



**KTH Electrical Engineering**

# **Fundamentals of Medium Access Control Design for Millimeter Wave Networks**

HOSSEIN SHOKRI-GHADIKOLAEI

Licentiate Thesis  
Stockholm, Sweden 2015

TRITA-EE 2015:030  
ISSN 1653-5146  
ISBN 978-91-7595-645-9

KTH Royal Institute of Technology  
School of Electrical Engineering  
SE-100 44 Stockholm  
SWEDEN

Akademisk avhandling som med tillstånd av Kungl Tekniska högskolan framlägges till offentlig granskning för avläggande av teknologie licentiatesexamen i electro och systemteknik fredag den 18 september 2015 klockan 14.00 i Drottning Kristinasväg 30, plan 3 Lantmäteri , KTH Campus.

© 2015 Hossein Shokri-Ghadikolaei, unless otherwise stated.

Tryck: Universitetsservice US AB

# Abstract

In current wireless communication systems, demands for extremely high data rates, along with spectrum scarcity at the microwave bands, make the millimeter wave (mmWave) band very appealing to provide these extremely high data rates even for a massive number of wireless devices. MmWave communications exhibit severe attenuation, vulnerability to obstacles (called blockage), and sparse-scattering environments. Moreover, mmWave signals have small wavelengths that allow the incorporation of many antenna elements at the current size of radio chips. This leads to high directivity gains both at the transmitter and at the receiver, directional communications, and, more importantly, possible noise-limited operations as opposed to microwave networks that are mostly interference-limited.

These fundamental differences between mmWave networks and legacy communication technologies challenge the classical design constraints, objectives, and available degrees of freedom. The natural consequence is the necessity of revisiting most of the medium access control (MAC) layer design principles for mmWave networks, which have so far received less attention in the literature than physical layer and propagation issues. To address this important research gap, this thesis investigates the fundamental MAC layer performance metrics, including coverage, fairness, connection robustness, collision probability, per-link throughput, area spectral efficiency, and delay. The original analysis proposed in this thesis suggests novel insights as to the solutions for many MAC layer issues such as resource allocation, interference management, random access, mobility management, and synchronization in future mmWave networks.

A first thread of the thesis focuses on the fundamental performance analysis and mathematical abstraction of mmWave wireless networks to characterize their differences from conventional wireless networks, i.e., high directivity, line-of-sight communications, and occurrence of deafness (misalignment between transmitters and receivers). A mathematical framework to investigate the impact of beam training (alignment) overhead on the throughput is established, which leads to identify a new *alignment-throughput* tradeoff in mmWave networks. A novel blockage model that captures the angular correlation of line-of-sight conditions using a new notion of “coherence angle” is proposed. The coverage and delay of directional cell discovery are evaluated, and an optimization approach to maximize long-term throughput of users with fairness guarantees is proposed. In addition, this thesis develops a tractable approach to derive the collision probability, as a function of density of the transmitters, transmission power, density and size of the obstacles, operating beamwidth, and sensitivity of the receiver, among the main parameters. The collision probability allows deriving closed-form expressions for the per-link and network throughput of mmWave networks, and thereby identifying that, contrary to mainstream belief, these networks may exhibit a non-negligible *transitional behavior* of interference from a noise-limited to an interference-limited regime.

The second thread of the thesis builds on the previous fundamental performance analysis and modeling to establish new, efficient MAC protocols. The de-

rived collision probability is used to evaluate per-link throughput, area spectral efficiency, and delay performance of common MAC protocols such as TDMA and slotted ALOHA, and to provide a fundamental comparison between pros and cons of contention-free and contention-based MAC protocols. The results suggest the use of on-demand interference management strategy for future mmWave cellular networks and collision-aware hybrid MAC protocols for mmWave ad hoc networks to reliably deliver messages without sacrificing throughput and delay performance. Moreover, the transitional behavior, together with significant mismatch between transmission rates of control and data messages, imposes the development of new hybrid proactive and reactive control plane architecture. This thesis identifies the prolonged backoff time problem, which happens in mmWave networks due to blockage and deafness, and proposes a new collision notification signal to solve this problem. Motivated by the significant mismatch between coverage of the control and data planes along with delay analysis of directional cell search, a novel two-step synchronization procedure is proposed for mmWave cellular networks. Also, the impact of relaying and multi-hop communication to provide reliable mmWave connections, to alleviate frequent handovers, and to reduce the beam training overhead is investigated.

The investigations of this thesis aim to demystify MAC layer performance of mmWave networks and to show the availability of many new degrees of freedom to improve the network performance, e.g., in terms of area spectral efficiency, energy efficiency, robustness, delay, coverage, and uniform quality of service provisioning. The results reveal many special behaviors of mmWave networks that are largely ignored in design approach of the current mmWave networks. Given that the standardization of mmWave wireless cellular networks has not started as yet, and that existing standards of mmWave ad hoc networks are highly sub-optimal, the results of this thesis will provide fundamental design guidelines that have the potential to be very useful for future mmWave standardizations.





# Acknowledgments

I would like to express my sincere appreciation towards my supervisor Associate Prof. Carlo Fischione, whose constructive supports and guidance throughout the last years have lead to this work. I am also grateful to my co-authors Prof. Michele Zorzi, Prof. Petar Popovski, Dr. Gábor Fodor, and Dr. Lazaros Gkatzikis. With them all, I had exciting collaborations that have allowed me to substantially develop my knowledge. I also thank Associate Prof. Ming Xiao for being my co-advisor.

I am also immensely grateful to people of Communication Theory department for many insightful discussions, and also to people of Automatic Control department for making every day at lab enjoyable. I would like to thank Anneli, Hanna and Kristina for their administrative supports and helps especially when I arrived Sweden.

Finally, I would like to express my appreciation to my family for their love and unconditional support throughout my life and my studies.

Hossein Shokri  
Stockholm, September 2015





---

# Contents

---

<b>Contents</b>	<b>ix</b>
<b>List of Figures</b>	<b>xiii</b>
<b>List of Acronyms</b>	<b>xv</b>
 <b>I Thesis Overview</b>	 <b>1</b>
<b>1 Introduction</b>	<b>3</b>
1.1 Background . . . . .	6
1.1.1 Millimeter Wave Wireless Channel . . . . .	6
1.1.2 Beamforming . . . . .	7
1.1.3 Deafness and Blockage . . . . .	9
1.1.4 Right Interference Model . . . . .	9
1.1.5 Network Architecture . . . . .	10
1.1.6 Control Channel . . . . .	10
1.1.7 Hybrid MAC . . . . .	11
1.1.8 Hidden and Exposed Node Problems . . . . .	12
1.2 Contributions of the Thesis . . . . .	13
1.2.1 MmWave Cellular Networks . . . . .	14
1.2.2 Short Range mmWave Networks . . . . .	15
1.2.3 Alignment-throughput Tradeoff in mmWave Networks . .	16
1.2.4 The Transitional Behavior of mmWave Networks . . . . .	18
1.2.5 Contributions not Covered in the Thesis . . . . .	21
1.3 Conclusions and Future Works . . . . .	22
 <b>II Included Papers</b>	 <b>25</b>
<b>A Millimeter Wave Cellular Networks: A MAC Layer Perspective</b>	<b>27</b>
A.1 Introduction . . . . .	29
A.2 Fundamentals . . . . .	31
A.2.1 The Directed mmWave Wireless Channel . . . . .	31

A.2.2	Heterogeneity . . . . .	32
A.2.3	Beamforming . . . . .	32
A.3	Realization of Physical Control Channels . . . . .	35
A.3.1	Essential Tradeoffs . . . . .	35
A.3.2	Available Options and Design Aspects . . . . .	38
A.4	Initial Access and Mobility Management . . . . .	40
A.4.1	Fundamentals of Initial Access . . . . .	41
A.4.2	Two-step Synchronization and Initial Access . . . . .	44
A.4.3	Mobility Management and Handover . . . . .	47
A.5	Resource Allocation and Interference Management . . . . .	49
A.5.1	Channelization . . . . .	49
A.5.2	Scheduling . . . . .	49
A.5.3	Interference Management . . . . .	53
A.5.4	Dynamic Cell . . . . .	53
A.6	Concluding Remarks . . . . .	58
<b>B</b>	<b>Design Aspects of Short Range Millimeter Wave Networks:</b>	
<b>A</b>	<b>MAC Layer Perspective</b>	<b>67</b>
B.1	Introduction . . . . .	69
B.2	Fundamentals . . . . .	71
B.2.1	The Directed mmWave Wireless Channel . . . . .	71
B.2.2	Beam-searching . . . . .	71
B.2.3	Deafness and Blockage . . . . .	71
B.2.4	Control Channel . . . . .	72
B.3	Standardization in mmWave Communications . . . . .	72
B.3.1	Personal Area Networks: IEEE 802.15.3.c . . . . .	73
B.3.2	Local Area Networks: IEEE 802.11ad . . . . .	74
B.4	Main Issues for MAC Design . . . . .	75
B.4.1	Alignment-Throughput Tradeoff . . . . .	75
B.4.2	Transitional Behavior . . . . .	75
B.4.3	Prolonged Backoff Time . . . . .	78
B.4.4	Reactive Control Plane . . . . .	79
B.4.5	Directional-mmWave Control Channel . . . . .	82
B.4.6	Multihop Communications . . . . .	82
B.5	Conclusions . . . . .	84
<b>C</b>	<b>Beam-searching and Transmission Scheduling in Millimeter Wave Communication</b>	<b>85</b>
C.1	Introduction . . . . .	87
C.1.1	Related Work . . . . .	88
C.1.2	Our Contribution . . . . .	89
C.2	System Model and Problem Formulation . . . . .	89
C.2.1	Alignment Overhead . . . . .	90
C.2.2	Effective Transmission Rate . . . . .	91
C.2.3	Maximizing Network Throughput . . . . .	93

---

C.3	Joint Beamwidth Selection and Transmission Scheduling . . . . .	93
C.3.1	Single Link Scenario . . . . .	93
C.3.2	Multiple Links Scenario . . . . .	94
C.4	Numerical Results . . . . .	97
C.5	Conclusion . . . . .	99
<b>D</b>	<b>The Transitional Behavior of Interference in Millimeter Wave Networks</b>	<b>101</b>
D.1	Introduction . . . . .	103
D.2	System Model . . . . .	107
D.3	Collision Analysis . . . . .	110
D.4	Throughput and Delay Analysis . . . . .	117
D.4.1	Noise-limited or Interference-limited . . . . .	118
D.4.2	Proper Resource Allocation Protocol . . . . .	119
D.4.3	Collision-aware Hybrid MAC . . . . .	128
D.5	Concluding Remarks . . . . .	129
	<b>Bibliography</b>	<b>135</b>



---

## List of Figures

---

1.1	Atmospheric absorbtion of electromagnetic waves . . . . .	4
1.2	United States frequency allocations chart . . . . .	5
1.3	General hybrid beamforming architectures . . . . .	7
1.4	Hidden and exposed node problems . . . . .	12
1.5	Performance of the proposed approach to mitigate the prolonged backoff time . . . . .	16
1.6	Alignment-throughput tradeoff in mmWave networks . . . . .	17
1.7	The Transitional Behavior of Interference . . . . .	19
1.8	Area spectral efficiency and delay performance of slotted ALOHA and TDMA . . . . .	20
A.1	Beamforming procedure . . . . .	33
A.2	Tradeoffs in realizing a physical control channel . . . . .	37
A.3	Coverage gain against directivity gain . . . . .	38
A.4	Coverage of different physical control channels . . . . .	41
A.5	Initial access and mobility management in mmWave networks . . . .	42
A.6	Complexity of spatial synchronization in mmWave cellular networks	46
A.7	Scheduling scenarios in mmWave cellular networks . . . . .	50
A.8	Example of the optimal association in mmWave cellular networks . .	57
A.9	Illustration of the angles between BSs and UEs . . . . .	64
B.1	Network architecture of existing mmWave WPAN and WLAN . . . .	73
B.2	Network timing structure of existing IEEE mmWave standards . . .	74
B.3	Performance comparison of slotted ALOHA and TDMA in mmWave WPANs . . . . .	77
B.4	A simple protocol for mitigating prolonged backoff time . . . . .	80
B.5	Performance of the proposed approach to mitigate the prolonged backoff time . . . . .	81
B.6	Different options to realize a control channel . . . . .	83
C.1	Time slot segmentation of each mmWave link . . . . .	90
C.2	Illustration of the angles between transmitters and receivers . . . .	91
C.3	Optimal region of transmission and reception beamwidths . . . . .	98
C.4	Alignment-throughput tradeoff in mmWave networks . . . . .	99
C.5	Network throughput in multiple links scenario . . . . .	99

D.1	Hatched lines show potential interference zone. Operating beamwidth $\theta$ is divided into $k$ sectors of angle $\theta_c$ . The typical receiver is on the origin. The tagged transmitter, shown by a green circle, is on sector $k$ at distance $\ell$ of the typical receiver. $S_i$ shows sector $1 \leq i \leq k-1$ . $SS_1$ and $SS_2$ are two sub-sectors of sector $k$ . Zones with orange hatched lines have both random interferers and obstacles, represented by a red triangle and a blue rectangle. Zones with green hatched lines have only random interferers. $d_{\max}$ is the interference range. . . . .	112
D.2	The probability of having LoS interference from sector $s$ , $1 \leq s \leq k-1$ , as a function of (a) link density and (b) obstacle density, as computed by Equation (D.3) and Monte Carlo simulations. . . . .	115
D.3	The probability of collision as a function of the length of the typical link $\ell$ , as computed by Equations (D.8) and Monte Carlo simulations, marked by filled circles. Upper and lower bounds are computed by Equation (D.10). . . . .	118
D.4	The probability of collision as a function of (a) link density and (b) obstacle density. The length of the typical link is $\ell = 5$ m. . . . .	120
D.5	The effective MAC throughput against transmission probability $\rho_a$ , as computed by the emulator and by Equation (D.12). The obstacle density is $\lambda_o = 0.11$ per unit area. . . . .	122
D.6	Achievable regions of (a) per-link throughput and (b) area spectral efficiency of slotted ALOHA with $\rho_a = 1$ . . . . .	124
D.7	(a) the optimal transmission probability and (b) the maximum per-link throughput against link density. "S-ALOHA" stands for slotted ALOHA. . . . .	126
D.8	Area spectral efficiency and delay performance of slotted ALOHA and TDMA. Area size is $10 \times 10$ m <sup>2</sup> . Different points of (b) represent different link densities from 0.02 to 2 links per unit area. The obstacle density is $\lambda_o = 0.25$ per unit area. Operating beamwidth in (b) is $10^\circ$ . Slotted ALOHA provides higher ASE with lower delay significantly. These performance gains may improve with the number of links. . .	127

---

## List of Acronyms

---

A-BFT	Association beamforming training
ADC	Analog digital converter
AP	Access point
ATI	Announcement transmission interval
BHI	Beacon header interval
BS	Base station
BTI	Beacon transmission interval
CAP	Contention access period
CBAP	Contention-based access period
CBR	Constant bit rate
CDF	Cumulative distribution function
CN	Collision notification
CSI	Channel estimation information
CSMA	Carrier sense multiple multiple access
CSMA/CA	Carrier sense multiple access/collision avoidance
CTAP	Channel time access period
CTS	Clear to send
D2D	Device to device
DoA	Direction of arrival
DTI	Data transfer interval
FCC	Federal Communications Commission
FDD	Frequency division duplexing
HARQ	Hybrid automatic repeat request
LoS	Line of sight
MAC	Medium access control
MACA	Multiple access with collision avoidance
MIMO	Multiple input multiple output

mmWave	Millimeter wave
NLoS	Non line of sight
OFDM	Orthogonal frequency division multiplexing
PBSS	Personal basic service set
PCP	PBSS control point
PHY-CC	Physical control channel
PMF	Probability density function
PNC	Piconet coordinator
QoS	Quality of service
RSRP	Reference signal received power
RSSI	Received signal strength indicator
RTS	Request to send
SINR	Signal to interference-plus-noise ratio
SNR	Signal to noise ratio
SP	Service period
STDMA	Spatial time division multiple access
TDD	Time division duplexing
TDMA	Time division multiple access
UE	User equipment
WiGig	Wireless gigabit alliance
WLAN	Wireless local area network
WPAN	Wireless personal area network



# Part I

## Thesis Overview



# Introduction

---

Increased demands for higher data rates in wireless communication systems, along with new applications such as massive wireless access, and limited available spectrum at the microwave bands have motivated enhancing spectral efficiency by using advanced technologies such as full-duplex communications, cognitive and cooperative networking, interference cancelation, and massive multiple input multiple output (MIMO). As these enhancements are reaching the fundamental capacity limits, the millimeter wave (mmWave) band is becoming an alternative and promising option to support extremely high data rate wireless access [1–6]. The main reasons are very simple: all the current (main) commercial wireless systems together have less than two percent of the bandwidth available at the mmWave spectrum, see Fig. 1.2; there are several unlicensed channels at the mmWave band, e.g., around 60 GHz, for short range wireless services, each having more than 2 GHz bandwidth. This huge bandwidth, even if utilized with a very low spectral efficiency, can easily provide gigabit-per-second data rate.

Currently, mmWave spectrum is primarily used for satellite communications, long-range point-to-point communications, military applications, local multipoint distribution service, and recently short range ad hoc networks [2, 7]. Due to severe attenuation of the signal at the mmWave band, especially at certain frequency bands such as 60 and 180 GHz, see Figure 1.1, mmWave communications were thought to be only applicable either for especial applications with especial hardware, mentioned above, or for “whisper radios” with coverage distances of a few meters (m) [3, 8] that is suited for wireless personal area networks (WPANs). However, recent studies on mmWave mobile networks have convinced the Federal Communications Commission (FCC) to publish notice of inquiries in late 2014 and early 2015, to evaluate the viability of mmWave bands for mobile radio services [9, 10]. These notice of inquiries were about technology specifications, bandwidth allocations, and health effects of mmWave communications, among others. In early 2015, Ofcom in UK also published similar public comments [11]. In all the answers to those inquiries, provided by numerous corporations and academic institutions, there was a common part: it is better to repurpose the mmWave band for future wireless networks.

MmWave communications are particularly attractive for ultra short range/high

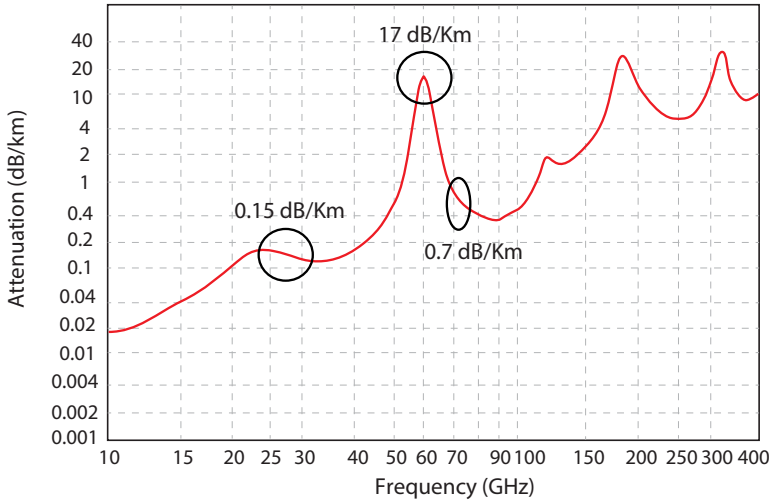


Figure 1.1: Atmospheric absorption of electromagnetic waves. High absorption have resulted in unlicensed short-range applications in the 60 GHz. See [www.mmwaveconcepts.com](http://www.mmwaveconcepts.com) for useful attenuation factors caused by rain, dust, and fog at mmWave bands. This figure is a modification of [12, Fig. 2].

rate communications and gigabit wireless applications such as wireless gigabit ethernet and uncompressed high quality video transmission, see Table 1.1. The commercial potential of mmWave networks initiated several standardization activities within wireless personal area networks (WPANs) and wireless local area networks (WLANs), such as IEEE 802.15.3c [13], IEEE 802.11ad [14], WirelessHD consortium, wireless gigabit alliance (WiGig), and recently IEEE 802.11ay study group on next generation 60 GHz.<sup>1</sup> Although there has been no dedicated standardization activity for mmWave in cellular networks so far, there are several ongoing discussions within research projects such as FP7 EU Project METIS [6] (2012-2015) on how to incorporate mmWave networks in 5G. The special propagation features [7] and hardware requirements [15] of mmWave systems bring multiple challenges at the physical, medium access control (MAC), and routing layers. These challenges are exacerbated due to the expected spectrum heterogeneity, that is, integration of and coexistence with the microwave communication standards. MmWave systems exhibit orders of magnitude higher attenuations, oxygen absorption, vulnerability to obstacles, sparse-scattering environments, smaller wavelength, higher number of antenna elements, high directivity gains, and possible noise-limited operation. These unique features distinguish mmWave systems from legacy microwave systems and

<sup>1</sup>Detailed information about these projects can be found at the following addresses: <http://www.wirelesshd.org> (WirelessHD), <http://wirelessgigabitalliance.org> (WiGig), and [http://www.ieee802.org/11/Reports/ng60\\_update.htm](http://www.ieee802.org/11/Reports/ng60_update.htm) (802.11ay), respectively. IEEE 802.11ay was approved in May 2015, and the study group has not released any stable document so far.

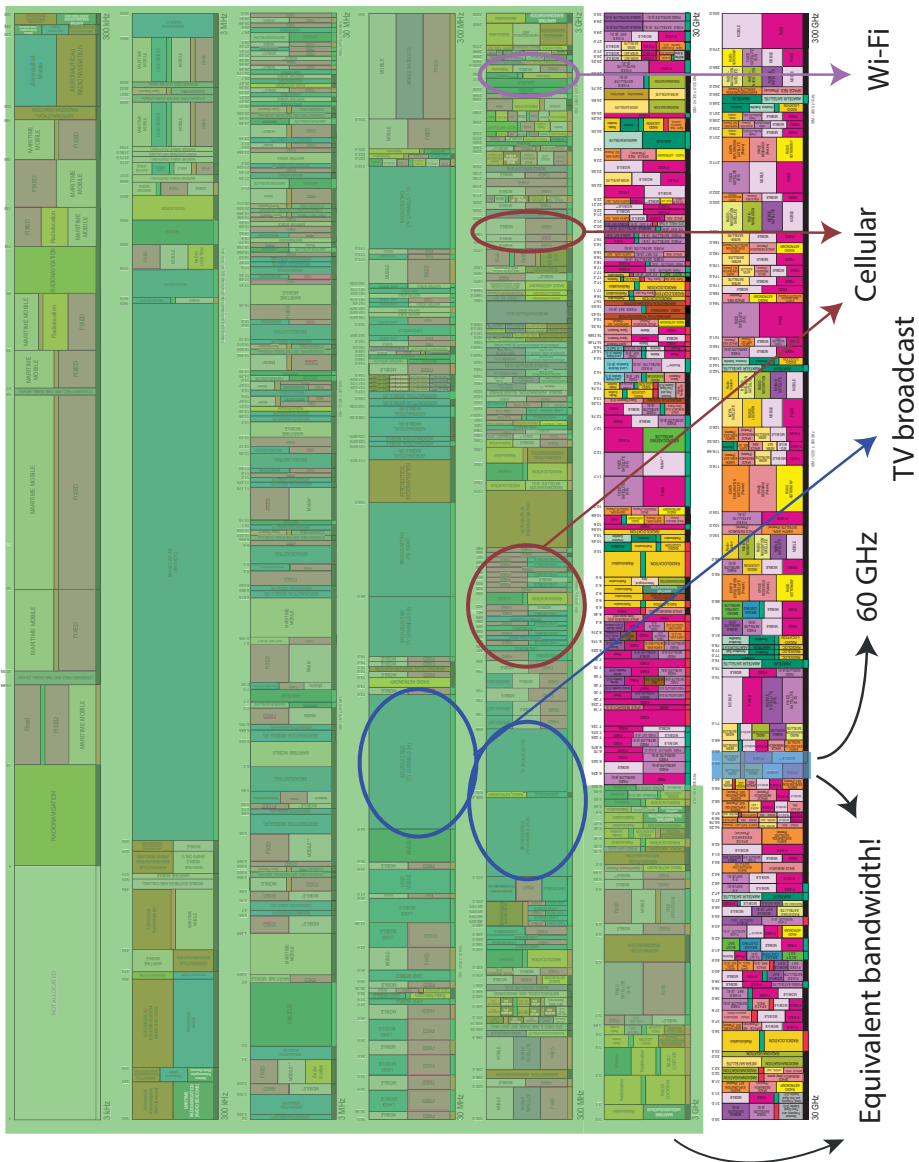


Figure 1.2: United States frequency allocations chart as of 2011. Below 6 GHz (microwave bands) are shaded by green color. Important commercial applications such as TV broadcast, WiFi, and cellular applications together have less than 1 GHz bandwidth. Areas colored by blue are 6 GHz free-licence channels around 60 GHz. The bandwidth of all existing commercial systems, shaded by green color, is equivalent to part of unlicensed bands available in the mmWave bands, shaded by blue color.

Table 1.1: Application scenarios for mmWave networks. This table is deduced from ongoing discussions inside IEEE 802.11ay study group. “NS” means not specified yet.

Usage models	Delay (s)	Availability	Range (m)	Rate (Gbps)	Application scenarios
Ultra short range communications	< 1	NS	< 10	10	Wireless tollgate and kiosks to transfer e-magazine, picture library, 4K movie trailers, 4K movies
8K Video transfer at smart home	< 0.005	NS	< 5	28	8K video stream between a source device (e.g., set-up box, tablet) and a sink device (e.g. smart TV, split TV), replacement of wired interface
Augmented reality	< 0.005	NS	< 10	20	Interface between a constantly moving high-end wearable devices and its managing device to deliver 3D video
Data center	< 0.1	99.99%	< 5	40	Inter-rack connectivity
Vehicular networks	< 0.1	NS	< 1000	NS	Intra- and inter-car connectivity, intersection collision avoidance, public safety
Video on-demand	< 0.1	NS	< 100	NS	Broadcast in crowd public places (e.g., classroom, in flight, train, ship, bus, exhibitions)
Mobile offloading	< 0.1	99.99%	< 100	20	Offload video traffic from cellular interface to the mmWave interface
Mobile fronthauling	< 0.035	99.99%	< 200	20	Wireless connections between remote radio heads and base band unit
Mobile backhauling	< 0.035	99.99%	< 1000	20	Small cell backhauling, mutihop backhauling, inter-building communications

demands a significant reconsideration in the design of the communication architecture and protocols, especially at the MAC layer, as pointed out in the editorials of two recent special issues dedicated to the use of mmWave in 5G [16, 17].

## 1.1 Background

In this section, we overview the essential properties of mmWave communications and briefly review the literature. Detailed literature review is provided in each chapter of the second part of this thesis.

### 1.1.1 Millimeter Wave Wireless Channel

MmWave communications use the part of the electromagnetic spectrum in the range 30–300 GHz, which corresponds to wavelengths from 10 mm to 1 mm. In the literature, however, mmWave frequencies casually refer to the frequency band between 6–300 GHz [7, 18, 19]. The main characteristics of mmWave are short wavelength/high frequency, large bandwidth, high interaction with atmospheric constituents such as oxygen (quantified in Fig. 1.1), and high penetration loss due to most solid materials. These characteristics lead to a sparse-scattering environment, where the

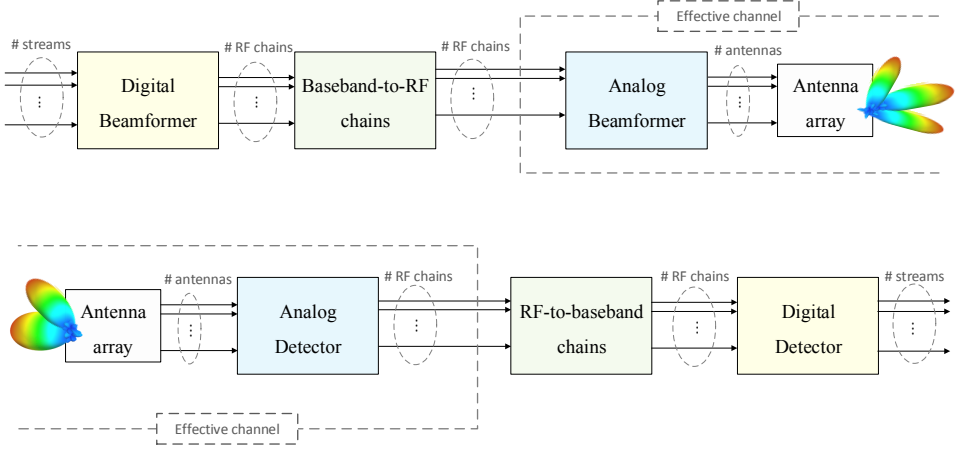


Figure 1.3: General hybrid beamforming architectures. Disabling analog (digital) beamformer and detector blocks and adopting proper number of RF chains result in a complete digital (analog) beamforming architecture. This figure is from our work [22, Fig. 1].

majority of the channel directions of arrivals are below the noise floor [7, 19–21]. Very small wavelengths allow implementation of a large number of antenna elements in the current size of radio chips. Using proper beamforming, this large antenna array provides high directivity gain both at the transmitter and at the receiver, which can largely compensate the high path-loss (that is, the distance-dependent component of the attenuation) without any extra transmission power. Due to directional transmissions, mmWave communication encounters a directed spatial channel, that is, a communication link can be established in a specific direction with a range that varies according to the directionality level.

### 1.1.2 Beamforming

Beamforming is the key technique to compensate the severe channel attenuation in mmWave systems. Generally speaking, there are three beamforming architectures, namely digital, analog, and hybrid, all illustrated in Figure 1.3.

Digital beamforming, as the defacto scheme in modern MIMO systems, provides the highest flexibility in beamforming at the expense of one baseband-to-RF chain (in short RF chain) per antenna. While this expense may be affordable in today's wireless systems with relatively small number of antenna elements, future mmWave devices are envisioned to have orders of magnitude more antenna elements. This large number of antenna elements each having one RF chain, operating in very wide bandwidth, increases the cost, complexity, and power consumption, which may limit the applicability of mmWave systems in low-cost energy-efficient future wireless networks [5, 6, 23–25]. Moreover, to have a proper digital beamforming,

the channel between every pair of antenna elements of the transmitter and the receiver should be estimated, which may be formidable in mmWave bands due to a coherence time that is around an order of magnitude smaller than that of microwave bands.<sup>2</sup> This limitation restricts the application of mmWave systems to only low-mobility scenarios, where coherence time is sufficiently large to first estimate the channel and then operate with the formed beams. Low-resolution ADCs (ideally with only one bit) and sparse channel estimation are recently proposed to address the aforementioned challenges (see [26, 27] and references therein).

Analog beamforming forms the beam with only one RF chain, but a series of phase shifters that are connected to individual antenna elements [25, 28]. Analog beamforming, besides having low complexity and cost, replaces complicated beamforming based on instantaneous channel estimation information (CSI) by a simple beam-searching procedure, as already established in existing mmWave WPAN and WLAN standards [13, 14]. Analog beamformer at the transmitter and at the receiver can sweep, by a sequence of pilot transmissions, all directions with a predefined resolution to find the pair of beams that maximize signal-to-noise ratio (SNR). These directions along with the corresponding resolutions are defined in a beamforming codebook. However, analog beamforming forms only one beam at a time without being able to multiplex within the beam, implying that this architecture provides only directivity gain. Although this might not be a big challenge in applications where one device communicates to only one device (typical ad hoc and device-to-device (D2D) scenarios),<sup>3</sup> applications where one device serves multiple devices (a typical cellular network) require several RF chains to serve devices that are separated geographically. This diminishes the advantages of this architecture such as low complexity and low power consumption.

A two-stage hybrid digital-analog beamforming is a promising architecture for future mmWave networks, both cellular [25, 27, 29] and short range in IEEE 802.11ay. This architecture allows the use of a very large number of antennas with a limited number of RF chains [29–31], typically 8–16 times fewer RF chains than the number of antenna elements [32]. Analog beamforming layer provides spatial division and directivity gains, whereas digital beamforming layer may be used to further reduce intra-beam interference and provide multiplexing gain inside one beam. To this end, the digital beamformer is applied on the effective channel consisting of the analog beamforming weights and the actual channel matrix. This complicates the estimation of CSI, as the CSI is available only after being processed by the analog beamformer. To address this problem, some recent works couple channel estimation and analog beamforming design [32, 33]; however, different time-scales over which analog and digital beamforming should be designed challenges these solutions. Digital beamformer requires instantaneous CSI while analog beamformer can be designed based on long-term CSI [22].

---

<sup>2</sup>The Doppler shift scales linearly with the operating frequency, and the operating frequency of mmWave systems is an order of magnitude higher than that of microwave systems.

<sup>3</sup>Study group of IEEE 802.11ay suggests the use of multiple RF chains per device to substantially improve the achievable throughput of the legacy IEEE 802.11ad with multiplexing gain.



### 1.1.3 Deafness and Blockage

Vulnerability to obstacles and directional communications in mmWave networks result in two consequences [2]: (1) blockage and (2) deafness.

*Blockage* refers to very high attenuation due to obstacles. As some examples, the penetration loss of mmWave signals due to human body, brick, and glass is as much as 35 dB, 80 dB and 50 dB, respectively [19, 34–38]. This severe loss cannot be compensated by just adding a few dB more transmission power or extra directivity gain using narrower beams. Instead, a mmWave connection may find alternative directed spatial channels that are not blocked or fall back to microwave band, if possible [14].

*Deafness* refers to the situation in which the main beams of the transmitter and the receiver are not aligned toward each other. Therefore, the link budget will not be boosted enough to establishment a high quality mmWave link. The consequences of deafness are threefold from a MAC layer perspective: (1) interference and collision avoidance mechanisms may be secondary design factors, as a receiver listens only to specific directed channel; (2) concurrent transmissions enables substantial increment in the spectral efficiency; and (3) complicated beamforming (alignment) and beam-tracking procedures may be necessary to establish and maintain a mmWave link.

### 1.1.4 Right Interference Model

One of the most challenging part in analysis of any wireless network is modeling the aggregated interference, as it depends on the transmit powers, unknown random channel attenuations, MAC protocol, and more importantly the network topology, which is (partially) not available in most of the wireless applications. Therefore, a very fundamental question in the design of a wireless network is: what is the right interference model for this wireless network?

The simplest model is the *interference range model*, in which a receiver may observe interference only from the closest interferer, interpreted as the strongest one in this model, and an outage event occurs if that interferer is located no farther than a constant maximum distance of the receiver, called interference range. A modified version of this model is the *protocol model*, formalized by the seminal work of Gupta and Kumar [39]. The only modification is that the interference range, instead of being a constant value, depends on the received power from the intended transmitter and a minimum signal-to-interference-plus-noise ratio (SINR) threshold. These interference models are extensively adopted to analyze the MAC and network layers of a wireless network in terms of network-layer capacity [39, 40], delay [41], fairness [42], throughput [43], backoff design [44], etc. However, both interference range and protocol models have a major disadvantage: they do not consider the impact of interference aggregation. It might be that there are several transmitters outside the interference range such that their aggregated interference downs the perceived SINR below the threshold. The most accurate but complicated interference model is the *physical model*, also formalized in [39], that considers the

impact of interference aggregation instead of considering only the closest interferer. This interference model is adopted mostly at the physical layer for beamforming design [45], capacity evaluation [39, 46], power control [47], coverage analysis [48], energy efficiency characterization [49], etc.

Recent study [50] reveals that the special characteristics of mmWave networks make the protocol model quite accurate in those networks. Essentially, as the probability of having no obstacle on a link decreases exponentially with the distance [51], far away transmitters will be most probably blocked and therefore cannot contribute in the interference a receiver observes. Therefore, considering only the impact of spatially close interferers, ideally only the closest one, introduces a negligible loss in the accuracy of the interference model, but significantly facilitates analysis and protocol design for mmWave networks.

### 1.1.5 Network Architecture

A mmWave network can be deployed either with infrastructure, where a centralized entity usually called base station (BS) or access point (AP) manages all tasks in the network, or ad hoc, where there is no such a predefined network manager. Cellular networks, adopt the first architecture, whereas most of the short range networks adopt the second architecture. The fundamental difference from MAC layer perspective is that the roles are predefined in the infrastructure networks, for instance a terminal that wants to connect always waits for a beacon signal from the infrastructure node, while the roles in ad hoc networks are dynamically assigned. Besides, short-range networks may rely on carrier sensing among terminals, they may use multihop communications, which may also affect traffic patterns, and WPAN/WLAN devices generally have much less capabilities compared to smart phones and base stations in cellular networks.

### 1.1.6 Control Channel

Control channels are instrumental for any wireless network. These channels facilitates device discovery, data channel establishment, neighbor discovery, resource allocation coordination, routing information exchange, feedback signals, and many other key information. While control channels should ensure different quality-of-service (QoS) levels for different control signals, very high reliability and availability are their indisputable requirements. These requirements introduce two new mismatches in mmWave networks: (1) a mismatch between transmission rate of control and data channels, and (2) a mismatch between coverage of control and data channels. We will discuss implications of these mismatches on the design of proper control plane for a mmWave network, later in the second part of this thesis.

While data channels of mmWave networks are implemented in mmWave frequency band, control channels can be implemented in mmWave [13, 14] or microwave [52] band. Each option has its own pros and cons. The mmWave channel is less reliable than the microwave counterpart, due to vulnerability to blockage; however, a dedicated microwave control channel demands higher hardware com-

plexity and energy consumption, since an extra transceiver should be tuned on the microwave control channel. Using mmWave band, still we can implement a control channel with or without directional communication. An omnidirectional control channel alleviates the deafness problem at the expense of being subject to a very short range;<sup>4</sup> whereas a directional one increases the coverage with extra alignment overhead.

Note that we may realize a hybrid mmWave/microwave control plane, as recently proposed in [22]. In this case, synchronization or channel access requests are transmitted in omnidirectional-microwave mode, and other control messages such as acknowledgement (ACK) or negative-acknowledgement (NACK) operate in directional-mmWave mode.

### 1.1.7 Hybrid MAC

Wireless networks are designed to serve diverse applications with different constraints and QoS requirements, ranging from low-data-rate event-driven monitoring applications to high data rate real-time video streaming applications. Adding different reliability requirements into the picture, most of the existing standards incorporate several resource allocation protocols to ensure supporting different QoS levels. Carrier sense multiple access/collision avoidance (CSMA/CA) is one of the most celebrated protocols in wireless networks due to its simplicity, flexibility, and robustness. Without network-wide synchronization or global topology information, CSMA/CA can handle dynamic device registration, almost avoid interference, realize spatial reuse, and provide fairness among the devices. The price is high overhead due to constant collision avoidance procedure, which can cause as high as 75% throughput reduction for wireless applications with short packets [54]. Time division multiple access (TDMA) is the simplest and most used contention-free resource allocation that activates only one link at a time to avoid any interference. TDMA requires tight synchronization among all devices and a coordinator that activate different links (transmitter-receiver pairs) at different time. To enable spatial reuse, original TDMA is extended to spatial TDMA (STDMA) protocol that activates a set of links with negligible mutual interference at a time. STDMA offers the maximum throughput for every link and for the network [55–58]; however, it requires precise knowledge of the network topology a priori. Scheduling based on partial topology information also leads to substantial loss on the network throughput, around 33% is reported in [59]. Even for a given network topology, finding the optimal STDMA scheduling is an NP-hard problem [58–60], which may be impractical to solve in a wireless network with fast rescheduling requirements due to time-varying channel conditions, physical environmental changes, battery outage, and device failures.

It is well-established that TDMA provides substantially lower channel utilization and higher delays than CSMA/CA, in low contention regimes. Still, TDMA

---

<sup>4</sup>The transmission range can be enhanced by using lower-rate or more efficient coding techniques [53].

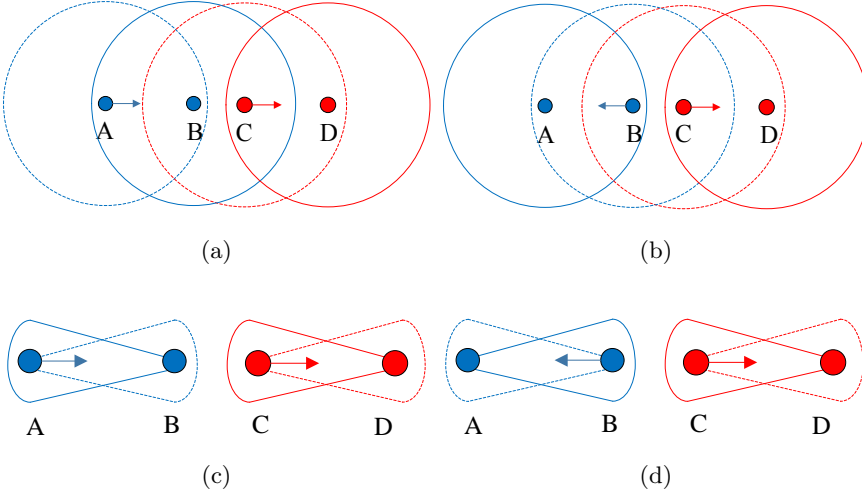


Figure 1.4: Illustration of the hidden and exposed node problems: (a) hidden node problem with omnidirectional communications, (b) exposed node problem with omnidirectional communications, (c) hidden node scenario with directional communications, and (d) exposed node scenario with directional communications. Circles and circle sectors show the transmission/reception ranges and directions. Solid lines show reception, and dashed lines show transmission. Similar colors correspond to similar transmitter-receiver pairs. Directional communications of mmWave networks alleviate the hidden and exposed node problems, and reduce the necessity of collision avoidance procedure of CSMA/CA.

can ensure certain QoS levels, which is usually very important for specific applications such as video streaming. Pros and cons of individual resource allocations motivate many hybrid MAC protocols to combine the strengths of TDMA and CSMA/CA, while offsetting their weaknesses. Examples include IEEE 802.15.3, 802.15.4, and 802.11 (various versions) [61, Table 5.8], and many other protocols such as Z-MAC [62] and T-MAC [63]. Current mmWave standards are also using a hybrid MAC with a CSMA/CA phase, mostly to register channel access requests, followed by a TDMA phase to provide guaranteed QoS levels [13, 14].

### 1.1.8 Hidden and Exposed Node Problems

Hidden and exposed node problems are amongst the most important problems in contention-based multiple access strategies, which demands adding protocol complexity to the MAC layer. The hidden node problem occurs when a transmitter is visible from a receiver, but not from other transmitters communicating with that receiver, see Figure 1.4(a) where node A is hidden from node C. Exposed node

problem occurs when a wireless device is prevented from sending packets to other devices due to a neighboring transmitter [64], see Figure 1.4(b) where nodes B and C mistakenly think their transmission will collide at their intended receivers. The widespread solution is incorporating collision avoidance signals, introducing multiple access with collision avoidance (MACA), firstly introduced in the seminal work of Karn [65]. As will be discussed later, current mmWave standards [13, 14, 52] adopt similar collision avoidance mechanisms as those of the legacy standards, developed for microwave band and primarily with omnidirectional operation. However, high directionality of mmWave communications both at the transmitter and at the receiver lead to negligible hidden and exposed node problems compared those legacy technologies, see Figures 1.4(c) and (d).

Note that we can have those problems for contention-based control channel(s) on microwave band, if any; however, the short size of control messages and their rare frequency make the hidden and exposed node problems of secondary importance. With very limited collisions, along with negligible hidden and exposed node problems, the essence of having proactive collision avoidance mechanisms for distributed multiple access in mmWave communications is challenged, especially because those mechanisms are a source of huge throughput loss in dense wireless networks [54, 66]. We discuss in the second part of this thesis how to solve collision problem (and in general manage the interference) in an on-demand manner. This leads to a substantial higher throughput compared to the existing resource allocation with a proactive collision avoidance strategy.

## 1.2 Contributions of the Thesis

This thesis investigates analysis and optimization of MAC layer performance of mmWave networks. The chapters presented in the second part of this thesis are based on the following published papers or submitted manuscripts. Below, we briefly present the main contributions of each chapter.

- [J1] H. Shokri-Ghadikolaei, C. Fischione, G. Fodor, P. Popovski, and M. Zorzi, “Millimeter wave cellular networks: A MAC layer perspective,” to appear in *IEEE Trans. Commun.*, 2015.
- [J2] H. Shokri-Ghadikolaei, C. Fischione, P. Popovski, and M. Zorzi, “Design aspects of short range millimeter wave wireless networks: A MAC layer perspective,” submitted to *IEEE Network*, May 2015, under second review round.
- [C1] H. Shokri-Ghadikolaei, L. Gkatzikis, and C. Fischione, “Beam-searching and transmission scheduling in millimeter wave communications,” in *Proc. IEEE International Conference on Communications (ICC)*, 2015.
- [J3] H. Shokri-Ghadikolaei and C. Fischione, “The transitional behavior of interference in millimeter wave networks,” submitted to *IEEE Trans. Commun.*, May 2015, under second review round.

- [C2] H. Shokri-Ghadikolaei and C. Fischione, “Millimeter wave ad-hoc networks: Noise-limited or interference-limited?,” in *Proc. IEEE Global Communications (GLOBECOM) Workshop*, San Diego, USA, Dec. 2015.

### 1.2.1 MmWave Cellular Networks

This chapter is based on [J1] and discusses the MAC layer design aspects of a mmWave cellular network. In this chapter, we focus on several MAC layer issues, such as synchronization, random access, handover, channelization, interference management, scheduling, and association. In particular, we show novel design approaches for three aspects:

**Control channel architecture:** We propose and develop fundamental design methods to realize an efficient physical control channel for mmWave cellular networks and provide application areas for each option. An omnidirectional channel on microwave bands is an imperative option wherever robustness to deafness, high channel reliability, and long range are necessary, e.g., in coordination among BSs during handovers. Directional physical control channels are more energy efficient and seems to be mandatory in cell search procedure to alleviate the possible mismatch between coverage of control and data channels. Considering advantages of all options, a combination of both omnidirectional microwave and directional millimeter wave control channels is proposed to realize efficient control plane for mmWave cellular networks. This novel hybrid architecture of the control plane is exemplified by proposing a two-step synchronization procedure that realizes macro-level time-frequency synchronization with an omnidirectional microwave channel and micro-level spatial synchronization with a directional mmWave channel. Performance evaluation confirms that a relatively small number of pilot transmissions guarantees discovery of a user with high probability. This number increases by using narrower beamwidths, which introduces a tradeoff between boosting link budget and reducing synchronization overhead.

**Initial access, mobility management, and handover:** We show that the contention-based random access procedure becomes more justifiable than contention-free counterpart to be incorporated in the initial access phase, as the operating beamwidths become narrower. However, to have this superior performance, we should solve a prolonged backoff time during random access, which we address by proposing a novel MAC layer signal. We also discuss how to manage the mobility and alleviate frequent handover problems in mmWave cellular networks using relay stations along with a central macro-level controller, which can be realized inside a macro-level BS.

**Resource allocation and interference management:** We demonstrate the implications of directional operation with pencil beams on proposing new definition of a cell, supplementing the definition of resource block with a spatial dimension, facilitating resource allocation, and simplifying intra- and inter-cell interference cancelation. We argue that the current interference-limited architecture of cellular networks should be revisited to leverage the potential of mmWave systems to improve the complex tradeoffs among throughput enhancement, fair scheduling, and

Table 1.2: The impact of directionality on resource allocation performance. All rates are measured in bit/s/Hz. See Table A.4 and Figure A.8 for more information.

Communication Mode	# RF chains per BS	Network sum rate	Minimum rate	Jain's fairness index
Directional	3	151.48	3.76	0.94
	6	322.74	7.73	0.89
	12	630.62	12.50	0.92
Omnidirectional	1	5.52	0.06	0.72

high connection robustness. We formulate an optimization problem based on long-term resource allocation, which shows that additional RF chains at the BS (or user) open new opportunities to redefine cells so as to better balance the total load of the network. This brings significant improvements in the network sum rate as well as enhancements in the minimum rate offered to a user and in fairness. We also discuss the limits on these gains when we use directionality at the BS and/or the users.

For instance, with 2 BSs and 30 users, distributed in 1 square kilometer, path-loss exponent  $\alpha = 3$ , 30 dBm transmission power of BSs, only one RF chain per user, Table 1.2 shows the performance of the network using the optimal association, resource sharing within every analog beam, operating beamwidths, and boresight angles of BSs as well as users. Directional communications bring significant performance gains even without using huge bandwidth of mmWave bands, as directionality improves the link budget, and at the same time, reduces the multiuser interference. In particular, with 12 RF chains at the BSs, we observe a sum rate enhancement by a factor of 113, a minimum rate enhancement by a factor of 207, and fairness enhancement by 20%, compared to the omnidirectional mode.

### 1.2.2 Short Range mmWave Networks

This chapter is based on [J2] and covers the substantial new achievements on the performance analysis of short range mmWave networks to identify the main challenges of existing mmWave standards at the MAC layer. We highlight a new alignment-throughput tradeoff, emphasize on the transitional behavior of interference in mmWave networks, and raise the necessity of new collision-aware hybrid resource allocation protocols. Then, we discuss the prolonged backoff time problem in mmWave networks with directional communication and propose a new MAC layer signal to alleviate this problem. We challenge the applicability of current mmWave MAC layer functions in dense deployment scenarios due to the significant mismatch between transmission rates of signaling and data packets, and highlight the need for an on-demand control plane. Finally, we discuss the potential of mul-

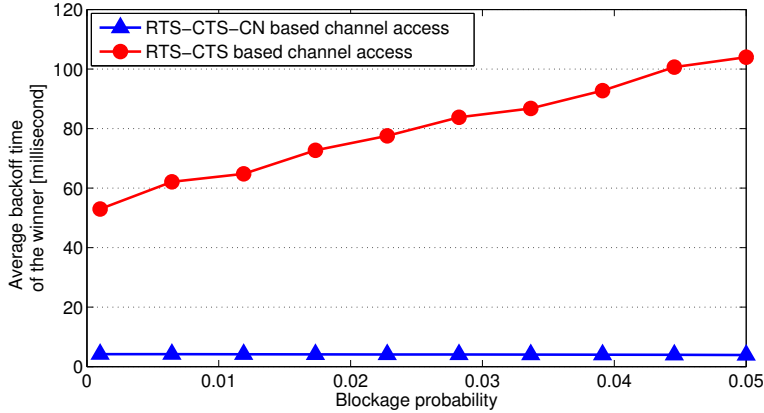


Figure 1.5: Average backoff time of the device winning the contention among 20 devices for accessing the same transmission resource (frequency and direction). The standardized collision avoidance approach of IEEE 802.11ad with request-to-send (RTS) and clear-to-send (CTS) signals leads to unnecessarily prolonged backoff time, while a slight modification of this standard negotiation, by introducing a collision-notification (CN) signal, effectively mitigates the problem. See Figures B.4 and B.5 for more information.

tihop communication techniques to compensate the error-prone mmWave physical layer and to provide reliable mmWave connections. Throughout this chapter, we identify critical MAC layer aspects of existing mmWave standards that may limit the efficacy and use cases of short range mmWave communications, and propose MAC design guidelines accordingly.

Considering a Bernoulli link failure model, that is, every link fails due to blockage independently and with constant blockage probability, Figure 1.5 shows the performance enhancement due to the introduction of the proposed collision-notification signal. With a blockage probability of 0.02, for instance, using collision-notification signal can dramatically reduce the average backoff time by about 95% (twenty times).

### 1.2.3 Alignment-throughput Tradeoff in mmWave Networks

This chapter is based on [C1] and identifies a new tradeoff between the alignment time and achievable throughput, called *alignment-throughput* tradeoff. That is, on the one hand, narrower beamwidths enhance the beam resolutions, so increases the alignment overhead and leaves less time for data transmission. On the other hand, it provides higher directivity gains, leading to higher transmission rates. Larger beamwidths also speed up alignment process at the expense of reduced transmission rates. In multiuser scenario, the problem becomes more complicated as narrow beamwidth, besides boosting the link budget, reduces multiuser interference, so in-



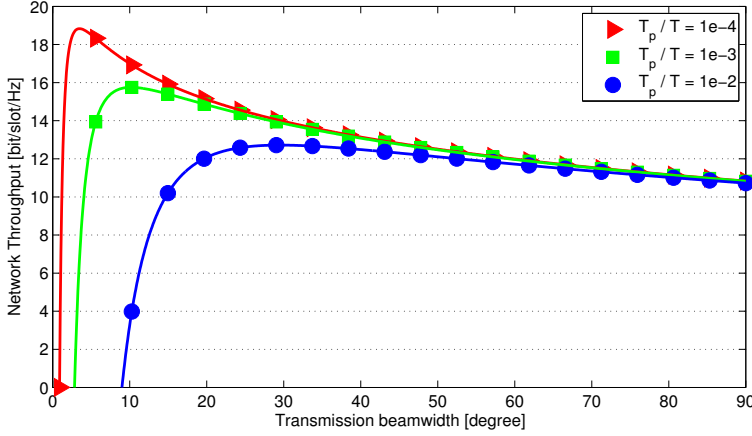


Figure 1.6: Alignment-throughput tradeoff in mmWave networks.  $T_p = 20\mu s$  is single pilot transmission time [13]. The time slot duration is  $T$ . The overhead of single pilot transmission is  $T_p/T$ . Adopting narrower beamwidths is not necessarily throughput-optimal. See Figure C.5 for more information.

creases SINR and thereby achievable transmission rate. More importantly, it may increase the spatial gain, that is, we may be able to activate higher number of links without harmful mutual interference. However, the price of this rate enhancement is higher alignment overhead per-link and complicated scheduling. We capture the alignment-throughput tradeoff by a unifying optimization problem that brings together beam-searching and transmission scheduling and explicitly addresses the major challenges of mmWave communications, namely deafness and interference management. Thanks to this optimization problem, we show that using extremely narrow beams (or equivalently excessively increasing the beamforming codebook size) is not beneficial in general due to the corresponding alignment overhead. We evaluate the computational and protocol complexities of solving the proposed optimization problem, and argue that it cannot be solved optimally, due to both NP-hardness of the problem and the need for knowing precise network topology a priori. To alleviate these complexities, we propose two low-complexity and standard-compliment protocols that rely on overestimation and underestimation of interference. The overestimation approach activates only a small subset of non-interfering links to ensure no harmful interference for active links. This overprotection underutilizes the available spatial resources, yet doubles the network throughput of the existing standards. The underestimation approach uses possible noise-limited behavior of a mmWave network and neglects the interference, yielding a close to the optimal performance with light computational complexity for small to modest size mmWave networks. Validity of the noise-limited assumption is subject of our work in [J3].

Figure 1.6 demonstrates the alignment-throughput tradeoff for a single link

mmWave network. For narrow beamwidths, beam-searching overhead limits the throughput performance, whereas as operating beamwidths increase, directivity gain becomes the limiting factor. Generally, the optimal point is a balance between directivity gain over the benefit of additional transmission time. Moreover, reduced overhead for single pilot transmission allows executing more beam-searching iterations with the same time budget. As a result, performance is improved, and narrower beams are more beneficial. From Figure 1.6, adopting narrower beamwidths is not necessarily throughput-optimal, due to the alignment overhead.

#### 1.2.4 The Transitional Behavior of mmWave Networks

This chapter is based on [J3] and [C2], and investigates if a mmWave network with pencil-beam operation is always noise-limited. This is a key question at the MAC layer, as the answer affects the design of almost all MAC layer functions such as resource allocation and interference management. For instance, in a noise-limited regime, there is no multiuser interference, hence activating all links without any coordination is throughput optimal, while we may need a complicated independent set-based scheduling in an interference-limited network to ensure throughput optimality of the scheduling. Although the increased directionality level in a mmWave network reduces multiuser interference, as we show in this chapter, this reduction may not be enough to take an action (e.g., scheduling) based on the assumption of being in a noise-limited regime. Specifically, activating all links at the same time may cause a significant throughput performance drop compared to the optimal resource allocation [C1]. It follows that a noise-limited assumption may be detrimental for proper MAC layer design. Still, the interference footprint may not be so large that we need to adopt a very conservative resource allocation protocol such as TDMA, which activates only one link at a time, adopted by existing mmWave standards.

In this chapter, we first introduce a novel blockage model that captures the correlation among LoS events of different links. This blockage model enables us to have a better approximation of the network behavior compared to existing models with independent blockage assumption used in [48, 67], especially as the number of links increases or if transmitters appears in spatial clusters. Tractable closed-form expressions along with tight bounds for the collision probability, per-link throughput, and area spectral efficiency of a mmWave network operating under slotted ALOHA and under TDMA are derived. We analytically evaluate the impact of the transmit power, transmission/reception beamwidth, transmitter density, and the density and size of the obstacles on the performance metrics. The new analysis shows that the noise-limited abstraction may not be accurate even for a modest-sized ad hoc network, and that *mmWave networks exhibit a transitional behavior from a noise-limited regime to an interference-limited regime*. Analytical and numerical performance analyses reveal that a simple slotted ALOHA may achieve the performance of STDMA and significantly outperforms TDMA in terms of throughput and delay performance. Still, TDMA may be necessary to ensure communication without any collision for a small subset of conflicting links. We conclude that the tran-

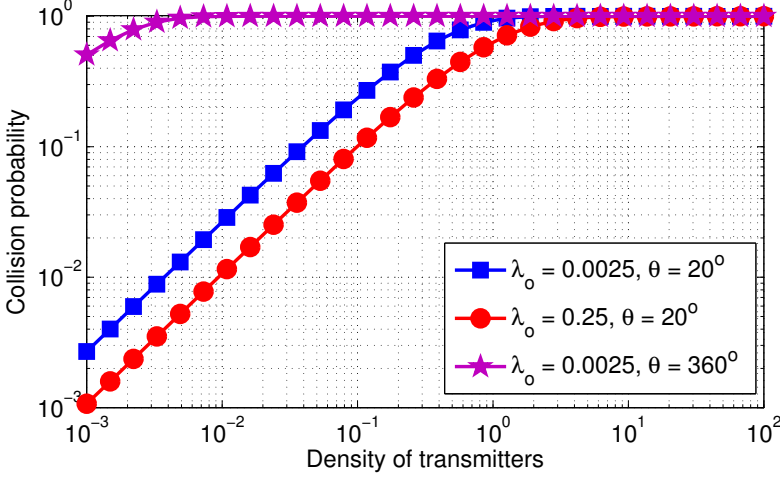


Figure 1.7: Collision probability against density of the transmitters.  $\lambda_o$  is the obstacle density,  $\theta$  is the operating beamwidth. MmWave networks exhibit a transitional behavior from a noise-limited to an interference-limited operating regime, as opposed to always interference-limited conventional networks. See Figure D.4 for more information.

sitional behavior of interference in mmWave networks necessitates collision-aware alternations between contention-based and contention-free phases in a hybrid MAC. In particular, the contention-based phase significantly improves throughput/delay performance of the network with light signaling overhead, while on-demand use of the contention-free phase to deliver only the collided packets guarantees a reliable mmWave connection with minimal drop in the throughput/delay performance. Detailed analysis of this chapter provide useful insights for designing proper resource allocation framework for future mmWave networks.

Consider a random number of aligned mmWave transmitter-receiver pairs and a random number of obstacles in the shape of lines with random orientation and random size between 0 and 1 m, all uniformly distributed in a  $10 \times 10 \text{ m}^2$  area. Every transmitter generates traffic with constant bit rate 384 Mbps, the size of all packets is 5 kB, time slot duration is  $100 \mu\text{s}$ , transmission rate is 1 packet per slot (link capacity around 1.5 Gbps), the transmitters have infinite buffer to save and transmit the packets, and the emulation time is 1 second. Under these simulation parameters, Figure 1.7 illustrates the transitional behavior of interference in mmWave networks. From this figure, the collision probability is not negligible even for a modest-size network. For instance, for 1 transmitter in a  $2 \times 2 \text{ m}^2$  area and 1 obstacle in a  $2 \times 2 \text{ m}^2$  area, the collision probability is as much as 0.24. Reducing the obstacle density increases the collision probability due to higher number of non-blocked interferers. Moreover, as can be observed in all curves of Figure D.4a, there

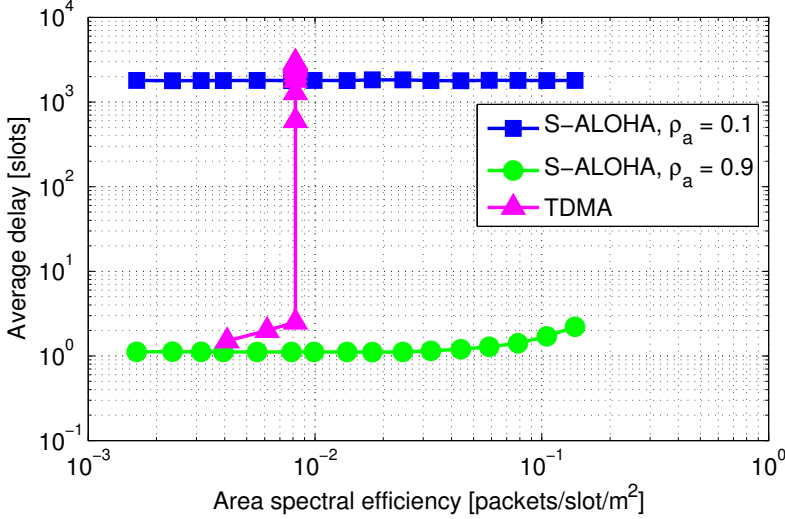


Figure 1.8: Area spectral efficiency and delay performance of slotted ALOHA and TDMA.  $\rho_a$  is the transmission probability of slotted ALOHA. Different points represent different link densities from 0.02 to 2 links per unit area. The obstacle density is 0.25 per unit area. Operating beamwidth is  $10^\circ$ . Slotted ALOHA provides significantly higher ASE with lower delay. These performance gains may improve with the number of links. See Figures D.7 and D.8 for more information.

is a transition from the noise-limited regime to the LoS interference-limited one in mmWave networks; whereas conventional networks with omnidirectional communications always experience an interference-limited regime without any transitional behavior under “realistic” set of parameters.

Figure 1.8 reports area spectral efficiency and the corresponding delay in slotted ALOHA and TDMA. Slotted ALOHA with transmission probability 0.9 significantly outperforms TDMA in terms of both throughput and delay. In particular, it requires, on average, less than two time slots to deliver a packet with one time slot transmission time, even in a very dense mmWave network with 2 transmitters in a unit area. The slotted ALOHA with transmission probability 0.1 may provide higher area spectral efficiency than that with 0.9 in ultra dense networks with around 9 transmitters in a unit area, not shown in this figure; however, its delay is very large for many practical set of parameters, around 3 orders of magnitude higher than that in slotted ALOHA with transmission probability 0.9. Increasing the number of links enhances the network throughput of TDMA in a saturating manner, where the saturation is achieved by 4 transmitters in the example considered. Further increasing the number of links will not improve the network throughput, but reduces the time share of every link and consequently reduces the average throughput of a link, and ultimately makes the queues of the transmitter may unstable. Superior throughput

and delay performances of slotted ALOHA is due to spatial gain. As the network goes to the noise-limited regime, spatial gain and consequently throughput/delay gains improve, making simple collision-base scheduling more justifiable than the contention-free counterparts.

### 1.2.5 Contributions not Covered in the Thesis

The following publications are not covered in this thesis, but contain related materials and applications:

- [J4] Y. Xu, H. Shokri-Ghadikolaei and C. Fischione, “Distributed association and relaying in millimeter wave networks,” submitted for journal publication, Sept. 2015.
- [J5] H. Shokri-Ghadikolaei, I. Glaropoulos, V. Fodor, C. Fischione, and A. Ephremides, “Green sensing and access: Energy-throughput tradeoffs in cognitive networking,” to appear in *IEEE Commun. Mag.*, 2015.
- [J6] H. Shokri-Ghadikolaei and C. Fischione, “Analysis and optimization of random sensing order in cognitive radio networks,” *IEEE J. Sel. Areas Commun.*, vol. 33, no. 5, pp. 803-819, May 2015.
- [C3] H. Shokri-Ghadikolaei, Y. Xu, L. Gkatzikis, and C. Fischione, “User association and the alignment-throughput tradeoff in millimeter wave networks,” in *Proc. IEEE Research and Technologies for Society and Industry (IEEE RTSI)*, Torino, Italy, Sept. 2015.
- [C4] S. Zhuo, H. Shokri-Ghadikolaei, C. Fischione, and Z. Wang, “Adaptive congestion control in cognitive wireless sensor networks,” in *Proc. IEEE International Conference on Industrial Informatics (IEEE INDIN)*, Cambridge, UK, Jul. 2015.
- [C5] H. Shokri-Ghadikolaei and C. Fischione, “Distributed random sensing order analysis and optimization in cognitive radio systems,” in *Proc. IEEE International Conference on Communications (IEEE ICC)*, Sydney, Australia, Jun. 2014.
- [C6] H. Shokri-Ghadikolaei, F. Yaghoubi, and C. Fischione, “Analysis and optimization of centralized sequential channel sensing in cognitive radio networks,” in *Proc. IEEE European Wireless (IEEE EW) Conference*, Barcelona, Spain, May 2014.
- [C7] H. Shokri-Ghadikolaei and C. Fischione, “Random Sensing Order in Cognitive Radio Systems: Performance Evaluation and Optimization,” in *Proc. IEEE International Conference on Computer Communications (IEEE INFOCOM) Workshops*, Toronto, Canada, May 2014.

### Contributions by the Author

The contributions of this Licentiate thesis' author on the mentioned above publications are the outcomes of the author's own work, in collaboration with the listed co-authors. The order of the name of the author reflects the contribution level in the papers. The author of this Licentiate thesis, when being first author of the paper, has been giving the substantial and vast majority of the contributions, especially in terms of theoretical analysis, computer simulations, and paper writing.

### 1.3 Conclusions and Future Works

Millimeter wave (mmWave) communications are promising enabler of extremely high data rate in future wireless networks and offer a significant improvement in per-user throughput, network throughput, and area spectral and energy efficiencies, compared to traditional wireless networks. The main characteristics of a mmWave system are very high path-loss, sparse-scattering environments, huge bandwidth, blockage, deafness, massive beamforming, and limited interference, all of which differentiate mmWave systems from legacy systems that operate at microwave band.

This thesis identified new challenges and tradeoffs that arise in mmWave networks, in the contexts of both ad hoc and cellular networks, and provided fundamental design guidelines for future mmWave networks, mostly from the medium access control (MAC) layer perspective. In particular, mismatch between control and data planes' coverage and transmission rates, tradeoff among cost-robustness-coverage of the control plane, inefficacy of current static cell definition, tradeoff among the number of RF chains-throughput-fairness-connection robustness, prolonged backoff time problem during random access, the alignment-throughput tradeoff, and the transitional behavior are investigated and analytically substantiated throughout the thesis.

To address these new tradeoffs and behaviors of a mmWave network, several protocols and solution approaches are proposed. For a mmWave cellular network, this thesis proposed four options to realize a physical control plane, a two-stage hierarchical synchronization protocol, a procedure for dynamic cell formation, a novel user association, an efficient handover procedure, and an on-demand inter-cell interference management. Delay and coverage of control plane were also studied, and design guidelines are provided accordingly. For short range mmWave networks, this thesis proposed a new MAC layer signal to solve the prolonged backoff time, new collision-aware hybrid resource allocation framework, novel random backoff procedure using a new collision notification signal, on-demand transmission of the control messages. Detailed mathematical analysis and discussions of this thesis aimed to provide original and important insights on the design of various MAC layer functions of future mmWave networks.

Although many open issues and future works are suggested in the second part of this thesis, followings are some additional possible future works:

- *Designing a heterogenous control plane for mmWave networks:* this thesis

identified different options to realize a physical control channel and provided initial performance evaluation to assess pros and cons of those options. The results suggest that we should redesign existing homogenous control plane to a heterogenous one that may include both mmWave and microwave bands and also both directional and omnidirectional communications. A comprehensive performance analysis and extensive numerical results in different situations are interesting topics for future studies to clarify the new architecture of the control plane.

- *Incorporating relaying techniques in mmWave networks:* Relaying techniques are key components of future mmWave networks for both access and backhaul, since they can provide more uniform quality of service by offering efficient mobility management, smooth handover operation, load balancing, indoor-outdoor coverage. Relaying is also essential for multihop backhauling, which is an important use case of IEEE 802.11ay. Still, very little done in analysis and design of efficient relaying schemes for mmWave networks [68], especially to evaluate the gain of relaying in a mobile environment with random blockage and extra alignment overhead between any device and the relays.
- *Evaluating the interplay between mmWave communications and D2D/cognitive networks:* As discussed throughout this thesis, pencil-beam operation shifts mmWave networks toward the noise-limited operation regime. Consequently, at the price of more complicated connection management, resource allocation and interference management procedures will be simplified. As recently pointed out, for instance, in [57,69–74], being closer to the noise-limited regime also increases the benefits of D2D and cognitive communications underlying a cellular networks. A thorough analysis of the interplay between D2D networks and underlying mmWave cellular networks is still missing in the literature. More interestingly, adding directionality to the users of D2D network, may change existing conclusions of possible huge adverse impact on cellular user with limited gain for D2D networks [75,76]. Performance evaluation of the coexistence of several network each having directional communications is an interesting future research direction.
- *Designing a proper retransmission policy for random access in mmWave networks:* To access the channel in a noise-limited regime, a wireless link may use retransmission only for time diversity if the original signal is severely attenuated by the random channel gain, so a very few retransmissions would be enough to access the channel. However, for an interference-limited network, retransmission policy should be designed to solve contention as well. This usually results in much higher retransmission attempts. Existing retransmission policies are designed for interference-limited microwave networks. However, as shown in this thesis, mmWave networks may exhibit both noise-limited and interference-limited regimes, demanding new collision-aware retransmission policy.





**Part II**

**Included Papers**



---

# Millimeter Wave Cellular Networks: A MAC Layer Perspective

---

Hossein Shokri-Ghadikolaie, Carlo Fischione, Gábor Fodor, Petar Popovski, and  
Michele Zorzi

To appear in  
*IEEE Transactions on Communications*

©2015 IEEE

The layout has been revised.

# Millimeter Wave Cellular Networks: A MAC Layer Perspective

Hossein Shokri-Ghadikolaei, Carlo Fischione, Gábor Fodor,  
Petar Popovski, and Michele Zorzi

## Abstract

The millimeter wave (mmWave) frequency band is seen as a key enabler of multi-gigabit wireless access in future cellular networks. In order to overcome the propagation challenges, mmWave systems use a large number of antenna elements both at the base station and at the user equipment, which lead to high directivity gains, fully-directional communications, and possible noise-limited operations. The fundamental differences between mmWave networks and traditional ones challenge the classical design constraints, objectives, and available degrees of freedom. This paper addresses the implications that highly directional communication has on the design of an efficient medium access control (MAC) layer. The paper discusses key MAC layer issues, such as synchronization, random access, handover, channelization, interference management, scheduling, and association. The paper provides an integrated view on MAC layer issues for cellular networks, identifies new challenges and tradeoffs, and provides novel insights and solution approaches.

## A.1 Introduction

The increased rate demand in the upcoming 5G wireless systems and the fact that the spectral efficiency of microwave links is approaching its fundamental limits have motivated consideration of higher frequency bands that offer abundance of communication bandwidth. There is a growing consensus in both industry and academia that millimeter wave (mmWave) will play an important role in 5G wireless systems [1–6] in providing very high data rates. The commercial potential of mmWave networks initiated several standardization activities within wireless personal area networks (WPANs) and wireless local area networks (WLANs), such as IEEE 802.15.3 Task Group 3c (TG3c) [13], IEEE 802.11ad standardization task group [14], WirelessHD consortium, and wireless gigabit alliance (WiGig). Although there has been no dedicated standardization activity for mmWave in cellular networks so far, there are several ongoing discussions within research projects such as FP7 EU Project METIS [6] (2012-2015) on how to incorporate mmWave networks in 5G. The high attenuation mitigates interference, while directionality supports wireless backhauling among micro and macro base stations (BSs) [77]; hence mmWave communication is suitable for dense heterogeneous deployments. The special propagation features [7] and hardware requirements [15] of mmWave systems bring multiple challenges at the physical, medium access control (MAC), and routing layers.

These challenges are exacerbated due to the expected spectrum heterogeneity in 5G, i.e., integration of and coexistence with the microwave communication standards. As pointed out in the editorials of two recent special issues dedicated to the use of mmWave in 5G [16, 17], the communication architecture and protocols, especially at the MAC layer, need to be revised to adapt signaling and resource allocation and cope with severe channel attenuation, directionality, and blockage.

In this paper, we identify the main challenges of mmWave cellular communications at the MAC layer. We show novel design approaches for three aspects:

### **Control channel architecture**

We highlight the necessity for a directional control plane in mmWave bands, identify the available options for that purpose, and discuss why an omnidirectional physical control channel in microwave bands can significantly boost the performance of the control plane.

### **Initial access, mobility management, and handover**

Leveraging the advantages of both omnidirectional microwave and directional millimeter wave control channel, we suggest a two-step synchronization procedure. We compare contention-free to contention-based random access protocols, and show that the latter becomes more justifiable to be incorporated in the initial access phase, as the transmission/reception beamwidths become narrower. However, the increased directionality may lead to a prolonged backoff time during random access, which we address by proposing a novel MAC layer signal. We also discuss how to manage the mobility and alleviate frequent handover problems in mmWave cellular networks.

### **Resource allocation and interference management**

The directional pencil-beam operation provides many options to form different cells and allocate resources, while significantly simplifying interference management. We identify new tradeoffs among throughput enhancement, fair scheduling, and high connection robustness, and formulate a suitable optimization problem based on long-term resource allocation. Finally, we show that additional RF chains at the BS can bring gains in terms of network throughput, fairness, and minimum UE rate, and discuss the limits on these gains when we use directionality at the BSs and/or the UEs.

The detailed discussions of this paper aim to demystify MAC layer design of mmWave cellular networks and show that there are many degrees of freedom that can be leveraged to significantly improve the performance, e.g., in terms of area spectral efficiency, energy efficiency, robustness, uniform QoS provisioning.

The rest of this paper is organized as follows. In Section A.2, we describe the essential aspects of mmWave cellular networks. In Section A.3, different options to realize a physical control channel will be discussed in detail. Section A.4 discusses design aspects of synchronization, random access, and handover procedures

in mmWave cellular networks. Resource allocation problems are discussed in Section A.5. Concluding remarks and future research directions are provided in Section A.6. To preserve the natural flow of the discussions, we present technical details, which are an integral part of the contributions of the paper, in the Appendices.

## A.2 Fundamentals

### A.2.1 The Directed mmWave Wireless Channel

MmWave communications use frequencies in the range 30–300 GHz, albeit the frequencies 10–30 GHz are also often referred to as mmWave [7, 18, 19]. The main characteristics of mmWave are short wavelength/high frequency, large bandwidth, high interaction with atmospheric constituents such as oxygen, and high attenuation through most solid materials. This leads to a sparse-scattering environment, where the majority of the channel directions of arrivals (DoAs) are below the noise floor [7, 19–21]. The sparsity in the angular domain (or equivalently the sparsity in the dominant channel eigenmodes) can be leveraged to realize efficient channel estimation and beamforming algorithms [32, 33, 78, 79]. Very small wavelengths allow implementation of a large number of antenna elements in the current size of radio chips, which boosts the achievable directivity gain, though at the price of extra signal processing. Such a gain can largely or even completely compensate the high path-loss (i.e., the distance-dependent component of the attenuation) without the need to increase the transmission power.

A channel in a mmWave system can be established in a specific direction (governed by nonzero channel eigenmodes) with a range that varies according to the directionality level. This results in two consequences: (1) blockage and (2) deafness. *Blockage* refers to high penetration loss due to obstacles and cannot be solved by just increasing the transmission power. The human body can attenuate mmWave signals by 35 dB [34, 35], and materials such as brick and glass attenuate them by as much as 80 dB and 50 dB [19, 36–38]. Overcoming blockage requires a search for alternative directed spatial channels that are not blocked, and this search entails a new beamforming overhead. This complicates mmWave MAC design for cellular networks compared to WPANs/WLANs, wherein short range still allows non-line-of-sight (NLoS) communications [13, 14]. Furthermore, the traditional notion of cell boundary becomes blurry in mmWave networks due to randomly located obstacles. This and other reasons, discussed later, demand reconsideration of the traditional cell definition. Early examples include the concepts of soft cell [80, 81] and phantom cell [82]. In mmWave cellular networks, instead, we can extend those concepts to that of *dynamic cell*, which is dynamically redefined to meet QoS demands of the UEs, overcome blockage, and optimize network utility, see Section A.5. *Deafness* refers to the situation in which the main beams of the transmitter and the receiver do not point to each other, preventing establishment of a communication link. On the negative side, deafness complicates the link establishment phase. On the positive side, it substantially reduces interference [43], as the receiver only listens to a specific directed spatial channel. This makes the conventional wisdom of

interference-limited microwave wireless networks not applicable to a noise-limited mmWave system,<sup>1</sup> heavily affecting both the initial access procedure and resource allocation, as will be discussed in Sections A.4 and A.5.

### A.2.2 Heterogeneity

To overcome the physical limitations of mmWave, the MAC mechanisms may have to exploit both microwave and mmWave bands simultaneously [19] and also facilitate co-existence of several communication layers with different coverage. Consequently, there will be two types of heterogeneity in mmWave cellular networks:

*Spectrum heterogeneity:* MmWave UEs may use both high (above 6 GHz) and low frequencies (microwave, such as the LTE band). While higher frequencies provide a massive amount of bandwidth for data communications, enabling very high data rates, the lower frequencies may be exploited for control message exchange, which demands much lower data rates but higher reliability than data communications. This facilitates the deployment of mmWave networks due to possible omnidirectional transmission/reception of control messages, as well as higher link stability, at lower frequencies.

*Deployment heterogeneity:* There will be macrocells, microcells, femtocells, and even picocells, all working together in 5G. This heterogeneity introduces two deployment scenarios for mmWave cellular networks: stand-alone and integrated networks [81]. In the stand-alone scenario, a complete mmWave network (from macro to pico levels) will be deployed in the mmWave band, whereas the integrated solution is an amendment to existing microwave networks for performance enhancement, and may be considered as an intermediate step in the migration from existing microwave networks to future mmWave networks. The integrated network includes mmWave small cells and/or mmWave hotspots [18].

Spectrum and deployment heterogeneity affect the options for realizing physical control channels, see Section A.3.

### A.2.3 Beamforming

Beamforming is the key technique to compensate the severe channel attenuation and to reduce interference in mmWave networks. Figure A.1(a) shows a typical cellular network where each entity may support multi-beam directional operation. This allows BSs to benefit from multiplexing to increase data rate or use spatial diversity to achieve robustness to blockage. Generally, a wireless link can be established in omnidirectional (both BS and UE are omnidirectional), semi-directional (either BS or UE is omnidirectional, the other directional), or fully-directional (both BS and UE are directional) communication modes. Figure A.1(a) shows that inter-cell

<sup>1</sup>Rigorously speaking, having negligible multiuser interference does not necessarily imply that the performance of the network is limited by noise; rather, it can be limited by the channel establishment and maintenance overhead [83]. However, the negligible (or, more generally, significantly reduced) multiuser interference is enough to establish our results especially in resource allocation and interference management in Section A.5.



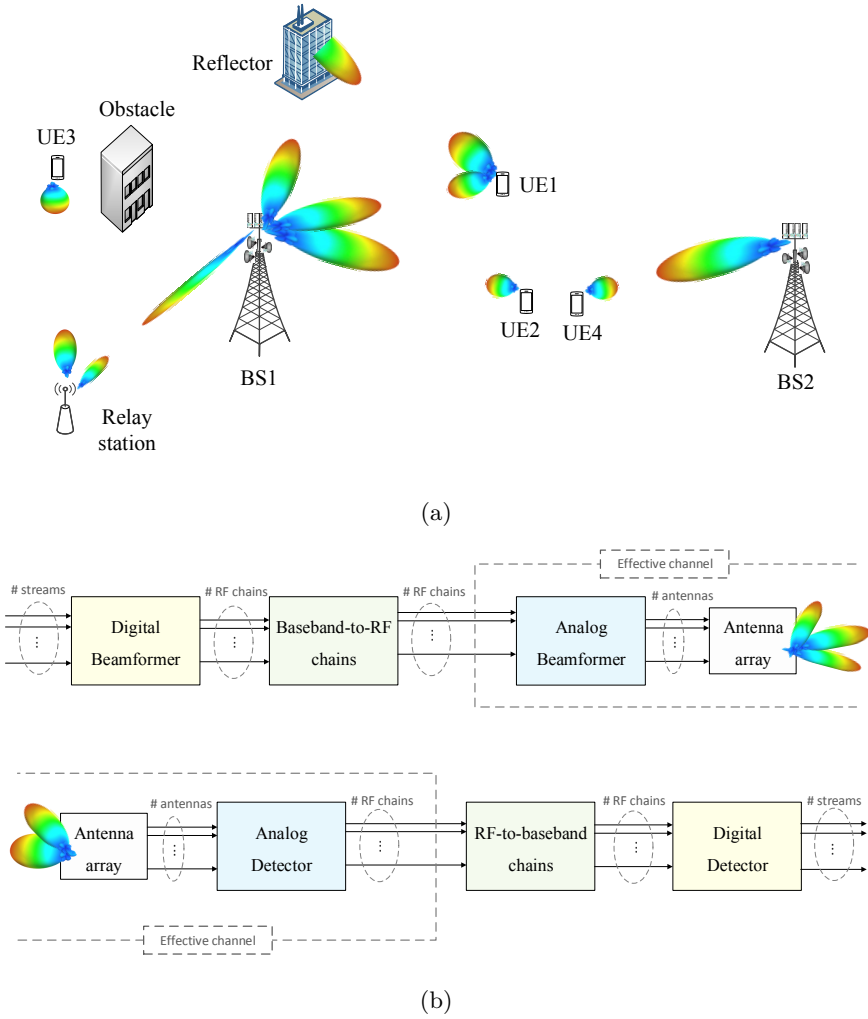


Figure A.1: Directional communications and beamforming: (a) a typical cellular network and (b) two-stage hybrid digital-analog beamforming architecture. Cell boundaries are intentionally omitted from (a) to indicate their loose meaning in mmWave cellular networks. The effective channel is illustrated in (b).

interference in both downlink and uplink is significantly reduced by fully directional pencil-beam communication, emphasizing the noise-limited trend of a mmWave cellular network. Generally speaking, there are three beamforming architectures, namely digital, analog, and hybrid.

### Digital beamforming

This architecture provides the highest flexibility in shaping the transmitted beam(s), however it requires one baseband-to-RF chain (in short RF chain) per antenna element. This increases the cost and complexity due to the large number of antenna elements operating in very wide bandwidth. Considering one high resolution analog-digital converter (ADC) per RF chain, digital beamforming also leads to high power consumption both at the BS and at the UEs, which is at odds with the design goals of 5G [5, 6, 23, 24]. Moreover, digital beamforming requires estimation of the channel between every pair of antenna elements of the transmitter and the receiver. Apart from a more complicated precoding, the complexity of this estimation scales at least linearly with the number of transmitter antenna elements [84].<sup>2</sup> In time division duplexing (TDD) systems, channel state information (CSI) at the transmitter can be obtained using uplink sounding signals. The advantage is that the overhead will be scaled with the combined number of UEs' antennas that can be much less than the number of BS antennas. However, the limited UE power and the possible lack of beamforming gains for the uplink reference signals may limit the performance of the network. Also, CSI acquisition by uplink reference signals requires the principle of channel reciprocity that holds if the duplexing time is much shorter than the coherence time of the channel. The coherence time in mmWave bands is around an order of magnitude lower than that of microwave bands, as the Doppler shift scales linearly with frequency. Therefore, TDD at mmWave bands needs to be restricted to low-mobility scenarios. In frequency division duplexing (FDD) systems, CSI estimation should be done in both uplink and downlink directions due to the lack of reciprocity. While CSI estimation overhead in the uplink is similar to the TDD case, the overhead in the downlink channel scales with the number of BS antennas, which becomes infeasible as the number of BS antennas grows large [25, 27, 84]. Altogether, for systems operating in very wide spectrum ranges, such as several hundreds of MHz, and employing a large number of antennas, a complete digital beamforming solution using the current requirements (one high resolution ADC per RF chain and channel estimation per antenna element), is hardly feasible and economical [25, 30]. Low-resolution ADCs (ideally with only one bit) and sparse channel estimation are promising solutions for enabling digital beamforming in mmWave systems (see [26, 27] and references therein).

### Analog beamforming

This technique shapes the output beam with only one RF chain using phase shifters [25, 28]. On the positive side, a simple beam-searching procedure can be used here to efficiently find the optimal beams at the transmitter and the receiver, as already established in existing mmWave WPAN and WLAN standards [13, 14]. With finite size codebooks each covering a certain direction, those standards recommend an exhaustive search over all possible combinations of the transmission and re-

---

<sup>2</sup>The complexity will be increased if the beamforming algorithm requires channel state information both at the transmitter and at the receiver [85, 86].

ception directions through a sequence of pilot transmissions. The combination of vectors that maximizes the signal-to-noise ratio is selected for the beamforming. This procedure alleviates the need for instantaneous CSI, at the expense of a new *alignment-throughput tradeoff* [57]. The tradeoff shows that excessively increasing the codebook size (or equivalently using extremely narrow beams) is not beneficial in general due to the increased alignment overhead, and there is an optimal codebook size (optimal beamwidth) at which the tradeoff is optimized. On the negative side, one RF chain can form only one beam at a time without being able to multiplex within the beam, implying that this architecture provides only directivity gain. For narrow beam operation, pure analog beamforming requires several RF chains to serve UEs that are separated geographically. This diminishes the advantages of this architecture such as low complexity and low power consumption.

### Hybrid beamforming

A promising architecture for mmWave cellular networks is a two-stage hybrid digital-analog beamforming procedure, allowing the use of a very large number of antennas with a limited number of RF chains [29–31]. With the hybrid solution, digital precoding is applied for the effective channel consisting of the analog beamforming weights and the actual channel matrix, see Figure A.1(b). Analog beamforming provides spatial division and directivity gains, which can be used to compensate the severe channel attenuation, by directing the transmitted signal toward different sectors. Furthermore, digital beamforming may be used to reduce intra-sector interference and provide multiplexing gain using CSI of an effective channel with much smaller dimension. Exploiting the sparse-scattering nature of mmWave channels, the complexity of hybrid beamforming design can be further reduced [27, 32, 78]. The analysis of [32] shows that, in a single user MIMO system, hybrid beamforming can almost achieve the throughput performance of a fully digital beamforming with 8 to 16 times fewer RF chains, leading to greatly reduced energy consumption and processing overhead with a negligible performance drop. However, analysis and optimization of the tradeoff between the number of employed RF chains and the achievable network throughput in multiuser MIMO system and in the presence of CSI errors in wideband mmWave systems requires further research, see [33, 87] and the references therein. In Sections A.4 and A.5, we will discuss this tradeoff and show how the hybrid beamforming architecture interplays with handover and scheduling decisions.

## A.3 Realization of Physical Control Channels

### A.3.1 Essential Tradeoffs

Reliable control channels are essential for synchronization, cell search, user association, channel estimation, coherent demodulation, beamforming procedures, and scheduling grant notifications, as well as multi-antenna transmission and reception configuration. While control channels are defined as logical channels, they have

to be mapped to some physical channels to be transmitted over the radio interface, thus the special characteristics of mmWave bands affect the control channel performance from several aspects. In particular, two types of tradeoffs arise when realizing a physical control channel (PHY-CC), namely fall-back and directionality tradeoffs, which do not exist in traditional cellular networks on microwave bands, see Figure A.2.

The *fall-back* tradeoff is the tradeoff between sending control messages over microwave or mmWave frequencies. While realizing a PHY-CC in mmWave bands enables the use of a single transceiver, the established channel is subject to high attenuation and blockage. On the other hand, a microwave PHY-CC facilitates broadcasting and network synchronization due to larger coverage and higher link stability compared to its mmWave counterpart, as will be discussed in Section A.4.1, at the expense of higher hardware complexity and energy consumption, since a dedicated transceiver should be tuned on the microwave PHY-CC.

The *directionality* tradeoff, from another perspective, refers to the option of establishing a PHY-CC in omnidirectional, semi-directional, or fully-directional communication modes. Although an omnidirectional PHY-CC has a shorter communication range, all devices within that range can receive the control messages without any deafness problem. The semi-directional option increases the transmission range, while introducing less interference to the network. However, mitigating the deafness problem in this case may require a spatial search that introduces extra delay. Finally, the fully-directional communication mode further increases coverage and decreases the interference caused to the network at the expense of even higher spatial search overhead.<sup>3</sup>

To have a better sense of the interplay between directionality and transmission range, we consider the simple distance-dependent path-loss model of [19, Equation (1)]. Fixing transmission power and required SNR at the UE, we depict in Figure A.3 the coverage enhancement factor in the downlink as a function of the combined directivity gains of the transmitter and receiver for three attenuation scenarios (good, fair, and severe attenuation). From Figure A.3, with a path-loss exponent of 3, a semi-directional communication with 16 dBi directivity gain increases the communication range roughly by a factor of 3.5 compared to omnidirectional communication. More interestingly, fully-directional communication further enhances the coverage gain to a factor of 10 with only 30 dBi transmitter and receiver combined gains, which can be readily achieved in practice.<sup>4</sup> This means that we need to have up to 100 BSs with omnidirectional communications to cover an area that one BS with fully-directional communication can cover by itself. The

<sup>3</sup>Alternatively, we can increase the transmission range of omnidirectional communication in the mmWave bands by using lower-rate or more efficient coding techniques [53].

<sup>4</sup>Note that a 16 dBi gain at the transmitter and a 14 dBi gain at the receiver, which yield a 30 dBi combined gain, can be achieved by adopting 3D beams with 32° horizontal and vertical half power beamwidths at the transmitter and 40° at the receiver, respectively, see [88, p. 1402]. Reducing half power beamwidths to 10°, the directivity gain increases to 25 dBi, providing 50 dBi combined gains, which is already being used for mmWave channel measurements in New York City [19].

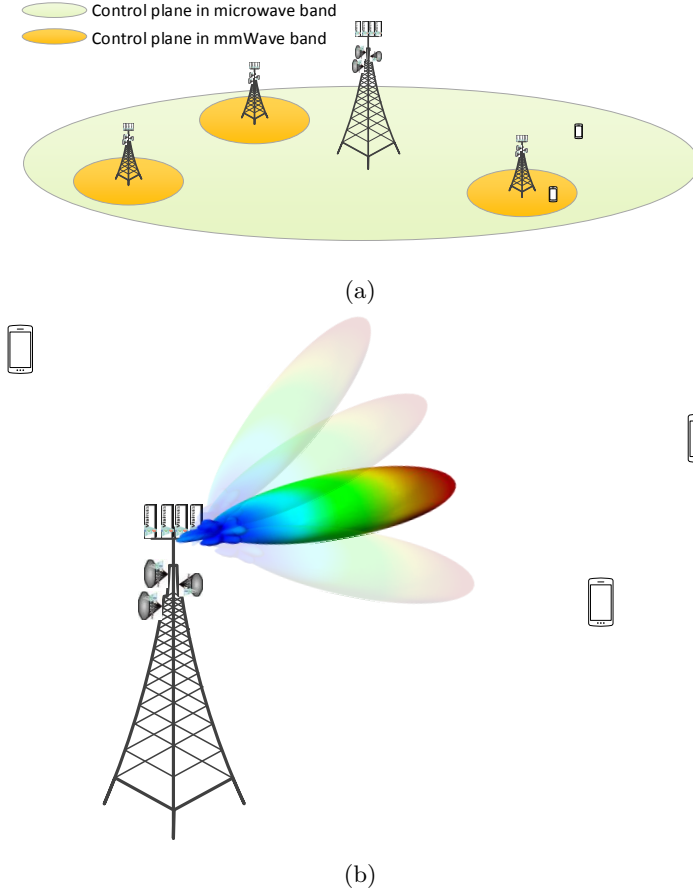


Figure A.2: Fall-back and directionality tradeoffs in realizing a PHY-CC. Microwave bands provide a reliable channel with much larger coverage compared to mmWave channels (a). Directional control channel increases coverage and may provide more efficient PHY-CC (in terms of energy and spectral efficiency) at the expense of extra spatial search (b). Different options of realizing a PHY-CC are various combinations of these tradeoffs.

coverage gain will be reduced as the attenuation factor increases, however even in a severely attenuated outdoor propagation environment (path-loss exponent 5), the coverage gain is still quite significant (2 and 4 with semi- and fully-directional communications, respectively). This significant gain comes at the expense of the alignment overhead [57], characterized in detail in Appendix A.

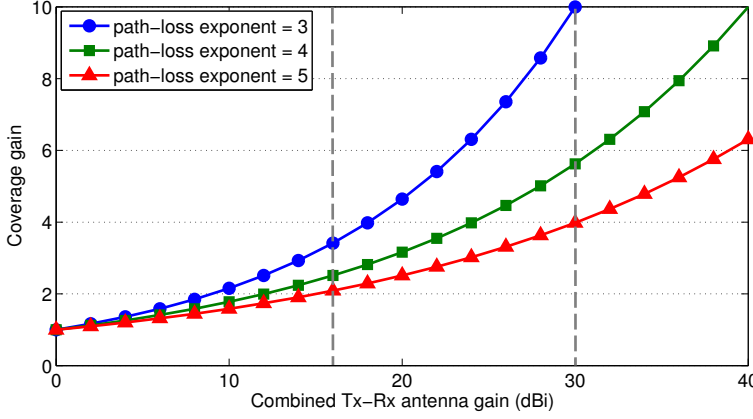


Figure A.3: Coverage gain against directivity gain for target SNR of 10 dB at the receiver and 15 dBm transmission power. The left vertical dashed line corresponds to a semi-directional communication with 16 dBi directivity gain at the BS. The right vertical dashed line corresponds to a fully-directional communication with 16 dBi and 14 dBi directivity gains at the BS and UE, respectively. Directional communications substantially increase transmission range, as expected.

### A.3.2 Available Options and Design Aspects

The identified tradeoffs lead to multiple options for realizing PHY-CC, which are analyzed in the sequel.

- (*Option 1*) *Omnidirectional-mmWave*: This option can provide a ubiquitous control plane but only in short range, which may be useful for broadcasting/multicasting inside small cells. However, this channel is subject to mmWave link instability, demanding the use of very robust coding and modulation schemes. More importantly, this option entails a mismatch between the transmission ranges of control and data channels due to the much higher directivity gains of the latter. This limits the applicability of omnidirectional mmWave PHY-CC, as will be discussed further in Section A.4.1.
- (*Option 2*) *Semi-directional-mmWave*: This option realizes a more selective PHY-CC in the spatial domain, increasing spectral and energy efficiency in the control plane. It is useful for multicasting inside small cells. The semi-directional-mmWave PHY-CC increases the protocol complexity for solving blockage and deafness problems. It can also be used for a feedback channel such as in hybrid automatic repeat request (HARQ), where the alignment phase has been conducted during the data channel establishment. Similarly, it is advantageous for realizing uplink/downlink shared (with data) and dedicated PHY-CCs, wherein user specific reference signals are transmitted for channel estimation and coherent demodulation.

- (*Option 3*) *Fully-directional-mmWave*: This option demands a good alignment between the BS and UE, with a minimal use of the spatial resources. Therefore, this option may be the best choice for HARQ feedback channel and uplink/downlink shared and dedicated PHY-CCs. It reduces the need for alignment overhead from two (one for control channel and one for data channel) to one (for both control and data channels), further improving spectral and energy efficiencies.
- (*Option 4*) *Omnidirectional-microwave*: This option offers statistically larger range that is more stable in time than its mmWave counterparts. This option was first introduced in the soft cell [80] and phantom cell [82] concepts, where the control plane is provided by a macrocell BS, whereas microcell BSs are responsible for providing only the data plane. Apart from being suboptimal in terms of energy efficiency, it is also not necessarily the best option for all types of PHY-CC such as HARQ feedback channel. Furthermore, transmissions in a microwave band cannot provide accurate information for estimating the DoA in the mmWave band due to different propagation characteristics. This hinders the applicability of this option for spatial synchronization and cell search procedures of mmWave cellular networks, as will be discussed in Section A.4.1.

In addition to these four options, a control channel can be established with the hierarchical use of several options, which is illustrated through the design of a novel two-step synchronization procedure in Section A.4.2.

In order to quantitatively compare the different PHY-CC options, we simulate a network with a random number of BSs. We consider a typical UE at the origin and evaluate the performance metric from its perspective, thanks to Slivnyak's Theorem [89, Theorem 8.1] applied to Poisson point processes. We assume that the typical UE can receive strong signals only from BSs with LoS conditions (in short LoS BSs). Further, we assume that the number of LoS BSs is a Poisson random variable with a density that depends on the transmission power of the BSs, the minimum required SNR at the UE side, the operating beamwidth  $\theta$ , and the blockage model, see Appendix A. The LoS BSs are uniformly distributed in a 2D plane. In the semi-directional option, only the BSs operate in the directional mode with beamwidth  $\theta$ , whereas the typical UE operates with beamwidth  $\theta$  only in the fully-directional mode (option 3). The bandwidth of the control channel is 50 KHz, so the noise power is  $-127$  dBm, the SNR threshold of the typical UE is 0 dB, and all BSs adopt a transmission power of 30 dBm, which can be employed even by low power BSs using power boosting to ensure appropriate control plane coverage [90]. At the MAC layer, the beamforming is represented by using an ideal sector antenna pattern [48, 91, 92], where the directivity gain is a constant for all angles in the main lobe and equal to a smaller constant in the side lobe. These constant values depend on the operating beamwidth, see Equation (A.6) in Appendix A. We use this model in Appendix A to characterize the spatial search overhead and delay in receiving control signals, imposed by options 2 and 3.

Figure A.4(a) shows the percentage of the areas that cannot be covered by the BSs (with SNR threshold 0 dB) for different PHY-CC options versus the density

of LoS BSs. Not surprisingly, for a given density of BSs, the coverage of option 1 is substantially lower than that of other options, due to the lack of directivity gain. In particular, for 1 LoS BS in a  $250 \times 250 \text{ m}^2$  area with path-loss exponent  $\alpha = 3$ , options 1, 2, and 3 cover 63.6%, 99.9%, and 100% of the area, respectively. A more sparse BS deployment highlights the benefit of having directivity gain both at the BS and at the UE. For instance, with LoS BS density of  $2 \times 10^{-6}$  (1 BS in a  $700 \times 700 \text{ m}^2$  area), option 3 can cover 99.8% of the area, whereas option 2 can only support 60% of the area when  $\alpha = 3$ . The extra coverage appears at the expense of more complicated alignment between the BS and the UE, as discussed in the next section. A higher attenuation  $\alpha = 3.5$  demands a denser BS deployment for the same coverage probability. Moreover, we can see that the coverage probability is an exponential function of the BS density, as also observed in [93] [94] for wireless sensor networks.

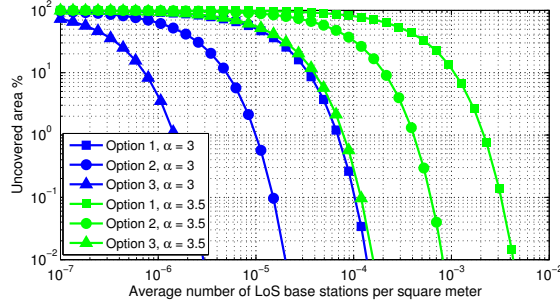
Figure A.4(b) demonstrates the impact of the operating beamwidth, and consequently the directivity gain, on the coverage probability with  $\alpha = 3$  and BS density  $10^{-5}$ . Increasing  $\theta$  reduces the coverage monotonically due to the reduced directivity gain. This reduction is more severe at 72 GHz, implying that a higher directionality level is required at 72 GHz to compensate for the higher channel attenuation and provide the same coverage as at 28 GHz. Recall that we depict coverage of the PHY-CC with an SNR threshold of 0 dB. Increasing the SNR threshold leads to a corresponding coverage reduction. With SNR threshold 10 dB, for instance, the coverage for the three options at 28 GHz would be close to the curves for 72 GHz with SNR threshold 0 dB in Figure A.4(b), so we omit the former for the sake of clarity in the figure.

Figure A.4(c) shows the minimum BS density per square meter required to ensure 97% coverage of the control channel as a function of the operating beamwidth. To support 97% coverage level, Option 1 requires ultra dense LoS BS density of  $5 \times 10^{-3}$  (1 LoS BS in a  $14 \times 14 \text{ m}^2$  area), while Options 2 and 3 may require substantially fewer BSs. For instance, with  $\theta = 30^\circ$ , Options 2 and 3 require 1 LoS BS in a  $31 \times 31 \text{ m}^2$  area and 1 LoS BS in a  $75 \times 75 \text{ m}^2$  area, respectively.

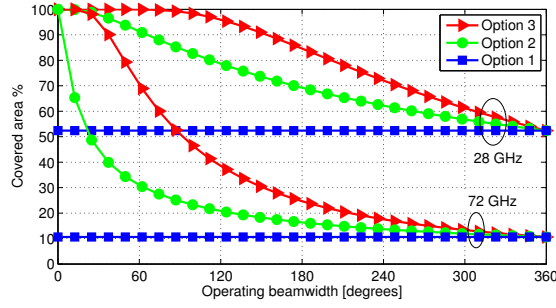
## A.4 Initial Access and Mobility Management

Initial access and mobility management are fundamental MAC layer functions that specify how a UE should connect to the network and preserve its connectivity. In this section, we identify the main differences and highlight important design aspects of initial access that should be considered in mmWave cellular networks using an illustrative example, depicted in Figure A.5. In the example, we have a macrocell with three microcells, two UEs, and one obstacle. UE1 aims at running an initial access procedure, whereas UE2 requires multiple handovers. Note that coverage boundaries and possible serving regions of the BSs, shown by dashed lines, do not necessarily follow regular shapes due to randomly located obstacles and reflectors. However, for the sake of simplicity, we neglect this aspect in the figure.

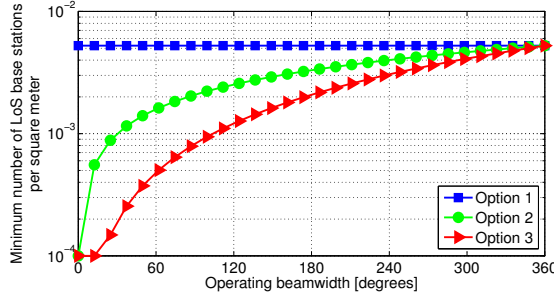




(a)



(b)



(c)

Figure A.4: Coverage probability for different options of realizing a PHY-CC.  $\alpha$  is the path-loss exponent. Operating beamwidth in (a) is  $20^\circ$ . BS density in (b) is  $10^{-5}$  per square meter. Coverage level in (c) is 97%.

#### A.4.1 Fundamentals of Initial Access

Once a new UE appears for the very first time, it will start the initial synchronization process, followed by extraction of system information. Then, it executes a random access procedure by which the network registers the UE as active. After these initial access procedures, the UE is connected to the data plane, and is able

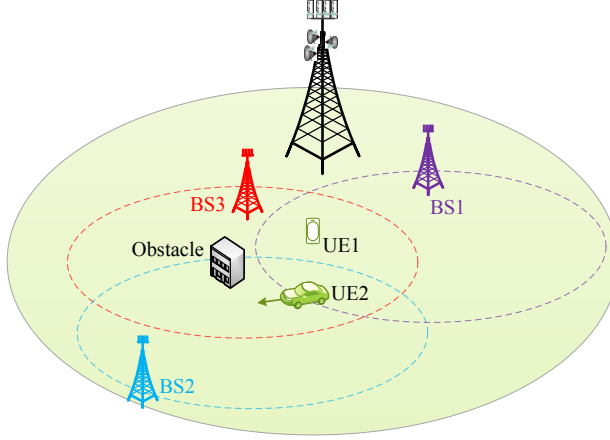


Figure A.5: Initial access and mobility management in mmWave cellular networks. UE1 starts the initial access procedure, and UE2 requires handover. Dashed lines show coverage boundaries (idealized to ease the discussion).

to transmit and receive actual data.

### Synchronization and Cell Search

In LTE systems, acquiring time-frequency domain synchronization during cell search is facilitated by the so-called primary and secondary synchronization signals, transmitted omnidirectionally in the downlink [95]. Each UE in the cell is aware a priori of when and where the synchronization control channel is, and thereby can extract synchronization signals along with cell identity. Hence, current cellular networks use beamforming only *after* omnidirectional synchronization and cell search procedure. However, as pointed out in [96], performing cell search on an omnidirectional PHY-CC (option 1) while having directivity gain in data transmission causes a mismatch between the ranges at which a link with reasonable data rate can be established and the range at which a broadcast synchronization signal along with cell identity can be detected, known as the problem of asymmetry in gain in ad hoc networks [53, 97]. For the example considered in Figure A.3, the data range can be at least 4 times larger than the synchronization range with only 30 dBi combined directivity gains even in a severely attenuated propagation environment. Therefore, option 1 does not seem a proper candidate for initial cell search procedure. Moreover, the synchronization signals over a microwave band (option 4) cannot provide sufficient information to extract spatial synchronization in the mmWave band due to different propagation characteristics. Thus, a fully-directional data plane demands a directional synchronization and cell search procedure in the mmWave band using options 2 or 3. These options, however, are subject to the directionality tradeoff, mentioned in Section A.3.1. They require spatial search that may cause

extra delay in obtaining system information at initial cell search. We evaluate the delay characteristics of options 2 and 3 in Section A.4.2, after proposing a two-step synchronization procedure, and in Appendix A.

### Extraction of System Information

System information includes cell configurations such as downlink and uplink bandwidth, frequency band, number of transmit antennas, cell identity, and random access procedure. LTE embeds system information in the so-called master and system information blocks that are transmitted in the physical broadcast channel, dedicated to control signaling, and physical downlink shared channel, respectively. While dedicated control channels can be established with omnidirectional communications, a UE still needs to decode a directional shared channel to extract system information in a mmWave cellular network. This is a fundamental MAC layer issue, which is not a problem in microwave cellular networks, as all the rendezvous signaling is done over omnidirectional control channels (option 4). Determining the exact information that should be transmitted over an omnidirectional control channel at microwave frequencies and a directional control channel at mmWave frequencies depends heavily on the initial access procedure. In Section A.4.2, we provide preliminary suggestions for an initial access procedure for mmWave cellular networks.

### Random Access

At the very beginning, a UE has no reserved channel to communicate with the BS(s), and can send a channel reservation request using contention-based or contention-free channel access. The contention-based requests, however, may collide due to simultaneous transmissions in the same cell, or not be received due to deafness. The comprehensive analysis of [69] shows that small to modest size mmWave networks operating with the slotted ALOHA protocol (a simple contention-based strategy) have a very small collision probability. In the contention-free scheme, the network defines and broadcasts multiple access signals that uniquely poll the individual UEs to avoid collisions. These signals should have spatial scheduling information to avoid deafness. Upon decoding a signal, each UE knows its uplink parameters: analog beam, random access preamble, and allocated resource for transmission of the preamble. Embedding all this information a priori is a challenging task especially due to the lack of spatial synchronization at the very beginning. As transmission and reception beamwidths become narrower, a reduced contention level makes contention-based procedures more justifiable than complex and wasteful contention-free ones [98].

In the contention-based random access procedure of LTE, a UE triggers a timer after sending a preamble, and if no response is received from the BS, it retransmits the preamble with an increased transmission power and/or after a random waiting (backoff) time. In a mmWave cellular network, the deafness problem cannot be solved by increasing the transmission power or waiting for a random backoff time. A UE may unnecessarily undergo multiple subsequent backoff executions in the deafness condition, resulting in a prolonged backoff time [83]. To solve this issue,

[83] introduces a novel MAC level collision-notification (CN) signal to distinguish collisions from deafness and blockage. During the spatial search, if a BS receives energy from a direction that is not decodable due to collisions, it sends back a CN message in that direction.<sup>5</sup> After transmitting a preamble, a UE will adopt one of the following three actions depending on the received control signal: (1) if a reservation grant is received before timeout, it starts transmission; (2) if a CN message is received before timeout, this is an indicator for contention in that spatial direction, hence retransmission after backoff is used; (3) if no signal is received before timeout, the UE knows that there is either deafness or blockage in this directed spatial channel, so it tries to investigate another direction or adjust the transmission beamwidth instead of executing an unnecessary backoff.

#### A.4.2 Two-step Synchronization and Initial Access

In this section, we utilize directional cell search and suggest a two-step synchronization procedure, followed by extraction of system information and random access procedures. In the *first step*, the macrocell BS broadcasts periodic time-frequency synchronization signals over an omnidirectional microwave control channel (option 4). When a new entity (either a UE or a microcell BS) turns on its radios, it first looks at the omnidirectional synchronization control channel, trying to detect the time-frequency synchronization signals. Here, the existing synchronization signals and procedure of LTE may be reused. After the first step, all entities in the macrocell, including microcell BSs and UEs, will be synchronized in time and frequency.<sup>6</sup> Moreover, the macrocell BS embeds some information about the cell in these time-frequency synchronization signals, for instance, its ID. In the *second step*, the microcell BSs perform a periodic spatial search using a sequence of pilot transmissions at mmWave frequencies. Upon receiving a pilot, the UE finds the remaining system information along with a coarse estimation of DoA, thanks to its multiple antennas. In this direction, the UE feeds back a preamble in a predetermined part of the time-frequency domain for which the corresponding microcell BS is receiving preambles. Note that the second phase can be initiated in semi- or fully-directional mode, leading to smaller collision probability compared to the omnidirectional case. The proposed two-step procedure enables us to support both cell-centric and UE-centric designs. In the former, the BSs periodically initiate both steps of the procedure, similar to existing cellular networks. In the latter, the second step (spatial synchronization) is triggered by the UE (on-demand), instead of the network.

In Appendix A, we have characterized the delay performance of spatial synchronization for options 2 and 3. We consider the same model for LoS BSs, whose

<sup>5</sup>Note that the energy that a BS will receive in a collision state with multiple received signals is substantially different from that in the deafness state with no received signal. Therefore, a simple hard decision based on the received energy (energy detector) would be enough to distinguish collisions from deafness.

<sup>6</sup>Some mapping, which may be as simple as some scalars, is necessary to map time-frequency synchronization in microwave band into mmWave band.

synchronization pilots can be received by a typical UE, with the same initial parameters as in Section A.3.2. Individually, every microcell BS divides a 2D space into  $N_s = \lceil 2\pi/\theta \rceil$  sectors, sorts them in a random order, and sends synchronization pilots toward sectors sequentially, that is, one sector per epoch. Upon receiving a pilot with high enough SNR, the UE extracts DoA along with other system information. Figure A.6(a) shows the average number of epochs required for discovering the UE for semi- and fully-directional options as a function of LoS BS density per square meter. The spatial search overhead for the semi-directional option is always less than that for the fully-directional one, as predicted by Remark A.6.5 in Appendix A. For a very sparse deployment of the BSs, for instance, one every 9 square kilometers, the delay performance of both options converges to  $(\lceil 2\pi/\theta \rceil + 1)/2$ , as predicted by Remark A.6.6. Moreover, increasing the beamwidth reduces the spatial search overhead in both options, at the expense of a smaller coverage and lower number of discovered UEs, see Figure A.4. Note that we have assumed a delay constraint for the synchronization procedure, thus some UEs may not have enough time to accumulate enough energy to detect the synchronization signal, and will therefore be in outage. Among those that can be discovered, however, the semi-directional option (or in general higher  $\theta$ ) offers less spatial search complexity than the fully-directional option, as verified by Figure A.6(a). It is important to see whether the performance enhancement in spatial search is significant when we consider the substantial coverage reduction of the semi-directional option. With a LoS BS density of  $10^{-5}$  (dense BS deployment), the enhancement of spatial search overhead due to the semi-directional option is less than 1 epoch on average, whereas it provides 10% less coverage compared to a fully-directional option with  $\theta = 60^\circ$ , see Figure A.4(b). Altogether, we can conclude that option 3 may provide a better solution when we consider both coverage and spatial search overhead. Another point from the figure is that increasing the path-loss exponent, with a fixed density of LoS BSs per square meter, implies that fewer BSs can participate in discovering the typical UE, as the pilots of the others cannot meet the SNR threshold of the UE. Therefore, discovering the UE requires more effort (epochs), as a compensation for fewer LoS BSs.

Figure A.6(b) shows the minimum number of epochs required to guarantee discovery of a typical UE with probability  $\mu$  with LoS BS density of 1 BS in a  $100 \times 100 \text{ m}^2$  area, see Remark A.6.4 in Appendix A. Full directionality (option 3) requires more epochs than semi-directionality (option 2) to guarantee a minimum discovery probability, as it has smaller search space per epoch. Increasing the search space per epoch of the fully-directional option reduces the performance difference with the semi-directional option, as can be verified by comparing the  $\theta = 20^\circ$  and  $\theta = 60^\circ$  curves. On the other hand, the difference increases as the number of LoS BSs used to discover a UE increases, e.g., due to favorable propagation ( $\alpha = 3$ ). Note that all curves refer to a dense deployment with 1 LoS BS in a  $100 \times 100 \text{ m}^2$  area. For the case of 1 LoS BS in a  $200 \times 200 \text{ m}^2$  area, which is omitted for the sake of clarity, the curves for  $\alpha = 3, \theta = 60^\circ$  will be very close to  $\alpha = 3.5, \theta = 60^\circ$  in Figure A.6(b), making the enhancement of semi-directionality negligible. The figure also shows that both options need more epochs to discover the typical UE as

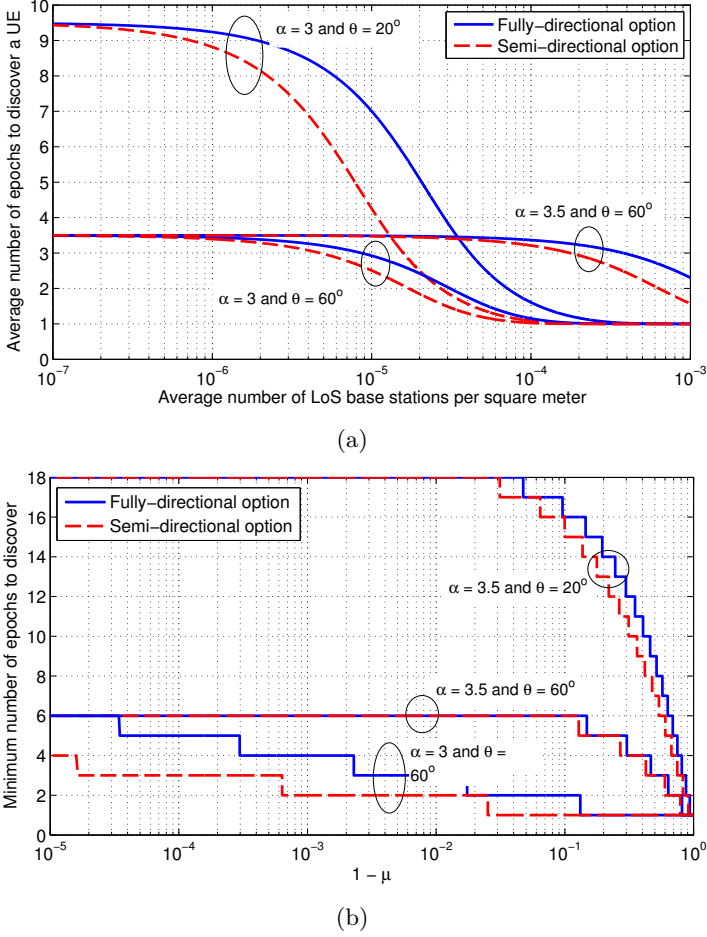


Figure A.6: Upper bound on the complexity of spatial synchronization given that a UE can receive synchronization pilots with high enough SNR: (a) Average number of epochs for discovering a UE, and (b) minimum number of epochs to guarantee discovering a UE with probability  $\mu$ . Semi-directional marginally outperforms the fully-directional option in both metrics.

$\mu$  increases, however the rate of such increment is not linear. That is, both options require searching over all  $N_s = 18$  sectors for  $\alpha = 3.5, \theta = 20^\circ$ , and all  $N_s = 6$  sectors for  $\alpha = 3.5, \theta = 60^\circ$ , to guarantee a minimum discovering probability of 0.99. From this perspective, option 2 has no advantage over option 3, emphasizing the previous conclusion. Instead of using option 2, we may optimize the operation of option 3 by selecting a proper  $\theta$  that reduces the spatial search overhead (in terms of both performance metrics depicted in Figure A.6) whilst providing a minimum

level of coverage.

### A.4.3 Mobility Management and Handover

The suppression of interference in mmWave systems with pencil-beam operation comes at the expense of more complicated mobility management and handover strategies. Frequent handover, even for fixed UEs, is a potential drawback of mmWave systems due to their vulnerability to random obstacles, which is not the case in LTE. Dense deployments of short range BSs, as foreseen in mmWave cellular networks, may exacerbate frequent handovers between adjacent BSs [99], if only the received signal strength indicator (RSSI) is used as a reassociation metric. Loss of precise beamforming information due to channel change is another criterion for handover and reassociation, since the acquisition of that information is almost equivalent to making a handover. For the example of Figure A.5, UE2 requires two subsequent handovers; one due to a temporary obstacle and the other due to the increased distance from BS2. Every handover may entail a spatial synchronization overhead, characterized in Figure A.6 and in Appendix A.

To avoid frequent handovers and reduce the overhead/delay of reassociation, the network should find several BSs for every UE. The cooperation among a UE, the associated BSs, and the macrocell BS can provide smooth seamless handover through efficient beam-tracking [100] and finding alternative directed spatial channels in case of blockage. Here, two scenarios are foreseeable. A UE may adopt multi-beam transmissions toward several base (relay) stations, so it will receive data from several directions at the same time, but with a corresponding SNR loss for each beam, if we consider a fixed total power budget. For the example considered in Figure A.5, smooth handover, robustness to blockage, and continuous connectivity is available if UE2 is served by both BS2 and BS3. The price, however, is a 3 dB SNR loss for each beam, on average, as well as the need for cooperation and joint scheduling between BS2 and BS3 for serving UE2. Alternatively, a UE may be associated to several base (relay) stations, but only one of them is the serving BS whereas the others are used as backup. This scenario mitigates joint scheduling requirements. Besides, backup connections enable switching without extra delay if the alignment and association to backup BSs are done periodically. In light of a user-centric design, the macrocell BS can record all connections of UE2, predict its mobility, give neighboring BSs some side information indicating when UE2 is about to make a handover, so they can better calibrate the directed channel and be *ready* for handover. Altogether, UE2 is served by either BS2 or BS3, however it is connected to both BSs for fast switch operation.

To facilitate handover negotiations, a reliable PHY-CC in the microwave band (option 4) seems an appropriate choice. Periodic connection checks between UEs and associated BSs can be done using more efficient PHY-CCs such as option 3. Table A.3 summarizes the pros and cons of different realizations of the control channel with possible application areas.

Table A.3: Comparison of different realizations of PHY-CC.

Control Channel	Advantages	Disadvantages	Possible PHY-CCs
Omnidirectional in mmWave band	(1) No need for spatial search (2) No deafness problem	(1) Very short coverage (2) Subject to mmWave link instability	(1) Broadcast channel inside small cells (2) Multicast channel inside small cells (3) Random access channel
Semi-directional in mmWave band	(1) Longer coverage (2) Energy-efficient transmission (3) Efficient use of spatial resources	(1) Extra complexity due to spatial search (2) Protocol complexity due to deafness and blockage (3) Subject to mmWave link instability	(1) Multicast channel inside small cells (2) Synchronization channel inside small cells (3) HARQ feedback channel (4) Uplink/downlink shared channel (5) Uplink/downlink dedicated channel (6) Random access channel
Fully-directional in mmWave band	Similar to option 2	Similar to option 2	(1) Synchronization channel inside small cells (2) HARQ feedback channel (3) Uplink/downlink shared channel
Omnidirectional in microwave band	(1) Macro-level coverage (2) No need for spatial search (3) No deafness problem (4) Link stability	(1) Hardware complexity due to the need for two radios (2) Inefficient use of spatial resources (3) Introduction of inter- and intra-cell interference in control plane	(1) Macro-level control plane (2) Macro-level synchronization channel (3) Macro-level Broadcast channel (4) Macro-level Multicast channel (5) Macro-level random access channel



## A.5 Resource Allocation and Interference Management

In order to leverage the special propagation characteristics and hardware requirements of mmWave systems, we suggest to migrate from the current interference-limited to a noise-limited architecture, from the current static to a dynamic cell definition, and from the current cell-centric to a user-centric design, all made possible under a proper software defined wireless network.

### A.5.1 Channelization

A key decision in MAC layer design is how to divide the physical resources in smaller units, called resource blocks. Although LTE defines a resource block as a portion of the time-frequency domain, directional transmission in mmWave cellular networks motivates to supplement the definition of resource block with a spatial dimension, leading to a block in the time-frequency-*space* domain. Proper utilization of such a resource block with a digital beamforming procedure requires precise CSI, imposing a large complexity during the pilot transmission phase, as stated in Section A.2.3. Instead, a hybrid beamforming technique provides a promising low overhead solution. Defining a group as a set of UEs that are non-distinguishable in the transmitted beam, the BS groups UEs together with one analog beamformer, as shown in Figure A.7(b), and serves every group with one analog beamforming vector [101]. Clearly, a macro BS can also group micro BSs and serve them together using a mmWave wireless backhaul link (in-band backhauling [102]). In fact, the analog beamformer partially realizes the spatial part of the new three dimensional resource blocks. Digital beamforming provides further spatial gain by multiplexing within a group, which is affordable due to a substantial reduction in the dimension of the effective channel, that is, the channel from a digital beamformer perspective [101].

### A.5.2 Scheduling

The time-frequency-space resources with narrow-beam operation allow a large number of concurrent transmissions and thus a high *area spectral efficiency*, measured in bit/s/Hz/m<sup>2</sup>. In the following, we discuss scheduling based on the hybrid beamforming structure, and leave the full digital beamforming option for future studies. Depending on the directionality level, three scheduling scenarios are foreseeable, see Figure A.7. In order to have insights and an illustrative comparison among different scenarios, and with no loss in generality, we elaborate on an example with the following assumptions: (1) the BS has 60 resource blocks in a slot, (2) there is no multiplexing inside a beam, (3) there is no inter-cell interference, (4) all UEs receive the same number of resource blocks (max-min scheduling), and (5) the base and relay stations have 4 RF chains (analog beams) each.

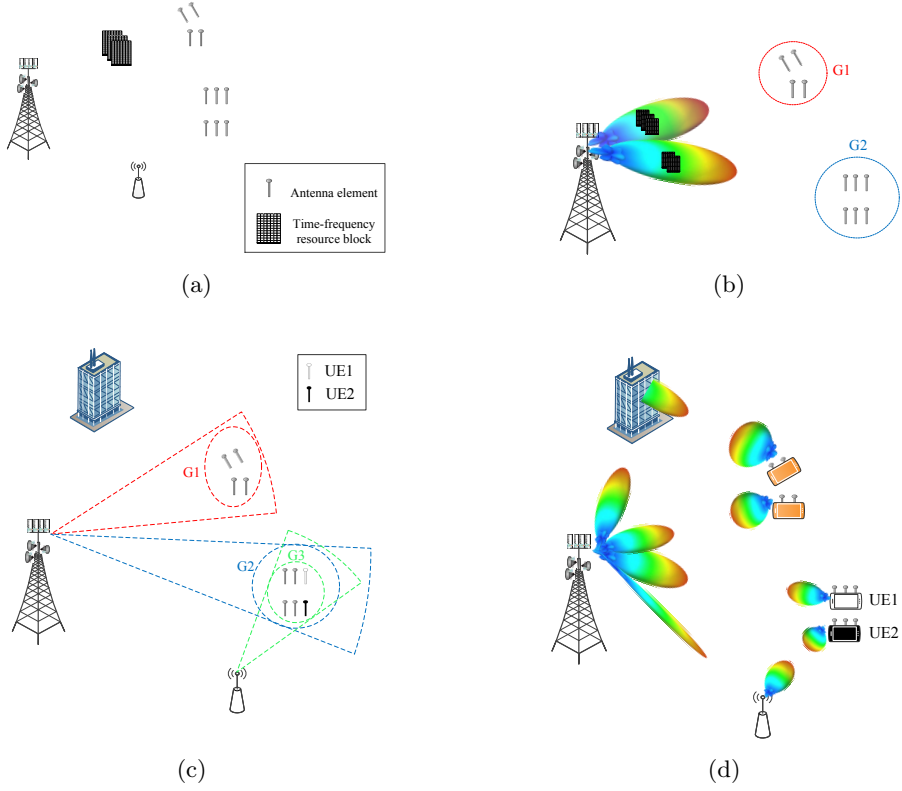


Figure A.7: Scheduling scenarios in mmWave cellular networks: (a) traditional time-frequency-dependent scheduling, (b) time-frequency-space-dependent scheduling using semi-directional communications, (c) time-frequency-space-dependent scheduling using semi-directional communications and relay stations, (d) time-frequency-space-dependent scheduling using fully-directional communications. The network throughput in scenarios (a) to (d) is 60, 120, 120, and 240 resource blocks, respectively.

### Omnidirectional communications

Traditionally, the scheduling procedure in cellular networks is designed based on the assumption of omnidirectional communication, which leads to an orthogonal use of time-frequency resource blocks through *time-frequency-dependent* scheduling inside a cell. The multiplexing gain, which depends on the channel rank, further increases the spectral efficiency, see Figure A.7(a). The elementary directional communication capabilities with a limited number of antennas, as in LTE, are not applicable to mmWave networks due to the large number of antennas both at the BS and at

the UEs. For the example considered, the BS (together with the relay station) can inject up to 60 resource blocks per slot in the cell, which is the maximum achievable network throughput. Considering 10 single antenna UEs in the cell, each UE can receive up to 6 resource blocks.

### Semi-directional communications

Considering a large number of antennas, with a limited number of RF chains, the BS can group UEs together based on the second order statistics of the channel and serve every group of UEs that have similar covariance matrix with one analog beamforming vector [101, 103]. To reuse time-frequency resource blocks for different groups, made by different analog beamformers, one needs a *time-frequency-space-dependent* scheduling. Hence, the design of analog beamformers is a fundamental MAC layer problem, since analog beamforming vectors are spatial resources that should be allocated to UEs together with time and frequency resources. However, we may have different time horizons over which spatial and time-frequency resources should be scheduled. Time-frequency scheduling should be recalculated after every channel coherence time and bandwidth, whereas spatial scheduling may be recalculated after a meaningful change in the covariance matrix of the channel, which is less frequent compared to the former. We use this property in the next subsections.

The new scheduling decisions may be complicated due to the complex interplay between different groups. A UE may belong to several groups in order to increase connection robustness to the blockages and provide smooth handover among groups, for instance, UE1 in Figure A.7(c) is in G2 and G3. In this case, time-frequency-dependent scheduling inside G2 depends on that of G3, as they have UE1 in common, demanding cooperation between the BS and the relay station in serving UE1. In other words, scheduling for G2 is correlated to that of G3. However, from a spectral efficiency perspective, decorrelating different groups increases the reuse factor footnote. The spatial reuse can be improved both in the sense that more BSs can be active simultaneously and in the sense that one BS can use more beams. The former is clear from Figure A.7(c). For the latter, replacing the relay station with a reflector, the BS serves G3 using a new beam, pointed toward the reflector. thereby enhancing spectral efficiency. This introduces a tradeoff between connection robustness and spectral efficiency, which is affected by the number of groups, i.e., the available degrees of freedom. Note that with single antenna UEs (semi-directional communication scenario), there is a one-to-one mapping between being spatially close to each other and belonging to the same group [101, 103, 104]. Therefore, the number of groups is dictated by two factors: (1) the number of RF chains and (2) the number of colocated UEs (UE clusters). While the former is a fundamental constraint, the latter can be relaxed if we incorporate fully-directional communications, since multiple antennas at the UEs enable control of the grouping from the UEs sides.

In the example, the BS can reuse all 60 resource blocks for G1 and G2. For the groupings depicted in Figs. A.7b and A.7c and without multiplexing gain inside groups, the network throughput is 120 resource blocks due to the spatial division

gain at the BS side, which is twice that with omnidirectional communications. Each single-antenna UE in G1 and G2 (G3) receives 15 and 10 resource blocks, respectively. Clearly, even though fairness is ensured per group, it has been violated at the macro level, due to the geographical (spatial) distribution of the UEs. Therefore, spatial grouping may violate fairness, even though it can potentially increase network throughput. The use of reflectors and relay stations is instrumental to form new groups and attain a good tradeoff among throughput enhancement, fair scheduling, and high connection robustness.

### Fully-directional communications

The existence of multiple antennas at the UEs promises spatial division gains at the UEs, which substantially increases the degrees of freedom compared to the semi-directional communication scenario where such a gain is available only at *one* entity of the network, the BS. The degrees of freedom can be further increased by envisioning multi-beam operation ability at the UEs [105].<sup>7</sup>

Managing the beamforming capabilities of the UEs, the BS can manipulate the effective channel that it will observe and make it a *proper channel* for scheduling purposes.<sup>8</sup> The notion of grouping needs an extension to include the impact of multiple antenna processing capabilities at the UEs. Colocated UEs do not necessarily belong to the same group, as they can match their beams to different beams offered by the BS (or different BSs) and be served in different groups by different analog beamformers. In Figure A.7(d), for instance, fully-directional communication makes G2 and G3 uncorrelated if UE1 points toward the BS and UE2 uses a beam toward the relay station, even though UE1 and UE2 are still colocated. This implies that all time-frequency resource blocks of G2 can be reused inside G3 without any joint scheduling. Moreover, UEs of G1 can be served separately due to spatial division gain at the UEs. With proper scheduling, the number of RF chains in the network infrastructure (base/relay stations) will be the only limiting factor, reflecting a tradeoff between hardware cost and achievable spectral efficiency. For dense BS deployment, capacity enhancement can be easily achieved by adding more RF chains, rather than more BSs. Hence, proper scheduling algorithms for mmWave cellular networks should be scalable with respect to the number of RF chains.

In the example, the BS can make four groups (three UEs and one relay station), and the relay station serves only UE2 (5 groups in total). The BS together with the relay station can reuse all 60 resource blocks for every multi-antenna UE. The network throughput is 240 resource blocks, twice that with semi-directional communications. This is due to spatial division gain at the multi-antenna UEs and no extra hardware complexity at the BS. Another important note is that the increased degrees of freedom in grouping have solved the above unfairness in the

<sup>7</sup>Multi-beam operation enables coherent combining of the strongest signals received from several distinct spatially-pointed beams at the UE. This coherent combination can give up to 24 dB link budget improvement at 28 GHz [105].

<sup>8</sup>The word “proper channel” is intentionally left fuzzy, since it depends on the ultimate goal of the beamforming at the BS, which may not be the same in all situations.

resource allocation, even though the UEs are still colocated. In Appendix B, we formulate an optimization problem for resource allocation in order to improve the throughput-fairness tradeoff with a minimum QoS level guarantees.

### A.5.3 Interference Management

In general, there are three types of interference that should be managed:

#### Intra-cell Interference

This is the interference among UEs within a cell. Using proper scheduling and beamforming design, the intra-cell interference can be mitigated. Pencil-beam operation substantially facilitates the intra-cell interference management strategy, due to spatial orthogonality of the directed channels of different UEs [69]. Intra-group interference, namely interference among UEs within a group, can be also mitigated using similar techniques.

#### Inter-cell Interference

The interference among different cells is called inter-cell interference. It is a challenge in traditional cellular networks, especially at the cell edges, where the reuse of the same resource block in adjacent cells causes strong interference. Inter-cell interference coordination, which is used in LTE, may not be necessary in mmWave cellular networks, since the scheduling based on time-frequency-space resource blocks along with fully-directional communication inherently significantly reduces the inter-cell interference, as illustrated in Figure A.1(a). In the case of rare interference, the UEs/BSs can initiate an *on-demand interference management* strategy [83]. Also, proper design of analog beamforming at the transmitter and the receiver can minimize inter-group interference.

#### Inter-layer Interference

It refers to interference among different layers, macro, micro, femto, and pico, which may be more severe compared to inter-cell interference among cells of the same layer due to directional communications.

It is worth mentioning that the role of interference is still prominent in omnidirectional control channels, which may need to be used for broadcasting, synchronization, and even channel estimation. This demands careful design of the pilots and control messages that aim at transmitting in omnidirectional communication mode to avoid inefficient utilization of the available resources, e.g., see the pilot contamination problem in massive MIMO [106, 107].

### A.5.4 Dynamic Cell

Most of the current standards define a cell by the set of UEs that are associated using a minimum-distance rule, which leads to non-overlapping Voronoi tessella-

tion of the serving area of every BS, exemplified by the well-known hexagonal cells [108, 109]. The minimum-distance rule leads to a simple association metric based on the reference signal received power (RSRP) and RSSI. However, the traditional RSRP/RSSI-based association may become significantly inefficient in the presence of non-uniform UE spatial distribution, and of heterogeneous BSs with a different number of antenna elements and different transmission powers [99, 108]. This association entails an unbalanced number of UEs per cell, which limits the available resources per UE in highly populated cells, irrespective of individual signal strengths, while wasting them in sparse ones. This is exacerbated by the directionality in mmWave systems, where the whole system becomes noise-limited, and it becomes pointless to use an association metric suited for an interference-limited homogenous system. The main disadvantage of the current static definition of a cell, as a predetermined geographical area covered by a BS, is that the static cell formation is independent of the cell load as well as of the UEs' capabilities.<sup>9</sup> In fact, three parameters should affect cell formation: (i) UE traffic demand, (ii) channel between UE and BSs, and (iii) BSs loads. Minimum-distance (RSRP/RSSI-based) association only considers the second parameter, such that reassociation is needed if this parameter is changed, which is inefficient in mmWave systems [99].

With the massive number of degrees of freedom that fully-directional communication offers and possible MAC layer analog beamforming, we can define a dynamic cell as a set of not necessarily colocated UEs that are served by the same analog beamformer of the BS and dynamically selected to improve some objective function. Upon any significant fluctuations of the above three parameters, dynamic cell redefinition may be required. To this end, we need a full database in the macro-cell BS, recording dynamic cell formations, UEs' traffic demands, their quality of service levels, and their connectivity to the neighboring BSs. Depending on the UEs' demands, microcell BSs dynamically group UEs together and form new cells so that (i) individual UE's demands are met (*QoS provisioning*), (ii) the trade-off between macro-level fairness and spectral efficiency is improved, e.g., through proportional fair resource allocation (*network utility maximization*), and (iii) every UE is categorized in at least two groups, to guarantee robustness to blockage (*connection robustness*). Two colocated UEs may belong to two different cells if their demands cannot be fully served with resource sharing inside a cell and if there exist proper directed spatial channels to form two independent cells. Moreover, a new UE is not necessarily served by a geographically close BS, if this violates the QoS of a UE that is already served by that BS. While serving a UE with a less-loaded but farther BS is not a good choice in interference-limited traditional cellular networks, it is feasible (and in fact desirable) in proper resource allocation based on fully-directional communication. All this may entail a substantial modification/extension of the methodology of cellular network analysis [89, 109–113] in general and mmWave cellular networks in particular [48, 67], as the main assumptions made in those frameworks of Voronoi serving regions do not hold. The notion of dynamic cell revolutionizes traditional cell-centric design and introduces a new

---

<sup>9</sup>Note that the state-of-the-art soft and phantom cell concepts have these problems as well.

user-centric design paradigm. This is especially important for uniform quality of experience provisioning throughout the network, which is one of the main goals in 5G.

In the following, we clarify the dynamic cell concept with an illustrative example. Consider a network with four UEs and two microcell BSs. BS1 serves colocated UE1 and UE2, and BS2 serves colocated UE3 and UE4. Therefore, we have two cells: one created by UE1 and UE2, and the other by UE3 and UE4. Assume that the traffic demands of UE1 and UE2 increase so that BS1 is no longer able to serve them both, while BS2 can serve one of them together with its own UEs. In this case, BS1 broadcasts a cell redefinition request, and a dynamic cell configuration reassociates UE2 from the first to the second cell. Now, the first cell contains only UE1, and the second cell contains UE2, UE3, and UE4.<sup>10</sup> The reconfiguration is done by changing the analog beamforming vectors of the BSs and UEs. The reconfiguration process can be managed at a macrocell BS that covers both BS1 and BS2, making the dynamic cell concept compatible with software defined networking and centralized radio network control [23, 114]. The benefit of dynamic cell formation depends heavily on the interference level, as pointed out partially in [108]. High directionality in mmWave systems with pencil-beam operation is a unique advantage, as microwave networks with omnidirectional operation are interference-limited.

To evaluate the performance gain due to the new degrees of freedom in mmWave networks, we simulate a network with 2 BSs and 30 UEs, distributed in 1 square kilometer. We consider a mmWave wireless channel with path-loss exponent  $\alpha = 3$ , and adopt the same initial parameters as in Section A.3.2. In Appendix B, cell formation is posed as an optimization problem aimed to ensure micro- and macro-level fairness with a predefined minimum rate for every UE. Given a network topology, the solution of optimization problem (A.9) in Appendix B gives the optimal association, resource sharing within every analog beam, operating beamwidths, and boresight angles of BSs as well as UEs. We conducted 10 experiments to evaluate the impact of directionality on the network performance in terms of sum rate in bps/Hz, maximum of the minimum rate of a UE in bps/Hz, and fairness using Jain's fairness index [115]. In all the experiments, we considered a summation over logarithmic functions for the network utility maximization formulated in (A.9) in Appendix B to guarantee fairness, as pointed out in Proposition A.1 in Appendix B. Furthermore, we assume that BSs and UEs can respectively make beams as narrow as  $5^\circ$  and  $10^\circ$ , if required. Experiments 1-3 are done as follows: the network topology and geometry is fixed, we consider only one RF chain for every UE, the number of RF chains per BS is varied, and we find the optimal solution of (A.9), which includes the optimal association. Experiments 4-6 are done as follows: the associations are fixed to those obtained in experiments 1-3, and we use Remark A.6.7 in Appendix B to find a sub-optimal solution of optimization problem (A.9) for semi-directional communications. Finally, in experiments 7-9, we solve optimization problem (A.9) for semi-directional communications, whose solution includes the optimal associa-

<sup>10</sup>Note that dynamic cell formation is fundamentally different from reassociation after a handover, as the former may be triggered without any change in the environment due to mobility or blockage.

Table A.4: The performance of resource allocation in omni-, semi-, and fully-directional communications with one RF chain per UE. All rates are measured in bit/s/Hz.

Experiment	Communication Mode	# RF chains per BS	Network sum rate	Minimum rate	Jain's fairness index
1	Fully-directional	3	151.48	3.76	0.94
2		6	322.74	7.73	0.89
3		12	630.62	12.50	0.92
4	Semi-directional	3	118.34	2.65	0.91
5		6	215.83	0.38	0.67
6		12	501.39	0.41	0.88
7		3	120.46	2.90	0.94
8		6	261.98	3.79	0.71
9		12	422.3	2.62	0.76
10	Omnidirectional	1	5.52	0.06	0.72

tion. The last experiment shows the omnidirectional performance, evaluated using Remark A.6.8 in Appendix B. For benchmarking purposes, we also show the optimal association for one random topology in Figure A.8, where squares represent BSs, and stars are UEs, solid red lines show association to one RF chain of BS1, and dashed green lines represent association to one RF chain of BS2. In particular, Figures A.8(a), (b), (c), and (d) represent the optimal associations for experiments 10, 7, 9, and 3, respectively.

Table A.4 shows the performance in all experiments, averaged over 10 random topologies. In general, the fully-directional mode outperforms other modes, as directionality improves the link budget on one side and reduces the interference on the other. In particular, compared to the omnidirectional mode in experiment 10, we observe a sum rate enhancement by factors of 113 and 75 in experiments 3 and 9, respectively. These enhancements are even more significant in terms of the minimum offered spectral efficiency, that is, 207 and 43 times in experiments 3 and 9, compared to experiment 10. Comparing Figure A.8(a) to Figures A.8(c) and (d), we can see that many UEs have to share the available resources in the omnidirectional communication, whereas in the semi- and fully-directional cases they share the available resources among significantly fewer UEs. Another point is that the increase of the number of RF chains adds new degrees of freedom, leading to further improvement in the sum and the minimum rates. For instance, increasing the number of RF chains by a factor of 4 improves the sum rate performance of



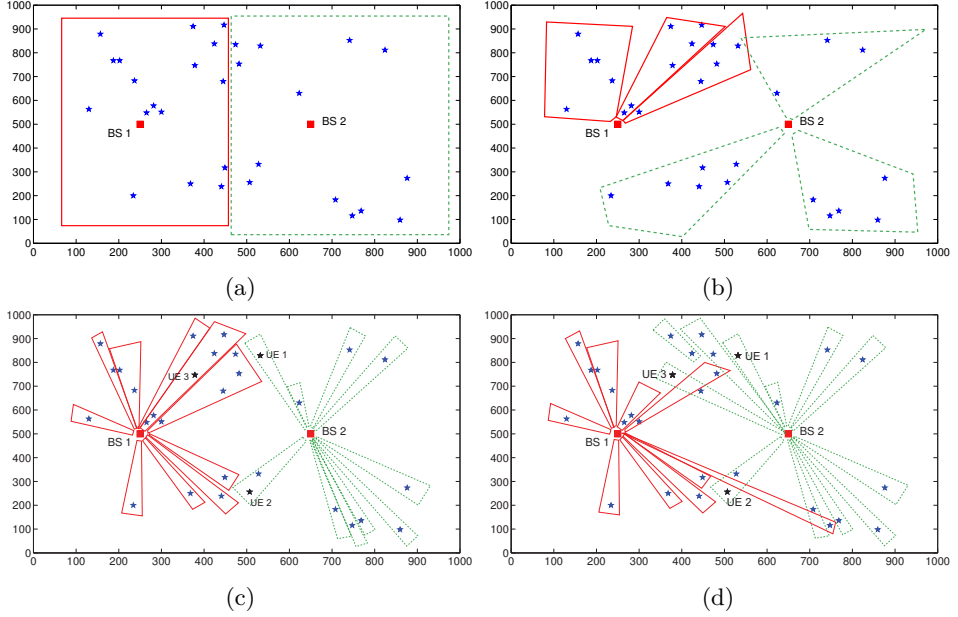


Figure A.8: Example of the optimal association. Squares represent BSs, and stars are UEs. (a) omnidirectional communication; (b) semi- and fully-directional communications with 3 RF chains at every BS; (c) semi-directional communication with 12 RF chains at every BS, and (d) fully-directional communication with 12 RF chains at every BS. Solid red lines show association to one RF chain of BS1. Dashed green lines represent association to one RF chain of BS2.

the fully-directional mode by a factor of 3.2, while also improving the minimum achievable rate by a factor of 2.3. Although the optimal resource allocation with semi-directional communication (experiment 9) experiences a high sum rate gain (2.5), the minimum rate performance of this mode cannot be further improved by adding more RF chains, as there are many colocated UEs served with the same analog beam. In this case, adding new degrees of freedom at the BSs (new RF chains) may not help as the system approaches its *maximum limit*. However, the fully-directional option leverages the beamforming capabilities of the UEs to manipulate the effective channel, thus improving the *maximum limit*, and serves even colocated UEs simultaneously with different analog beams transmitted from different directions, see Figure A.8(d). This reduces the number of UEs that share the resources of any given analog beam, improving both the network sum rate and the UEs' minimum rate. We verify the claim above on Figure A.8. With 3 RF chains per BS, the optimal association for both semi- and fully-directional communications are the same, as shown in Figure A.8(c). By increasing the number of RF chains per BS to 12, the semi-directional communication can reduce the size of the

groups of UEs. However, there are still some UEs that are indistinguishable in the angular domain, and should therefore be served together. This limits the improvement on the UE's minimum rate. The fully-directional communication mode, from another perspective, leverages directionality at the UEs, and associates UEs to a less-loaded RF chain of a preferably closer BS.<sup>11</sup> However, some UEs, such as UE3 in Figure A.8(d) will be associated to a further BS instead of sharing an analog beam with 4 other UEs as in Figure A.8(c). In addition to more efficient load balancing, the fully-directional option offers both higher link budget and lower interference. For instance, UE1 and UE2 in Figure A.8(c) receive a large amount of interference from BS1, whereas the interference will be almost canceled in the fully-directional option in Figure A.8(d) due to deafness. Last but not least, the fully-directional option also outperforms other options in terms of fair resource allocation, as verified by Jain's fairness index in Table A.4.

## A.6 Concluding Remarks

Millimeter wave (mmWave) communications, as a promising enabler of 5G cellular networks, offer a significant improvement in area spectral and energy efficiencies. The main characteristics of a mmWave system are very high attenuation, vulnerability to obstacles, sparse-scattering environments, high directionality level, and limited interference. The mmWave cellular networks are based on different constraints and degrees of freedom compared to traditional microwave cellular networks and therefore require fundamental changes in almost all design aspects, especially at the MAC layer. This paper focused on the changes required at the various MAC layer functionalities, such as synchronization, random access, handover, channelization, interference management, scheduling, and association. Design aspects, new challenges, and new tradeoffs were identified, and initial solution approaches, based on the special characterizes of mmWave systems, were investigated.

There are multiple options to design a physical control channel (PHY-CC) for mmWave systems. An omnidirectional PHY-CC on microwave bands is an indisputable option wherever robustness to deafness, high channel reliability, and long range are necessary, for instance, in initial access procedures and in coordination among BSs during handovers. A semi- or fully-directional PHY-CC on mmWave band is also mandatory to realize directional cell search to alleviate the possible mismatch between coverage of control and data channels. As some critical procedures in a cellular network, including initial access, need all the above requirements, we suggested a novel hierarchal architecture for a PHY-CC. The proposed two-step initial access procedure leverages macro-level coverage and reliability of an omnidirectional PHY-CC on microwave band and efficiency of a directional PHY-CC on mmWave band to enhance the performance of synchronization. Performance evaluations showed that a relatively small number of pilot transmissions guarantees discovery of a UE with high probability. This number increases with the direc-

<sup>11</sup>If we add the alignment overhead into the picture, association to a closer less-loaded easy-to-find BS may be preferable, especially if we have frequent reassociation.

tionality level, introducing a tradeoff between boosting link budget and reducing synchronization overhead. Comprehensive performance analysis of different PHY-CC options is an interesting topic for future studies.

Directional operation with pencil beams, which is mandatory to boost link budget in mmWave band, provides a large number of degrees of freedom to form different cells and allocate resources, while significantly simplifying intra- and inter-cell interference cancelation. As stated in Section A.5.2, leveraging the potential of mmWave systems to improve the complex tradeoffs among throughput enhancement, fair scheduling, and high connection robustness demands revisiting the current interference-limited architecture. An example was provided to highlight that a proper scheduling with fully-directional communication with a limited number of RF chains leads to a significant throughput gain over existing omnidirectional operation, while improving the fairness among the UEs. The performance of both semi- and fully-directional operations improves with the number of RF chains per BS, but in a saturating manner. The former generally faces the saturation point for a small number of RF chains, while the latter will still benefit from having more RF chains, as new RF chains open new opportunities to redefine cells so as to better balance the total load of the network. This will lead to a significant improvement in the network sum rate as well as enhancements in the minimum rate offered to a UE and in Jain's fairness index.

Software defined wireless networking as well as relaying techniques must be considered as primary building blocks in next generation cellular networks for both access and backhaul, since they can provide more uniform quality of service by offering efficient mobility management, smooth handover operation, load balancing, and indoor-outdoor coverage. As the system goes to a noise-limited regime, resource allocation and interference management procedures will be simplified, whereas connection establishment (initial access) and recovery (handover) become complicated. As recently pointed out, for instance, in [57, 69–74], the noise-limited regime also facilitates concurrent transmissions and increases the benefits of device-to-device (D2D) and cognitive communications underlying a cellular networks. At the same time, a noise-limited system simplifies the required MAC layer intelligence for spectrum sharing and inter-network interference avoidance. An interesting topic for future studies is in which conditions (for instance, in terms of UE and BS densities, transmission powers, operating beamwidths, and UE traffic) we are in the noise-limited regime. The answer to this fundamental question will shed light on the complexity of various MAC layer functions.

## Appendix A: Spatial Search Overhead

In this appendix, we compute an upper bound for the delay of spatial search using options 2 and 3 of Section A.3.2. To this end, we assume that there are  $n_b$  BSs whose pilots can be received with high enough SNR at a typical UE, located at the origin. The UE and all BSs are aware of the time-frequency portions over which the directional synchronization pilots are transmitted, thanks to the proposed two-step

synchronization procedure. All the BSs transmit pilot signals with the same power  $p$  and beamwidth  $\theta$ . We only consider a 2D plane, so there are  $N_s = \lceil 2\pi/\theta \rceil$  non-overlapping sectors that a BS should search over to find the typical UE. The upper bound is set by assuming that each BS randomly selects a new sector, among the  $N_s$  sectors with uniform distribution, to search using pilot transmission. In semi-directional mode, the UE has omnidirectional reception. In fully-directional mode, the UE is assumed to listen in one direction while the BSs do the search. A joint search by UE and BS is left as future work. For the sake of simplicity, we only count the BSs with LoS links. Thanks to this assumption, we end up with tractable closed-form expressions that give new insights on the overhead of the spatial search required by options 2 and 3. Note that we still find an upper bound on the delay performance, because the UE may receive a pilot of a close NLoS BS, even though this event does not happen frequently due to very high attenuation with every obstacle. Supposing that the process of obstacles forms a random shape process, for instance, a Boolean scheme of rectangles as considered in [51], and under some further assumptions such as independent blockage events [48], we can assume that the number of LoS BSs  $n_b$  is a Poisson random variable with mean  $\rho$ , which depends on the average LoS range of the network [48, 51]. Note that  $\rho$  is equal to the density of LoS BSs per square meter, denoted by  $\rho_u$ , times the effective area, whose value depends on the option chosen to realize the physical control channel and will be characterized later. Further, the LoS BSs are located uniformly in the 2D plane. In the following, we compute the probability that the typical UE can be found after  $n_e$  epochs of pilot transmission for an arbitrary density of LoS BSs  $\rho$ . We then characterize  $\rho$  as a function of the transmission power and beamwidth for both semi- and fully-directional case.

The UE can be discovered if and only if there is at least one BS, that is,  $m \geq 1$ , which happens with probability  $1 - e^{-\rho}$  [93]. Under this condition, we denote by  $\Pr[n_e = n, n_b = m | m \geq 1]$  the joint probability of discovering the typical UE at epoch  $n$  and having  $m$  LoS BSs, given  $m \geq 1$ .  $\Pr[n_b = m | m \geq 1]$  follows a zero-truncated Poisson distribution [116]. Given  $m \geq 1$ , the UE will be discovered by epoch  $n$  (cumulative distribution function), with probability  $\Pr[n_e \leq n | n_b = m, m \geq 1]$ , if it falls in at least one of the  $n$  sectors that any BS has investigated. Since each BS chooses uniformly and independently  $n$  out of  $N_s$  sectors, we have

$$\Pr[n_e \leq n | n_b = m, m \geq 1] = 1 - \left(1 - \frac{n}{N_s}\right)^m.$$

The probability mass function is

$$\Pr[n_e = n | n_b = m, m \geq 1] = \left(1 - \frac{n-1}{N_s}\right)^m - \left(1 - \frac{n}{N_s}\right)^m$$

for  $n > 0$ . Therefore, we can find  $\Pr[n_e = n, n_b = m | m \geq 1]$  for all  $n, m \geq 1$  as

$$\Pr[n_e = n, n_b = m | m \geq 1] = \left( \left(1 - \frac{n-1}{N_s}\right)^m - \left(1 - \frac{n}{N_s}\right)^m \right) \frac{e^{-\rho} \rho^m}{1 - e^{-\rho} m!}, \quad (\text{A.1})$$

and consequently  $\Pr[n_e = n | m \geq 1]$  as

$$\begin{aligned}
\Pr[n_e = n | m \geq 1] &= \sum_{m=1}^{\infty} \Pr[n_e = n, n_b = m | m \geq 1] \\
&\stackrel{(A.1)}{=} \sum_{m=1}^{\infty} \left( \left(1 - \frac{n-1}{N_s}\right)^m - \left(1 - \frac{n}{N_s}\right)^m \right) \frac{e^{-\rho}}{1 - e^{-\rho}} \frac{\rho^m}{m!} \\
&= \frac{e^{-\rho}}{1 - e^{-\rho}} \left( \sum_{m=1}^{\infty} \frac{\left(\left(1 - \frac{n-1}{N_s}\right)\rho\right)^m}{m!} - \sum_{m=1}^{\infty} \frac{\left(\left(1 - \frac{n}{N_s}\right)\rho\right)^m}{m!} \right) \\
&\stackrel{(\star)}{=} \frac{e^{-\rho}}{1 - e^{-\rho}} \left( e^{\left(1 - \frac{n-1}{N_s}\right)\rho} - e^{\left(1 - \frac{n}{N_s}\right)\rho} \right) \\
&= e^{-n\rho/N_s} \left( \frac{e^{\rho/N_s} - 1}{1 - e^{-\rho}} \right), \tag{A.2}
\end{aligned}$$

For  $(\star)$  in (A.2), we used the Taylor series of the exponential function. Using (A.2), we can derive closed-form expressions for several interesting performance metrics. Recalling the assumptions from the beginning of this appendix and observing a UE that *can* be discovered, the following remarks hold:

*Remark A.6.1.* The average number of pilot transmission epochs for discovering the UE, denoted by  $\mathcal{N}_d$ , is

$$\begin{aligned}
\mathcal{N}_d &= \sum_{n=1}^{N_s} n \Pr[n_e = n | m \geq 1] = \frac{e^{\rho/N_s} - 1}{1 - e^{-\rho}} \sum_{n=1}^{N_s} n e^{-n\rho/N_s} \\
&= \frac{e^{\rho+\rho/N_s} - (N_s + 1) e^{\rho/N_s} + N_s}{(e^{\rho} - 1)(e^{\rho/N_s} - 1)}. \tag{A.3}
\end{aligned}$$

*Remark A.6.2.* The probability that the UE is discovered within  $l$  epochs is

$$\begin{aligned}
\Pr[\text{Discovering a discoverable UE in } l \text{ epochs}] &= \sum_{n=1}^l \Pr[n_e = n | m \geq 1] \\
&= \frac{e^{\rho} - e^{\rho-\rho l/N_s}}{e^{\rho} - 1}. \tag{A.4}
\end{aligned}$$

*Remark A.6.3.* The probability that the UE is discovered within  $N_s = \lceil 2\pi/\theta \rceil$  epochs is 1. To verify, we should simply put  $n = N_s$  in (A.4).

*Remark A.6.4.* Consider Equation (A.4). The minimum number of epochs required to guarantee discovery of the UE with probability  $\mu$  is the smallest integer not less than

$$N_s - \frac{N_s}{\rho} \ln(\mu + (1 - \mu)e^{\rho}). \tag{A.5}$$

The last step to find the spatial search overhead is finding the density of the LoS BSs in semi- and fully-directional scenarios, which requires further assumptions on the antenna radiation pattern and the channel model.

For analytical tractability, we approximate the actual antenna patterns by a commonly used sectored antenna model [48,91,92]. This simple model captures the interplay between directivity gain, which ultimately affects the transmission range and half-power beamwidth. In an ideal sector antenna pattern, the directivity gain is constant for all angles in the main lobe and equal to a smaller constant in the side lobe. That is,

$$\begin{cases} \frac{2\pi-(2\pi-\theta)\epsilon}{\theta}, & \text{in the main lobe} \\ \epsilon, & \text{in the side lobe} \end{cases}, \quad (\text{A.6})$$

where typically  $\epsilon \ll 1$ . The main lobe gain can be derived by fixing the total radiated power of the antennas over a parameter space of  $\epsilon$  and  $\theta$ . In omnidirectional operation  $\theta = 2\pi$ , and there is no directivity gain.

Similar to [43,88], we consider a simple distance-dependent attenuation with path-loss exponent  $\alpha > 2$ . This leads to a closed-form expression, based on which we provide interesting insights.<sup>12</sup> The power that the typical UE receives from the pilot transmission of a LoS BS, located at distance  $d$ , is

$$\begin{cases} p \left( \frac{2\pi-(2\pi-\theta)\epsilon}{\theta} \right) \left( \frac{\lambda}{4\pi d} \right)^\alpha, & \text{semi-directional} \\ p \left( \frac{2\pi-(2\pi-\theta)\epsilon}{\theta} \right)^2 \left( \frac{\lambda}{4\pi d} \right)^\alpha, & \text{fully-directional} \end{cases},$$

where  $\lambda$  is the wavelength and  $p$  is the pilot transmission power. Considering a minimum required SNR  $\beta$  at the receiver and noise power  $\sigma$ , the typical UE can receive the synchronization pilot of a LoS BS at maximum distance  $d_{\max}$ , where

$$d_{\max} = \begin{cases} \frac{\lambda}{4\pi} \left( \frac{p(2\pi-(2\pi-\theta)\epsilon)}{\sigma\beta\theta} \right)^{1/\alpha}, & \text{semi-directional} \\ \frac{\lambda}{4\pi} \left( \frac{p(2\pi-(2\pi-\theta)\epsilon)^2}{\sigma\beta\theta^2} \right)^{1/\alpha}, & \text{fully-directional} \end{cases}, \quad (\text{A.7})$$

which can be reduced to

$$d_{\max} = \begin{cases} \frac{\lambda}{4\pi} \left( \frac{2\pi p}{\sigma\beta\theta} \right)^{1/\alpha}, & \text{semi-directional} \\ \frac{\lambda}{4\pi} \left( \frac{4\pi^2 p}{\sigma\beta\theta^2} \right)^{1/\alpha}, & \text{fully-directional} \end{cases} \quad (\text{A.8})$$

as  $\epsilon \rightarrow 0$ . The density of LoS BSs  $\rho$  in (A.5)–(A.1) is essentially equal to the product of the density of the LoS BSs per square meter, which is an input parameter, and

<sup>12</sup>Some preliminary results in the presence of Nakagami fading (not presented in this paper) show that these insights also apply to more general channel models, though the exact expressions will be different.

the effective area over which the typical UE can receive a pilot signal with high enough SNR. In semi-directional communications with omnidirectional UE, the UE can receive from all directions, hence the effective area is  $\pi d_{\max}^2$ , whereas in fully-directional communications the UE can receive only from LoS BSs located in a specific circle sector, hence the effective area is  $\theta d_{\max}^2/2$ , with  $d_{\max}$  given in (A.7) or (A.8).

*Remark A.6.5.* Consider the assumptions stated at the beginning of Appendix A. Consider Equation (A.8). Given that a UE can be discovered, semi-directional PHY-CC (option 2) requires fewer epochs, on average, for discovering the UE compared to fully-directional control channel (option 3).

*Proof.* Let  $\rho$  be the density of LoS BSs that can discover the typical UE. Let  $\rho_u$  denote the density of the LoS BSs per square meter. The effective area for the semi- and fully directional modes are  $\pi d_{\max}^2$  and  $\theta d_{\max}^2/2$ , respectively. Hence,

$$\frac{\rho \text{ in semi-directional mode}}{\rho \text{ in fully-directional mode}} = \frac{\pi \left( \frac{\lambda}{4\pi} \left( \frac{2\pi p}{\sigma\beta\theta} \right)^{1/\alpha} \right)^2 \rho_u}{\frac{\theta}{2} \left( \frac{\lambda}{4\pi} \left( \frac{4\pi^2 p}{\sigma\beta\theta^2} \right)^{1/\alpha} \right)^2 \rho_u} = \left( \frac{2\pi}{\theta} \right)^{1-2/\alpha},$$

where  $0 \leq \theta \leq 2\pi$  and  $\alpha > 2$ . Therefore, the semi-directional control channel offers higher density of LoS BSs than the fully-directional one. Considering that the average number of epochs required for discovering a typical UE, formulated in (A.3), is a strictly decreasing function of  $\rho$ , Remark A.6.5 is proved.  $\square$

*Remark A.6.6.* Consider the assumptions stated at the beginning of Appendix A. Consider Equation (A.3). Given that a UE can be discovered, for a sparse network where there is only one BS for discovering every UE, the average number of epochs for discovering a UE is  $(\lceil 2\pi/\theta \rceil + 1)/2$ , irrespective of using semi- or fully-directional modes.

*Proof.* Recall that in this appendix we characterize the spatial search overhead given that the UE can be discovered ( $m \geq 1$ ). Therefore, if we let the density of the LoS BSs go to zero, we inherently simulate a network where there is only one BS per UE. Using Taylor expansion of (A.3) at  $\rho \rightarrow 0$ , the limit of (A.3) as  $\rho \rightarrow 0$  is  $(N_s + 1)/2$ , which completes the proof by replacing  $N_s = \lceil 2\pi/\theta \rceil$ .  $\square$

## Appendix B: Optimal Cell Formation

In this appendix, we formulate an optimization problem to optimize cell formation. We first formulate the problem for fully-directional communications, and then show how this can be simplified to semi-directional and omnidirectional communications.

Let  $n_i$  be the number of RF chains (analog beams) at BS  $i$ . We replace BS  $i$  with  $n_i$  virtual BSs, hereafter called BSs, located at the same position, each having one

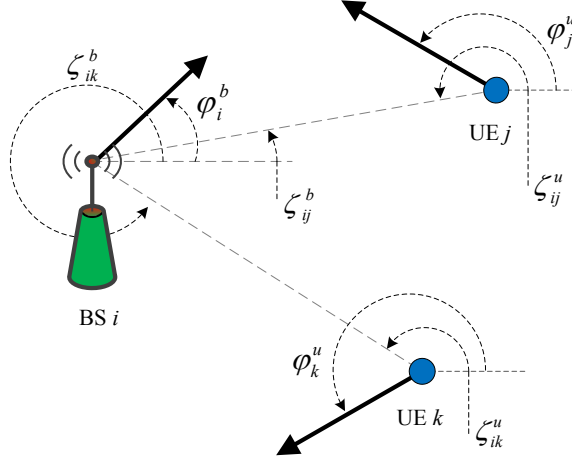


Figure A.9: Illustration of the angles between BSs and UEs  $\zeta_{ij}^b$  and  $\zeta_{ij}^u$ ,  $\varphi_i^b$ , and  $\varphi_j^u$ . Solid arrows show the boresight directions.

RF chain. We denote by  $\mathcal{U}$  the set of UEs, by  $\mathcal{B}$  the set of all BSs, by  $p$  the transmission power of a BS, by  $\sigma$  the power of white Gaussian noise, and by  $g_{ij}^c$  the channel gain between BS  $i$  and UE  $j$ , capturing both path-loss and shadowing effects. Here, we assume that the impact of fast fading on the received signal and consequently on the signal-to-interference-plus-noise ratio (SINR) is averaged out, since the association will execute on a large time scale compared to the instantaneous channel fluctuations. Such a long-term channel model implies the use of a long-term SINR, which is often effectively used for long-term resource allocation [108, 110]. Let  $\theta_i^b$  and  $\theta_j^u$  be the operating beamwidths of BS  $i$  and UE  $j$ , respectively. Let  $\zeta_{ij}^b$  be the angle between the positive  $x$ -axis and the direction in which BS  $i$  sees UE  $j$ , and let  $\zeta_{ij}^u$  be similarly defined by changing the roles of BS  $i$  and UE  $j$ . Note that these angles are imposed by the network topology, and that  $|\zeta_{ij}^u - \zeta_{ij}^b| = \pi$ . Let  $\varphi_i^b$  and  $\varphi_j^u$  be the boresight angles of BS  $i$  and UE  $j$  relative to the positive  $x$ -axis, see Figure A.9. We denote by  $g_{ij}^b$  the directivity gain that BS  $i$  adds to the link between BS  $i$  and UE  $j$  (transmission gain), and by  $g_{ij}^u$  the directivity gain that UE  $j$  adds to the link between BS  $i$  and UE  $j$  (reception gain). Using the sectorized antenna model introduced in Appendix A, we have

$$g_{ij}^b = \begin{cases} \epsilon, & \text{if } \frac{\theta_i^b}{2} < |\varphi_i^b - \zeta_{ij}^b| < 2\pi - \frac{\theta_i^b}{2} \\ \frac{2\pi - (2\pi - \theta_i^b)\epsilon}{\theta_i^b}, & \text{otherwise} \end{cases},$$

and

$$g_{ij}^u = \begin{cases} \epsilon, & \text{if } \frac{\theta_j^u}{2} < |\varphi_j^u - \zeta_{ij}^u| < 2\pi - \frac{\theta_j^u}{2} \\ \frac{2\pi - (2\pi - \theta_j^u)\epsilon}{\theta_j^u}, & \text{otherwise} \end{cases}.$$



Then, the power received by UE  $j$  from BS  $i$  is  $pg_{ij}^b g_{ij}^c g_{ij}^u$ . Hence, the SINR at UE  $j$  due to the transmission of BS  $i$  is

$$\frac{pg_{ij}^b g_{ij}^c g_{ij}^u}{\sum_{k \in \mathcal{B} \setminus i} pg_{kj}^b g_{kj}^c g_{kj}^u + \sigma},$$

which depends on the transmission power  $p$ , operating beamwidths  $\theta_i^b$  and  $\theta_j^u$ , boresight angles  $\varphi_i^b$  and  $\varphi_j^u$ , and network topology  $\zeta_{ij}^b$  and  $\zeta_{ij}^u$ . It is straightforward to see that narrower beams at the BSs and/or at the UEs lead to a higher SINR, on average, due to an increased received power from BS  $j$  and a decreased interference level. We denote by  $c_{ij}$  the achievable rate of the link between BS  $i$  and UE  $j$ , which we assume to be a logarithmic function of the corresponding SINR, and by  $y_{ij}$  the fraction of resources used by BS  $i$  to serve UE  $j$ . We first observe that  $r_{ij} = y_{ij}c_{ij}$  and  $r_j = \sum_{i \in \mathcal{B}} y_{ij}c_{ij}$  are the long-term rate that UE  $j$  will receive from BS  $i$  and from all BSs, respectively. Let  $U_j$  be a general utility function of  $r_j$ . Let  $x_{ij}$  be a binary association variable, equal to 1 if and only if UE  $j$  is associated to BS  $i$ . Let  $r_{i,\min}$  be the minimum required rate of UE  $j$ . Let  $\theta_{i,\min}^b$  and  $\theta_{j,\min}^u$  be the minimum possible operating beamwidth of BS  $i$  and UE  $j$ , which depend on the corresponding number of antenna elements and antenna configurations [117].

Given that the network topology is known a priori (that is,  $\zeta_{ij}^b$ ,  $\zeta_{ij}^u$ , and  $g_{ij}^c$  are known for every BS  $i$  and UE  $j$ ), the optimal cell formation attempts to find the optimal values for  $\varphi_i^b$ ,  $\theta_i^b$ ,  $\varphi_j^u$ ,  $\theta_j^u$ ,  $x_{ij}$ , and  $y_{ij}$  to maximize some network utility. If we collect all control variables  $x_{ij}$  and  $y_{ij}$  in matrices  $\mathbf{X}$  and  $\mathbf{Y}$ , and collect all  $\varphi_i^b$ ,  $\varphi_j^u$ ,  $\theta_i^b$ , and  $\theta_j^u$  in vectors  $\boldsymbol{\phi}^b$ ,  $\boldsymbol{\phi}^u$ ,  $\boldsymbol{\theta}^b$ , and  $\boldsymbol{\theta}^u$ , the cell formation optimization problem can be formally stated as

$$\underset{\boldsymbol{\phi}^b, \boldsymbol{\theta}^b, \boldsymbol{\phi}^u, \boldsymbol{\theta}^u, \mathbf{X}, \mathbf{Y}}{\text{maximize}} \quad \sum_{j \in \mathcal{U}} U_j \left( \sum_{i \in \mathcal{B}} y_{ij} c_{ij} \right), \quad (\text{A.9a})$$

$$\text{subject to} \quad \sum_{j \in \mathcal{U}} y_{ij} \leq 1, \quad \forall i \in \mathcal{B}, \quad (\text{A.9b})$$

$$\sum_{i \in \mathcal{B}} x_{ij} = 1, \quad \forall j \in \mathcal{U}, \quad (\text{A.9c})$$

$$\begin{cases} 0 \leq y_{ij} \leq x_{ij}, x_{ij} \in \{0, 1\} & \forall i \in \mathcal{B} \\ x_{ij} = 0 & \text{if } r_{ij} < r_{j,\min} \end{cases}, \quad \forall j \in \mathcal{U} \quad (\text{A.9d})$$

$$0 \leq \varphi_i^b \leq 2\pi, \quad \forall i \in \mathcal{B}, \quad (\text{A.9e})$$

$$0 \leq \varphi_j^u \leq 2\pi, \quad \forall j \in \mathcal{U}, \quad (\text{A.9f})$$

$$\theta_{i,\min}^b \leq \theta_i^b \leq 2\pi, \quad \forall i \in \mathcal{B}, \quad (\text{A.9g})$$

$$\theta_{j,\min}^u \leq \theta_j^u \leq 2\pi, \quad \forall j \in \mathcal{U}. \quad (\text{A.9h})$$

Observe that, for notational simplicity, function arguments have been discarded. Constraint (A.9c) guarantees association to only one BS, mitigating joint scheduling requirements among BSs, and constraint (A.9d) guarantees a minimum QoS for every UE. Further, constraint (A.9d) ensures that every BS  $i$  will provide a positive resource share only to its associated UEs. The solution of (A.9) provides a long-term association policy along with proper orientation and operating beamwidths for fully-directional communications. This solution is valid as long as the inputs of the optimization problem, that is, network topology and UE demands, remain unchanged. Once a UE requires more resources or loses its connection (for instance, due to a temporary obstacle), optimization problem (A.9) has to be re-executed. In the latter, the UE will use its backup connection, and will handover to the right BS once the new solution of (A.9) is available. We can easily extend optimization problem (A.9) to find proper backup associations for UEs. Note that the main aim of this paper is to understand the fundamental limitations, and an efficient solution method for (A.9) is left as future work.

**Proposition A.1.** *Consider optimization problem (A.9). Replacing  $y_{ij}$  by  $1/\sum_{j \in \mathcal{U}} x_{ij}$ , the solution of (A.9) gives the optimal cell formation with equal resource allocation inside every analog beam (micro-level fairness). Further, using a logarithmic function for  $U_j$ , the solution of (A.9) ensures a macro-level proportionally fair resource allocation.*

*Proof.* Following similar steps as those in [110, Appendix A], the proof is straightforward.  $\square$

*Remark A.6.7.* Consider optimization problem (A.9). Using  $\theta_{j,\min}^u = 2\pi$  for all  $j \in \mathcal{U}$ , the solution of (A.9) gives the optimal cell formation in the semi-directional mode with directional operation of BSs and omnidirectional operation of the UEs.

*Remark A.6.8.* If we use  $\theta_{i,\min}^b = 2\pi$  for all  $i \in \mathcal{B}$  and  $\theta_{j,\min}^u = 2\pi$  for all  $j \in \mathcal{U}$ , the solution of optimization problem (A.9) gives the optimal cell formation in the omnidirectional mode.

**Proposition A.2.** *Consider optimization problem (A.9). For a given network topology, the optimum of the problem (namely, the utility at the optimal value) for the omnidirectional communication mode is upper bounded by the semi-directional one, and the optimum of the problem for the semi-directional communication mode is upper bounded by the fully-directional one.*

*Proof.* According to Remark A.6.7, the feasible set of solutions for the optimization problem for semi-directional communications is a subset of that for fully-directional communications. Similarly, Remark A.6.8 implies that the feasible set of solutions for the optimization problem for omnidirectional communications is a subset of that for semi-directional communications. Therefore, the proposition follows.  $\square$

---

# Design Aspects of Short Range Millimeter Wave Networks: A MAC Layer Perspective

---

Hossein Shokri-Ghadikolaei, Carlo Fischione, Petar Popovski, and Michele Zorzi

Submitted to  
*IEEE Network*

©2015 IEEE

The layout has been revised.

# Design Aspects of Short Range Millimeter Wave Networks: A MAC Layer Perspective

Hossein Shokri-Ghadikolaie, Carlo Fischione, Petar Popovski, and  
Michele Zorzi

## Abstract

Increased density of wireless devices, ever growing demands for extremely high data rate, and spectrum scarcity in microwave bands make the millimeter wave (mmWave) band an important player in next generation wireless networks. MmWave communication systems exhibit severe attenuation, blockage, deafness, and may need microwave networks for coordination and fall-back support. To compensate high attenuation, mmWave systems exploit highly directional operation, which in turn substantially reduces the interference footprint. The significant differences between mmWave networks and legacy communication technologies challenge the classical design approaches, especially at the medium access control (MAC) layer, which has received comparatively less attention than PHY and propagation issues in the literature. In this paper, the MAC layer design aspects of short range mmWave networks are discussed. In particular, this paper discusses challenges and inefficiencies of current mmWave standards to fully exploit all potentials of short range mmWave networks, and argues for the necessity of new collision-aware hybrid resource allocation frameworks with on-demand control packets, the advantages of a collision notification signal, and the potential of multihop communication to provide reliable mmWave connections.

## B.1 Introduction

There is a growing consensus both in industry and in academia that millimeter wave (mmWave) communications appears as one of the most promising candidates for supporting extremely high data rates in the next generation wireless networks [1, 2, 19]. MmWave communications are particularly attractive for gigabit wireless applications such as gigabyte file transfer, wireless gigabit ethernet, wireless gaming, and uncompressed high definition video transmission. Due to the mmWave great commercial potential, several industry-led efforts and international organizations have emerged for their standardization in wireless personal and local area networks (WPANs and WLANs). Examples include IEEE 802.15.3c [13], IEEE 802.11ad [118], ECMA 387 [52], the WirelessHD consortium, and the wireless gigabit alliance (WiGig).

Special propagation features and hardware constraints of mmWave systems introduce many new challenges in the design of efficient physical, medium access control (MAC), and routing layers. The challenges become even more complex, as

in next generation wireless networks we envision the integration and coexistence of mmWave systems with more traditional communication standards working around the microwave frequencies of 2.4 GHz and 5 GHz, which is already possible with fall-back support of IEEE 802.11ad [118]. Directional communications with pencil-beam operation significantly reduces multiuser interference in mmWave networks. In the extreme case, multiuser interference no longer limits the network throughput, which results in a noise-limited network as opposed to conventional interference-limited networks.<sup>1</sup> This unique feature makes mmWave suitable for very dense deployments of infrastructure nodes and terminals.

The severe channel attenuation, vulnerability to obstacles, directionality of millimeter wave communications, the reduced interference footprint, and high signaling overhead demand a thorough reconsideration of traditional protocols, especially at the MAC layer, where signaling and resource allocation procedures need new architectures and algorithms able to cope with these unique challenges. MAC layer design considerations of mmWave networks in general and in mmWave cellular networks in particular are discussed in [2] and [22], respectively. In this paper, we focus on short range mmWave networks. The main differences between short range mmWave networks and mmWave cellular networks, reviewed in [22], are: (i) short-range networks may rely on carrier sensing among terminals, (ii) they have an ad hoc infrastructure, rather than a predefined infrastructure, (iii) they may use multihop communications, which may also affect traffic patterns, and (iv) WPAN/WLAN devices generally have much less capabilities compared to smart phones and base stations in cellular networks. Compared to [2], we cover the substantial new achievements on the performance analysis of short range mmWave networks to identify the main challenges of existing mmWave standards at the MAC layer. We highlight a new alignment-throughput tradeoff that should be optimized. We show that, contrary to mainstream belief, a mmWave network may exhibit both noise-limited and interference-limited regimes, challenging the efficacy of resource allocation protocols of existing standards and raising the necessity of new collision-aware hybrid resource allocation protocols. Then, we discuss the prolonged backoff time problem in mmWave networks with directional communication and propose a new MAC layer signal to alleviate this problem. We challenge the applicability of current mmWave MAC layer functions in dense deployment scenarios due to the significant mismatch between transmission rates of signaling and data packets, and highlight the need for an on-demand reactive control plane. Finally, we discuss the potential of multihop communication techniques to compensate the error-prone mmWave physical layer and to provide reliable mmWave connections. Throughout this paper, we identify critical MAC layer aspects of existing mmWave standards that may limit the efficacy and use cases of short range mmWave communications, and propose MAC design guidelines accordingly.

The rest of this paper is organized as follows. In Section B.2, we describe the

---

<sup>1</sup>Not being in an interference-limited regime does not necessarily imply that a network operates in a noise-limited regime, rather it only implies that the throughput per channel use is limited by the noise power. The network throughput performance, however, can be limited by other factors such as signaling overhead, as will be argued in Section B.4.

essential aspects of mmWave networks. In Section B.3, existing mmWave standards are briefly reviewed. Section B.4 investigates several MAC layer aspects of short range mmWave networks. Concluding remarks and future research directions are presented in Section B.5.

## B.2 Fundamentals

### B.2.1 The Directed mmWave Wireless Channel

MmWave communications use frequencies in the range 30–300 GHz, though the frequencies 6–30 GHz are also often referred to as mmWave [19]. The main characteristics of mmWave are high path-loss (i.e., the distance-dependent component of the attenuation), large bandwidth, short wavelength/high frequency, and high attenuation through most solid materials. Very small wavelengths allow the implementation of massive numbers of antenna elements in the current size of radio chips, which boosts the achievable directivity gain at the cost of some extra signal processing. Such a gain can largely or even completely compensate the high path-loss of mmWave systems without the need to increase the transmission power. Moreover, directional communications introduce the concept of directional spatial channel, that is, a channel can be established in a specific direction with a range that varies according to the directionality level.

### B.2.2 Beam-searching

The use of low-complexity and low-power mmWave devices, along with the massive number of antennas, make traditional digital beamforming based on instantaneous channel state information very expensive. Instead, the existing standards establish a mmWave link using analog beamforming (also called beam-searching) based on pre-defined beam steering vectors (beamforming codebook), each covering a certain direction with a certain beamwidth [1, 2, 13, 118]. Current standards suggest a three-stage beam-searching technique to reduce alignment overhead. After a quasi-omnidirectional (low resolution pattern) sweep, a coarse grained sector-level sweep (second level resolution pattern) is performed, followed by a beam-level refinement phase (the highest resolution pattern specified in the codebook). An exhaustive search over all possible transmission and reception directions is applied in each level through a sequence of pilot transmissions. The combination of vectors that maximizes the signal-to-noise ratio is then selected for the beamforming.

### B.2.3 Deafness and Blockage

Vulnerability to obstacles and directional communications in mmWave networks result in two consequences [2]: (1) deafness and (2) blockage. *Deafness* refers to the situation in which the main beams of the transmitter and the receiver do not point to each other, preventing the establishment of a directional communication link. Deafness introduces a time consuming beam-searching (alignment) procedure,

which complicates the link establishment phase. However, it substantially reduces multiuser interference [43], as the receiver listens only to a specific directed channel. *Blockage* refers to very high attenuation due to obstacles (e.g., 35 dB due to the human body [19]) that cannot be solved by just increasing the transmission power or increasing the directivity gain using narrower beams. Overcoming blockage requires a search for alternative directed mmWave channels that are not blocked, entailing a new alignment overhead.

Deafness and blockage are the main bottlenecks of mmWave communications at the MAC layer, requiring novel adaptive mechanisms in the protocol design.

### B.2.4 Control Channel

Many operations such as establishing a communication channel, discovering neighbors, exchanging routing information, and coordinating channel access rely on the exchange of signaling messages on a control channel. The characteristics of mmWave communications introduce fall-back and directionality tradeoffs, which also appear in mmWave cellular networks [22]. The *fall-back* tradeoff is the tradeoff between sending control messages through a mmWave or a microwave channel. The mmWave channel is subject to blockage, reducing the reliability of the control channel. A dedicated microwave control channel facilitates network synchronization and broadcasting at the expense of higher hardware complexity and energy consumption, since an extra transceiver should be tuned on the microwave control channel. The *directionality* tradeoff refers to the option of establishing a control channel in omnidirectional or directional operation modes. An omnidirectional control channel alleviates the deafness problem at the expense of being subject to a very short range, whereas a directional one increases the coverage with extra alignment overhead. Altogether, we may have two justifiable control channels: (1) omnidirectional-microwave, which is employed in ECMA 387, and (2) directional-mmWave,<sup>2</sup> which is employed in IEEE 802.15.3c and IEEE 802.11ad. The delay and coverage performance of these control channels are evaluated for a cellular context in [22]. Note that we may not necessarily adopt one type for all control messages; rather we can have a hybrid control plane. For instance, synchronization or channel access requests are transmitted in omnidirectional-microwave mode, and other control messages such as ACK or NACK operate in directional-mmWave mode.

## B.3 Standardization in mmWave Communications

In this section, we shortly review the recent IEEE standardization activities of mmWave MAC in the 60 GHz band for personal and local area networks. Broadly speaking, the standards define a network with one coordinator and several mmWave

<sup>2</sup>Note that realizing a control channel in the mmWave band with omnidirectional transmission and/or reception while having directivity gains for data transmission introduces a mismatch between the ranges at which a link with reasonable data rate can be established and the range at which control signals can be exchanged [22]. Such a mismatch substantially degrades the system performance.



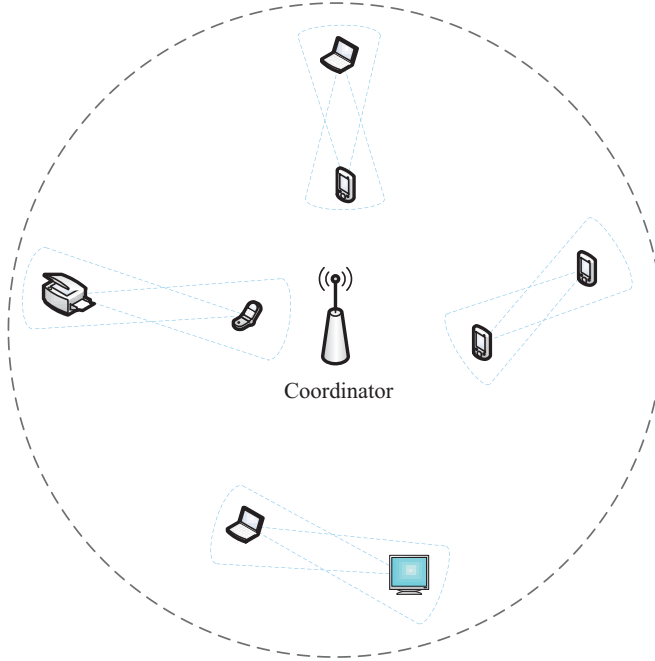


Figure B.1: Network architecture of existing mmWave WPAN and WLAN. The coordinator broadcasts synchronization commands and manages available resources.

devices.<sup>3</sup> The coordinator, which can be a device itself, is responsible for broadcasting synchronization beacons and managing radio resources. Figure B.1 shows a mmWave network with four directional links.

### B.3.1 Personal Area Networks: IEEE 802.15.3.c

The IEEE 802.15.3c standard [13] has been considered as one of the prominent MAC candidates to support mmWave wireless personal area networks, known as piconets. Supporting up to 5.78 Gbps data rate, it enables several applications such as high speed internet access, streaming content, video on demand, and high definition TV.

Among a group of devices, one will be selected as piconet coordinator (PNC), broadcasting beacon messages. Time is divided into successive super-frames, each consisting of three portions: beacon, contention access period (CAP), and channel time allocation period (CTAP), as shown in Figure B.1(a). In the beacon, the coordinator transmits an omnidirectional or multiple quasi-omnidirectional beacons to facilitate the discovery procedure. In the CAP, devices contend to register their

<sup>3</sup>ECMA 387 supports distributed network architecture as well [52].

Beacon	CAP	CTAP			
		CTA	CTA	...	CTA

(a) Superframe of IEEE 802.15.3c

BHI			DTI			
BTI	A-BFT	ATI	CBAP/SP	CBAP/SP	...	CBAP/SP

(b) Beacon interval of IEEE 802.11ad

Figure B.2: Network timing structure of existing IEEE mmWave standards. In IEEE 802.15.3c, beacon messages are transmitted in beacon. Channel access requests are made in CAP and served in CTAP using TDMA. Similar procedures are adopted in IEEE 802.11ad.

channel access requests at the PNC, based on carrier sense multiple access with collision avoidance (CSMA/CA). Although some devices with low QoS requirements may use this period for data transmission, PNC serves requests with high QoS demands, registered in CAP, during CTAP. Resource allocation in CTAP is based on time division multiple access (TDMA). CTAP consists of several channel time allocations (CTAs), serving data transmission with guaranteed QoS level.

### B.3.2 Local Area Networks: IEEE 802.11ad

IEEE 802.11ad adds modifications to the IEEE 802.11 physical and MAC layers to enable mmWave communications at 60 GHz. It provides up to 6.7 Gbps data rate using spectrum bands of 2.16 GHz over a short range. IEEE 802.11ad supports many applications including uncompressed high-definition multimedia transmissions and wireless docking stations.

IEEE 802.11ad defines a network as personal basic service set (PBSS) with one coordinator, called PBSS control point (PCP), and several stations. A superframe, called beacon interval, is divided into beacon header interval (BHI) and data transfer interval (DTI). BHI consists of beacon transmission interval (BTI), association beamforming training (A-BFT), announcement transmission interval (ATI). DTI consists of contention-based access period (CBAP) or service period (SP). In BTI, PCP transmits directional beacon frames that contain basic timing for personal BSS, followed by beamforming training and association to PCP in the A-BFT period. AT is allocated for request-response services where PCP sends information to the stations. Depending on the required QoS level, a device will be scheduled in the CBAP to transmit data using CSMA/CA, or in the SP to access using contention-free TDMA. This schedule is announced to the participating stations prior to the start of DTI. Figure B.1(b) illustrates generic timing segmentation of a superframe in IEEE 802.15.3c and a beacon interval in IEEE 802.11ad.

## B.4 Main Issues for MAC Design

In this section, we discuss the main MAC design issues that arise in mmWave communications, and state the weaknesses of the current solutions, including existing standards, when they are applied to support next generation short range wireless communications.

### B.4.1 Alignment-Throughput Tradeoff

The existing standards adopt beam-searching, as a low-complexity alternative to digital beamforming, to overcome the deafness problem while providing the required directivity gain. Beam-searching introduces an alignment overhead, which depends on the number of directions that have to be searched, which in turn depends on the selected transmission and reception beamwidths. For a given beamwidth, [119] suggests a new technique based on Rosenbrock search as a replacement for the two-stage exhaustive search to reduce the alignment overhead by up to 65% for a given operating beamwidth.

Besides choosing more efficient search procedures, we need to optimize the operating beamwidth, as claimed in [57]. Narrower beamwidths increase the search granularity, thus the alignment overhead, but provide a higher transmission rate due to higher directivity gains and lower interference footprint. Adopting larger beamwidths speeds up the search process at the expense of a degraded transmission rate. This introduces an alignment-throughput tradeoff [57]. The tradeoff shows that using extremely narrow beams (or excessively increasing the beamforming codebook size) is not beneficial in general due to the increased alignment overhead, and there is an optimal beamwidth (optimal codebook size) at which the tradeoff is optimized [57].

### B.4.2 Transitional Behavior

Directional communications with pencil-beam operation significantly reduces multiuser interference in mmWave networks. An interesting question is whether a mmWave network is noise-limited, as opposed to conventional interference-limited networks. This is a fundamental question at the MAC layer that affects the design principles of almost all MAC layer functions. For instance, as the system goes to the noise-limited regime, the required complexity for proper resource allocation and interference avoidance functions at the MAC layer is substantially reduced [69]. Instead, pencil-beam operation complicates negotiation among different devices in a network, as control message exchange may require a time consuming alignment procedure between transmitter and receiver [22]. In the extreme noise-limited case, sending expensive collision avoidance signals such as RTS and CTS in a network with negligible collision probability may be unjustifiable, as stated in Section B.4.4. The seminal work in [43] confirms the feasibility of a *pseudowired* (noise-limited) abstraction in outdoor mmWave mesh networks. However, as shown in [57], activating all links may cause a significant performance drop compared to the optimal resource

allocation in dense deployment scenarios due non-negligible multiuser interference. Further, the comprehensive analysis of [69] illustrates that mmWave networks may not be necessarily noise-limited; rather they show a *transitional behavior*, from a noise-limited to an interference-limited regime.

To have a better understanding on multiuser interference-level, and thereby on proper resource allocation strategies for mmWave networks with transitional behavior, we compare the average throughput of a link, the network throughput, and the delay performance of slotted ALOHA to those of TDMA –a simple collision-based versus a simple collision-free protocol– in a mmWave ad hoc network. We define delay as the difference between the time a new packet is inserted into the transmission queue of the transmitter and the time it is correctly received at the receiver. Both slotted ALOHA and TDMA use the same directionality level. We simulate a mmWave WPAN with a random number of mmWave aligned links (aligned transmitter-receiver pairs), all operating with the same beamwidth. The number of links is a Poisson random variable with density  $\lambda_l$  per unit area. They are uniformly distributed in a  $10 \times 10 \text{ m}^2$  area and operate at 60 GHz. For slotted ALOHA, in a given time slot, every link will be active with probability  $p$ . Active links are transmitting with power 2.5 mW. We also uniformly distribute a random number of obstacles with density 0.25 (on average 1 obstacle in a  $2 \times 2 \text{ m}^2$  area) in the environment. The obstacles are in the shape of lines with random orientation and their length is uniformly distributed between 0 and 1 m. Attenuation due to an obstacle is -30 dB, path-loss exponent is 3, and the minimum required SNR at the receiver is 10 dB. Every transmitter generates traffic with constant bit rate (CBR) 300 Mbps, the size of all packets is 10 kB, time slot duration is  $25 \mu\text{s}$ , transmission rate is 1 packet per slot (link capacity around 3 Gbps), the transmitters have infinite buffer to save and transmit the packets, and the emulation time is 1 second.

Figure B.3 illustrates several performance aspects of slotted ALOHA and TDMA. Assuming transmission of one packet per slot, Figure B.3(a) shows the average throughput of a link as a function of the transmission probability. For relatively not-so-dense networks, for instance, 1 transmitter in a  $2 \times 2 \text{ m}^2$  area ( $\lambda_l = 0.25$ ), increasing the transmission probability is always beneficial due to the small multiuser interference level. As the link density increases, the negative effect of a higher transmission probability (higher multiuser interference) overweighs its positive effect (more aggressive transmission). In a very dense network, for instance, with  $\lambda_l = 4$ , we should adopt a very small transmission probability to maximize the throughput of a link. Figure B.3(b) shows the behavior of the optimal transmission probability that maximizes the throughput as a function of link density and operating beamwidth. From the figure, we can observe that in many cases, the optimal transmission probability is 1, implying that we can simply activate all links with no penalty for the average link throughput (noise-limited regime). However, as the operating beamwidth or the link density increases, we should activate fewer links through reducing the transmission probability to decrease the high contention level inside the network (interference-limited regime).

Figs. B.3(c) and B.3(d) compare the performance slotted ALOHA to TDMA. Specifically, Figure B.3(c) reports the maximum throughput of a link in slotted

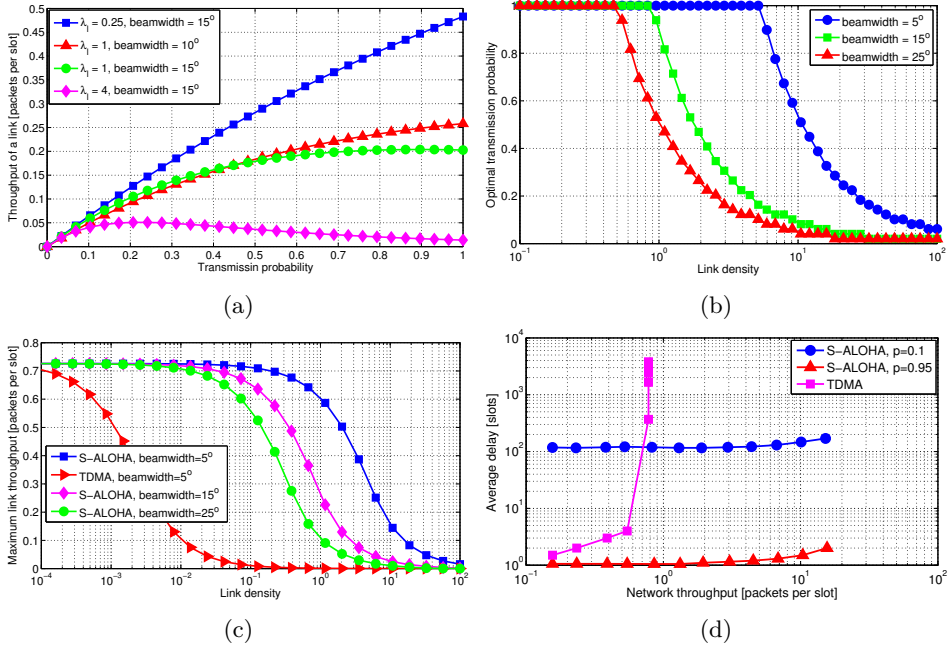


Figure B.3: Performance comparison of slotted ALOHA and TDMA in mmWave WPANs. “S-ALOHA” stands for slotted ALOHA,  $\lambda_l$  is the link density, and  $p$  is the transmission probability in slotted ALOHA. Different points of (d) represent different link densities from 0.02 to 2 links per unit area. Operating beamwidth in (d) is  $10^\circ$ . Increasing the link density may reduce the link throughput, increase the network throughput, and increase the delay. Slotted ALOHA significantly outperforms TDMA in terms of link throughput, network throughput, and delay performance. On the other hand, TDMA guarantees no collision on the communication.

ALOHA, associated with the optimal transmission probability in Figure B.3(b), and Figure B.3(d) shows the network throughput against the corresponding average delay obtained by changing the link density. First, neglecting the alignment overhead, the throughput of a link in slotted ALOHA will decrease with the operating beamwidth, due to higher collision probability. Moreover, TDMA activates one link at a time—orthogonal use of time resources—irrespective of the number of links. Considering the traffic generation rate of this example, which is 0.1 of the link capacity, the network will be saturated roughly with 10 links, and further increasing the number of links will not improve the network throughput (see Figure B.3(d)),<sup>4</sup> but reduces the time share of every link and consequently reduces the average throughput of a link, see Figure B.3(c). Besides, every link experiences a

<sup>4</sup>The network throughput of TDMA is up to 1 packet per slot. This upper bound is achieved if there is no obstacle in the environment.

higher delay to access the channel and transmit its data, see different points of the TDMA curve in Figure B.3(d). Note that with a fixed packet generation rate, the *effective link capacity* (link capacity multiplied by its time share) of every link in TDMA reduces with the number of links in the network, so the queues of the transmitter may become unstable. Instead, slotted ALOHA leverages small multiuser interference and re-uses time resources (spatial gain). The network can handle more traffic due to a higher effective capacity. From Figure B.3(d), slotted ALOHA significantly outperforms TDMA in terms of both network throughput and delay, all possible due to significant spatial gain. However, unlike slotted ALOHA, TDMA can guarantee communication with no collision, which may be of importance in some applications. Also, Figure B.3(c) explicitly discloses the transitional behavior of mmWave ad hoc networks. Increasing the link density will not initially affect the average throughput of a given link due to negligible multiuser interference; however, the throughput will rapidly drop with link density once the network transits to the interference-limited regime. The transitional region depends on the density of the transmitters, the density and the average size of the obstacles, and the operating beamwidth, among the main parameters.

The transitional behavior of mmWave networks shows the inefficacy of existing standards and suggests a dynamic incorporation of both contention-based and contention-free phases in the resource allocation. Current mmWave standards, such as IEEE 802.15.3c and IEEE 802.11ad, adopt the existing resource allocation approaches that were originally developed for interference-limited microwave networks. In particular, the network traffic is mostly served in the contention-free phase even in a noise-limited regime. We can (should) leverage the transitional behavior of mmWave networks and dynamically serve the network traffic partially on the contention-based and partially on the contention-free phase. Using a flexible phase duration, adjusted according to the collision level of the network, we can reduce the use of inefficient contention-free phase, improve the network throughput (especially as the network goes to the noise-limited regime), and also guarantee communication without collisions.

### B.4.3 Prolonged Backoff Time

Suppressing interference in mmWave networks with pencil-beam operation comes at the expense of complicated link establishment. Traditional CSMA/CA fails to provide efficient multiple access for mmWave systems [43], since it had been originally developed for omnidirectional transmissions. To elaborate, assume that a mmWave transmitter tries to access the channel by sending an RTS message after the backoff timer expires (see Scenario 3 in Figure B.4). The receiver does not hear the RTS due to deafness or blockage, and therefore does not send the CTS message. The traditional CSMA/CA protocol assumes that a collision occurred and therefore increases the backoff time exponentially. In mmWave, this is the wrong decision, which may lead to a *prolonged backoff time*. Similar issues may also exist in the random access phase of mmWave cellular networks, as mentioned in [22].

To enhance the performance of CSMA/CA in directional communications, [120]

modifies traditional CSMA/CA such that each device exponentially increases the contention window size upon a missing ACK, while this increment is linear with each missing CTS. Although this proposal is better than the original CSMA/CA in the sense that different events demand different actions, it fails to solve the prolonged backoff time in mmWave systems. In fact, blockage, deafness, and collision, which are caused by different physical reasons, deserve a different handling at the MAC layer, a fact that is totally ignored in [120]. This problem may be alleviated by introducing additional signaling messages for establishing a mmWave link.

A simple scheme, illustrated in Figure B.4, may work as follows. After sending a directional (or omnidirectional) RTS to a receiver that is ready to receive, three possible scenarios might occur.

- Scenario 1 (success): The transmitter receives a CTS before timeout. Then, it extracts the beamforming information from the CTS and starts transmission based on the CSMA/CA mechanism.
- Scenario 2 (collision): The receiver fails to decode the RTS due to a collision. It sends a collision-notification (CN) signal. Upon receiving the CN message, the transmitter knows that there is a contention to access this channel in this direction, and therefore sends another RTS after running the backoff procedure.
- Scenario 3 (deafness or blockage): The transmitter does not receive a CTS nor a CN. In this case, after timeout, it knows that there is either deafness or blockage. Hence, it tries to find another directed spatial channel instead of running an unnecessary backoff.

Note that the energy that the mmWave receiver will observe in a collision state with multiple simultaneous received signals is substantially higher than that in the deafness state with no received signal. Therefore, a simple hard decision based on the received energy (energy detector) would be enough to distinguish collisions from deafness. Thanks to the CN signal, the transmitter can sense the presence of contention in the channel and take the proper action to avoid the prolonged backoff time, which is the result of deafness and blockage, and not of contention on the channel.

We simulate a network with a Bernoulli link failure model, that is, every link fails due to blockage independently and with constant blockage probability. Figure B.5 shows the performance enhancement due to the introduction of CN. With a blockage probability of 0.02, for instance, the average backoff time will be dramatically decreased by about 95% (twenty times) if CN is used.

#### B.4.4 Reactive Control Plane

Current collision avoidance mechanisms suggest that a network with uncoordinated users will benefit by accepting collisions on tiny signaling packets such as request-to-send (RTS) and clear-to-send (CTS) to avoid retransmission of large

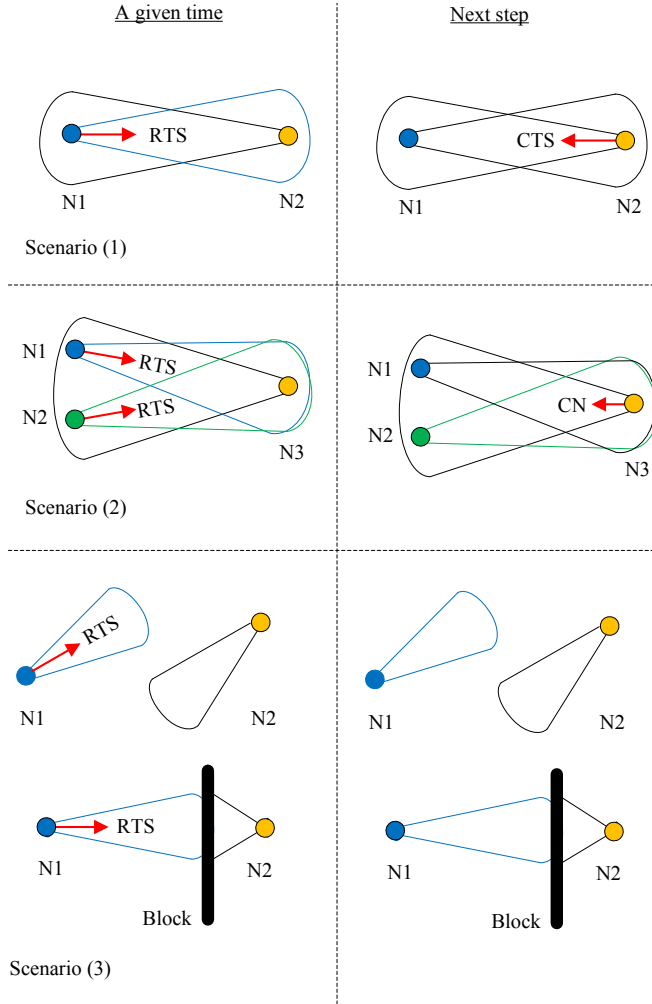


Figure B.4: A simple protocol for mitigating prolonged backoff time. For a given time, in Scenario 1, device N2 detects an RTS. The next step is to send a CTS signal by device N2 to reserve the channel for the communication. In Scenario 2, device N3 receives more than one RTS at the same time. It sends a CN signal to let the transmitters run the backoff procedure. In Scenario 3, device N2 will not receive the RTS of device N1 due to either deafness or blockage, and it will be silent at the next step.

data packets. To increase the robustness of signaling messages, current mmWave standards transmit control packets at much lower rate compared to the data packets. IEEE 802.11ad, for instance, supports a peak transmission rate of 27.7 Mbps



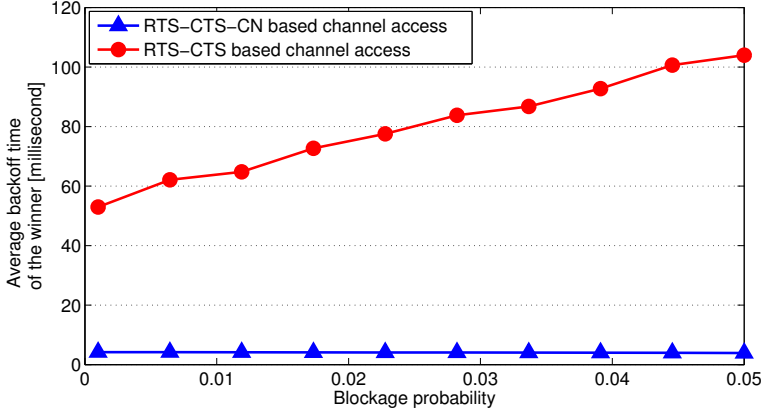


Figure B.5: Average backoff time of the device winning the contention among 20 devices for accessing the same transmission resource (frequency and direction). Standard RTS-CTS based negotiation leads to unnecessarily prolonged backoff time, while a slight modification of this standard negotiation, by introducing CN, effectively mitigates the problem.

for control and 6.7 Gbps for data packets [118]. This significant mismatch between transmission rates of control and data packets substantially increases the cost of collision avoidance procedures and challenges the efficacy of current mmWave standards in handling packets with short size. To illustrate this inefficiency, we provide the following example.

Let  $t_i$  be the time required to transmit message  $i$ . With negligible propagation and queuing delays and with no collision on a directed spatial channel, the current CSMA/CA protocol introduces the following delay to transmit a payload:  $3t_{\text{SIFS}} + t_{\text{RTS}} + t_{\text{CTS}} + t_{\text{DIFS}} + t_{\text{DATA}} + t_{\text{ACK}}$ , where  $t_{\text{DATA}} = t_{\text{header}} + t_{\text{payload}}$ . Note that the transmitter should wait for a SIFS duration before sending every RTS, CTS, and ACK, and wait for a DIFS duration before every regular data frame. In IEEE 802.11ad,  $t_{\text{SIFS}} = 2.5 \mu\text{s}$  and  $t_{\text{DIFS}} = 6.5 \mu\text{s}$ . Considering 20 Bytes for RTS, CTS, and ACK messages, we have  $t_{\text{RTS}} = t_{\text{CTS}} = t_{\text{ACK}} = 5.5 \mu\text{s}$ . Every data packet contains an 8-Byte header, which should be transmitted at 27.7 Mbps, so  $t_{\text{header}} = 2.2 \mu\text{s}$ . To transmit 10 KBytes of payload, we need only  $t_{\text{DATA}} = 13.6 \mu\text{s}$ , while the total delay is  $44.1 \mu\text{s}$ , leading to 30% channel utilization. This inefficiency increases as the size of the payload reduces, for instance, only 9.8% channel utilization for 1 KByte of payload. This means that CSMA/CA consumes more than 90% of the time resources only to ensure avoidance of collisions even in a noise-limited scenario. This inefficient handling of packets with short size hinders the applicability of current mmWave technology solutions (with Gbps data rate and small interference footprint) to massive wireless access scenarios where we have frequent transmissions of packets with small payloads. In fact, the huge overhead of having an unnecessary proactive collision avoidance protocol may be one of the

main bottlenecks of future applications of mmWave networks.

Significant mismatch between transmission rates of control and data packets, along with reduced average collision probability in mmWave networks, demands development of new MAC layer protocols with on-demand and minimal use of signaling. Note that proactive transmission of some vital control signals, such as beam-searching pilots for avoiding deafness, may still be mandatory. These mandatory control overheads may limit delay/channel utilization performance and therefore the applicability of mmWave networks to use cases with sporadic infrequent transmissions of small payloads. This suggests the existence of a minimal payload size to make establishment of a costly mmWave link beneficial.

#### B.4.5 Directional-mmWave Control Channel

A directional mmWave control channel is an inseparable part of mmWave networks to realize efficient channel estimation, coherent demodulation, association to coordinator, and spatial synchronization. To implement a directional-mmWave control channel, two possible solutions are available, as illustrated in Figure B.6: time splitting and resource table. In the *time splitting* approach, which is adopted by the current standards, a time slot is divided into signaling and data phases, see Figure B.2(b). During the signaling phase, each terminal overhears the control messages in all (some) directions, in order to be aware of the network status. Then, transmissions are performed in the data phase. [121] suggests that the network coordinator operates in the omnidirectional mode by activating all its beams during the signaling phase, and uses only one beam for data transmission in the next phase. Although the time splitting approach offers a simple protocol and facilitates realization of simple TDMA collision-free transmissions, tight synchronization is required and a large portion of the available time-frequency-space resources that are wasted for the signaling phase cannot be used for data transmission. On the other hand, in the *resource table* approach, each transmitter estimates the topology of the network in a neighbor discovery phase. Then, it creates a table of proper spatial resources (directions) based on the feedback received from previous transmission attempts (piggybacking over data transmissions). The table is updated upon every received feedback, and each transmitter tries to communicate with other devices using the most updated table. The resource table approach can be implemented in a distributed manner with a directional-mmWave control channel, making this approach suitable for mmWave ad hoc networks.

#### B.4.6 Multihop Communications

Multihop communications is a solution for range extension and for blockage [2, 88, 122]. In [122], range extension using a relay node is investigated for an outdoor sport broadcasting system. Extensive analysis demonstrated that high quality live videos of 10 sources can be efficiently transmitted over 300 m. Besides range extension, [88] showed that having an alternative path using relay node(s) can significantly alle-

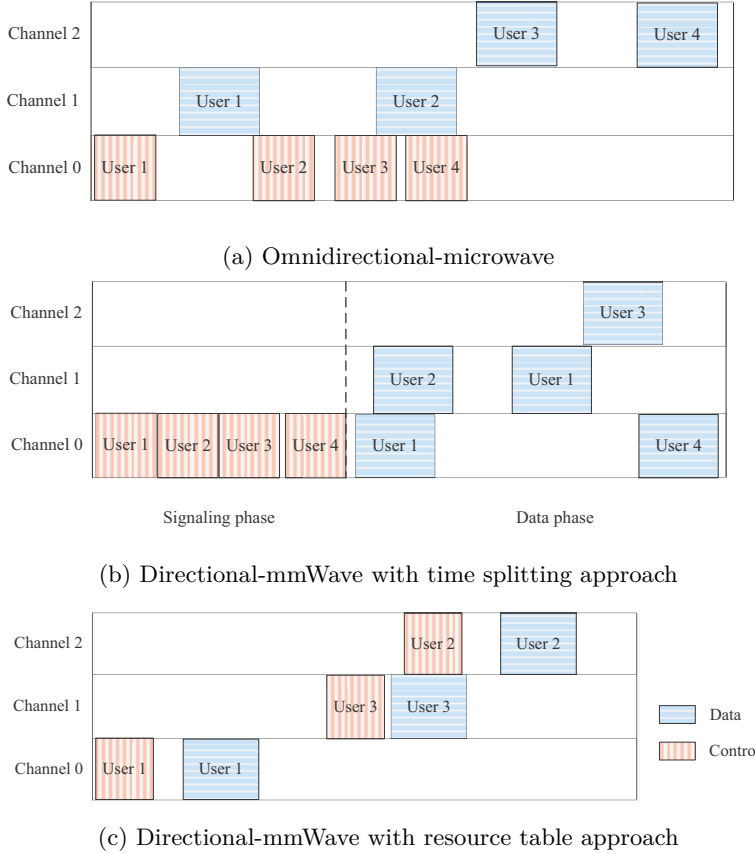


Figure B.6: Different options to realize a control channel in mmWave WPANs/WLANs. Channel 0 in (a) is on microwave frequencies, channels 1 and 2 are on mmWave frequencies. Omnidirectional-microwave control channel requires two radios to manage signaling and data transmissions, but facilitates the exchange of control messages. In the time splitting approach, all the devices perform negotiation in the signaling phase, and then the available resources are reserved for the devices in the data phase. In the resource table approach, a distributed implementation with minimal overhead is available. Fall-back support enables users to transmit on the microwave frequencies if there is no channel on the mmWave frequencies.

viate blockage. The backup paths are recorded in the coordinator and established upon blockage on the direct path, increasing connectivity to about 100%.

Unfortunately, current standards support only single- or two-hop links with a relay node rather than a complete multihop communications capability.<sup>5</sup> Having a

<sup>5</sup>IEEE 802.15.3c supports only single-hop communications, while ECMA 387 and

reliable control channel is the most challenging part of multihop mmWave communications. An omnidirectional-microwave control channel along with a directional data channel can be a simple and practical solution. A joint routing and scheduling approach is necessary here to leverage the low interference footprint in mmWave communications using scheduling, while guaranteeing connectivity using routing protocols.

## B.5 Conclusions

Millimeter wave (mmWave) communication systems are promising solutions to provide extremely high data rate and support massive uncoordinated access in next generation wireless networks. Severe channel attenuation, blockage, and deafness, along with reduced interference footprint, differentiate mmWave systems from legacy systems that operate at microwave frequencies. MmWave networks may face alignment-throughput tradeoff, huge overhead of control packets, transitional behavior, and prolonged backoff time. This paper discussed how the MAC layer functions of existing mmWave standards are not effective in addressing these new challenges. It was argued that new collision-aware hybrid resource allocation, collision notification signal, on-demand control packets, and multihop communication are required, which are very interesting future research directions in the area of short range mmWave networks.

Moreover, while the average collision probability is derived in [43, 69], the distribution of the number of links in the same collision domain (links with strong mutual interference) is an open problem. This distribution clarifies the number of mmWave devices that can be supported in the network with predetermined QoS level, helps in designing efficient retransmission policies, and reveals if reactive execution of a random backoff procedure is a better option than proactive executions of collision avoidance mechanisms in mmWave networks.

---

IEEE 802.11ad support also two-hop communications.

---

# Beam-searching and Transmission Scheduling in Millimeter Wave Communication

---

Hossein Shokri-Ghadikolaei, Lazaros Gkatzikis, and Carlo Fischione

in Proc.  
*IEEE International Conference on Communications (ICC), 2015*

©2015 IEEE

The layout has been revised.

# Beam-searching and Transmission Scheduling in Millimeter Wave Communications

Hossein Shokri-Ghadikolaei, Lazaros Gkatzikis, and Carlo Fischione

## Abstract

Millimeter wave (mmWave) wireless networks rely on narrow beams to support multi-gigabit data rates. Nevertheless, the alignment of transmitter and receiver beams is a time-consuming operation, which introduces an alignment-throughput tradeoff. A wider beamwidth reduces the alignment overhead, but leads also to reduced directivity gains. Moreover, existing mmWave standards schedule a single transmission in each time slot, although directional communications facilitate multiple concurrent transmissions. In this paper, a joint consideration of the problems of beamwidth selection and scheduling is proposed to maximize effective network throughput. The resulting optimization problem requires exact knowledge of network topology, which may not be available in practice. Therefore, two standard-compliant approximation algorithms are developed, which rely on underestimation and overestimation of interference. The first one aims to maximize the reuse of available spectrum, whereas the second one is a more conservative approach that schedules together only links that cause no interference. Extensive performance analysis provides useful insights on the directionality level and the number of concurrent transmissions that should be pursued. Interestingly, extremely narrow beams are in general not optimal.

## C.1 Introduction

Millimeter wave (mmWave) communications appear as a promising option to meet the ever growing demand for multi-gigabit data rates. MmWave communications refer to the electromagnetic spectrum between 30 and 300 GHz, which corresponds to wavelengths from 10 mm to 1 mm. Small wavelength facilitates the integration of numerous antenna elements in the current size of radio chips, which in turn promises a significant directivity gain. The main characteristics of mmWave are directionality, large bandwidth, but also high attenuation [19].

MmWave has been considered lately by several standardization bodies as an ideal candidate for short range communications. Specifically, IEEE 802.15.3 task group 3c [13] works on the development of high rate wireless personal area networks (WPAN), whereas IEEE 802.11ad task group [14] focuses on wireless local area networks (WLAN). In both standards, one of the network devices is assigned the role of the coordinator, who schedules transmissions in a centralized manner. In particular, channel access is determined through a hybrid carrier sense multiple access/collision avoidance (CSMA/CA) and time division multiple access (TDMA)

scheme. A superframe consists of three phases. A beacon period, a contention access period, where devices compete to register their channel access requests to the coordinator, and a channel time allocation period, which is further divided into several time slots and each is assigned to a *single* transmitter-receiver pair. The existing standards do not exploit the full potential of mmWave communications. In fact, high data rates are achieved due to the high signal-to-noise ratio (SNR), which is a result of directional communications, and the extended bandwidth availability in mmWave bands. Pencil beams, however, promise extensive frequency reuse while simplifies interference management [43].

In this paper, we suggest that efficient transmission scheduling mechanisms could significantly improve network throughput (spectral efficiency), by scheduling multiple transmissions at the same time slot, as long as they do not cause harmful interference to each other. The level of interference depends also on the selected beamwidths, which in turn determine the time required for alignment of transmitter and receiver beams. Thus, an alignment-throughput tradeoff is introduced. A narrower beamwidth leads to significant alignment overhead, since many directions have to be searched, but provides a higher transmission rate due to higher directivity gains and lower interference. Larger beamwidths speed up alignment process at the expense of reduced transmission rate. In order to address those problems, we propose a joint formulation of the beamwidth selection and transmission scheduling problems in mmWave communications, and analyze the impact of each of the system parameters on network throughput.

### C.1.1 Related Work

A main issue in mmWave communications is deafness, which is a direct consequence of directional transmission and reception. It occurs when the main beams of a transmitter and the intended receiver are not aligned. To address this issue, a beam-searching procedure has been proposed to establish a communication link [119]. In this case, an exhaustive search over all possible combinations of transmission and reception directions is performed through a sequence of pilot transmissions. In fact, mmWave devices adopt analog beamforming, also called beam-searching, using simple phase shifters, rather than a complex digital beamforming based on instantaneous channel state information. The latter would impose formidable complexity due to the large number of antennas in mmWave [19]. Beam-searching introduces an alignment overhead, i.e., the time required to find the best beams. This overhead is proportional to the number of directions that have to be searched, which in turn depends on the selected transmission and reception beamwidths. Current standardization activities [13, 14] suggest a two-stage beam-search technique, to reduce alignment overhead and power consumption. Initially, a coarse grained sector-level sweep is performed, followed by a beam-level alignment phase. An exhaustive search over all possible transmission and reception directions is applied in each level. For a given beamwidth (fixed granularity of searching), [119] suggests a new search technique as a replacement of the two-stage exhaustive search to reduce the alignment overhead. Here, we suggest that the alignment-throughput tradeoff



should be addressed by optimizing beamwidth per se. Thus, our work and [119] are complementary.

The option of concurrent transmissions scheduling to optimally exploit the directionality of mmWave communications was proposed only recently. The authors of [123] consider the problem of maximizing the number of scheduled flows such that their quality of service requirement is not violated. A greedy scheduling scheme is proposed, where in each time slot an additional link is activated if its contribution to total throughput is positive, i.e., throughput gain from this additional link is larger than the interference caused. A similar greedy heuristic is proposed in [124], where a priority ordering of links is assumed. Additional links are activated according to this priority order and as long as signal-to-interference-plus-noise ratio (SINR) at all receivers exceeds a threshold. The main issue of those approaches is that they are reactive protocols, i.e., a link has to be activated to deduce if it is compatible with other transmissions. Instead, here we demonstrate that directionality and high attenuation in mmWave communications can be exploited to derive accurate scheduling mechanisms.

### C.1.2 Our Contribution

The main contributions of this paper are summarized into the following

- We identify the tradeoffs and the corresponding controls that differentiate mmWave from other communication technologies.
- We provide a unifying optimization-based framework that brings together beam-searching and transmission scheduling and explicitly addresses the major challenges of mmWave communications, namely deafness and interference management. We show that using extremely narrow beams (or equivalently excessively increasing the beamforming codebook size) is not beneficial in general due to the increased alignment overhead.
- We demonstrate how the proposed framework can be translated into protocols that extend the capabilities of existing standards.
- We evaluate the performance gains arising from the proposed protocols. Our performance analysis provides useful insights on the directionality level and the number of concurrent transmissions that should be pursued.

## C.2 System Model and Problem Formulation

Consider a mmWave network consisting of one coordinator and  $N$  transmitter-receiver pairs (links). As shown in Figure C.1, a time slot consists of two phases: *i*) alignment and *ii*) data transmission. Without loss of generality, we assume that sector-level alignment has been established prior to the alignment phase, i.e., as a part of routing [88]. In the first phase, the transmitter and receiver of each link  $i$  have to decide on the optimal refined beams within their sectors, by searching over

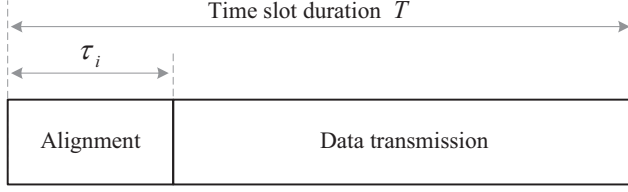


Figure C.1: The time slot segmentation of link  $i$ . Increasing alignment time  $\tau_i$  reduces time available for data transmission, but increases achievable rate.

all possible combinations to find the one of maximum SNR. This exhaustive search is compliant with IEEE 802.15.3c.

### C.2.1 Alignment Overhead

Let  $T_p$  denote the time required for a pilot transmission, which has to be performed for every possible direction, and  $\{\psi_i^t, \varphi_i^t\}$  and  $\{\psi_i^r, \varphi_i^r\}$  be sector-level and beam-level beamwidths at the transmitter and receiver sides of link  $i$ , respectively. Therefore, under exhaustive search, the total duration of this searching (alignment) procedure within a given sector is

$$\tau_i(\varphi_i^t, \varphi_i^r) = \left\lceil \frac{\psi_i^t}{\varphi_i^t} \right\rceil \left\lceil \frac{\psi_i^r}{\varphi_i^r} \right\rceil T_p, \quad (\text{C.1})$$

where  $\lceil \cdot \rceil$  is the ceiling function, returning the smallest following integer, since the number of pilots has to be integer. In practice, we may adopt different beam-search strategies; however, the proposed framework can still be applied by revising (C.1). Once the optimal directions for transmission and reception have been determined, the communication link can be established, and the data transmission phase starts. We assume that after the alignment procedure, any transmitter/receiver pair finds a path to establish data communications, e.g., through a reflection if the direct link is not available. By discarding the noncontinuous ceiling function, we derive a continuous approximation of alignment time  $\tau_i$ . The latter cannot exceed total time slot duration  $T$ , and hence a lower bound on feasible beamwidths can be derived:

$$\varphi_i^t \varphi_i^r \geq \frac{T_p}{T} \psi_i^t \psi_i^r. \quad (\text{C.2})$$

Besides, since alignment takes place within the sector-level beamwidths, we have  $\varphi_i^t \leq \psi_i^t$  and  $\varphi_i^r \leq \psi_i^r$ .

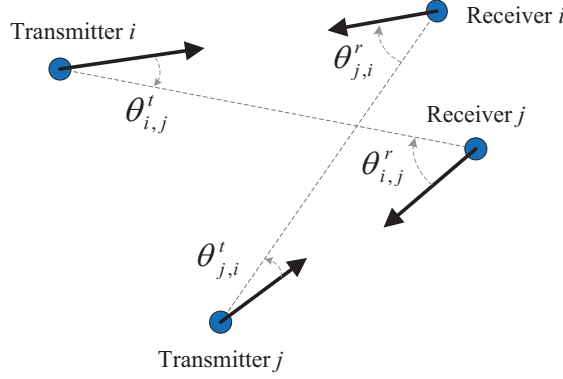


Figure C.2: Illustration of the angles between transmitters and receivers  $\theta_{i,j}^t$  and  $\theta_{i,j}^r$ . Solid arrows correspond to the boresight directions.

### C.2.2 Effective Transmission Rate

Let  $g_{i,j}^c$  denote channel gain between transmitter of link  $i$  and receiver of link  $j$  (in short, transmitter  $i$  and receiver  $j$ ), capturing both path loss and block fading,  $n$  be the power of white Gaussian noise, and  $p_i$  be the transmission power of transmitter  $i$ . Table C.5 summarizes the main notations used throughout the paper. For analytical tractability, we approximate the actual antenna patterns by a sectored antenna model [92]. This simple model captures directivity gains, the front-to-back ratio, and the halfpower beamwidth, which are considered the most important features of an antenna pattern. In ideal sector antenna pattern, the gains are a constant for all angles in the main lobe, and equal to a smaller constant in the side lobe. Let  $\theta_{i,j}^t$  and  $\theta_{i,j}^r$  be the angles between transmitter  $i$  and receiver  $j$  relative to their respective boresight directions (see Figure C.2). Let  $g_{i,j}^t$  and  $g_{i,j}^r$  be the transmission and reception gains at transmitter  $i$  and receiver  $j$  toward each other. Then,

$$g_{i,j}^t(\theta_{i,j}^t, \varphi_i^t) = \begin{cases} \frac{2\pi - (2\pi - \varphi_i^t)z}{\varphi_i^t}, & \text{if } |\theta_{i,j}^t| \leq \frac{\varphi_i^t}{2} \\ z, & \text{otherwise} \end{cases}, \quad (\text{C.3})$$

and

$$g_{i,j}^r(\theta_{i,j}^r, \varphi_j^r) = \begin{cases} \frac{2\pi - (2\pi - \varphi_j^r)z}{\varphi_j^r}, & \text{if } |\theta_{i,j}^r| \leq \frac{\varphi_j^r}{2} \\ z, & \text{otherwise} \end{cases}, \quad (\text{C.4})$$

where  $0 \leq z \ll 1$  is the gain in the side lobe. The gain in the main lobe can be derived by fixing the total radiated power of the antennas over parameter space of  $z$ ,  $\varphi_i^t$ , and  $\varphi_j^r$ . Then, the received power at receiver  $j$  from transmitter  $i$  is  $p_i g_{i,j}^t g_{i,j}^c g_{i,j}^r$ ,

Table C.5: Summary of main notations

Symbol	Definition
$T$	Time slot duration
$T_p$	Pilot transmission time
$N$	Number of links
$\text{SINR}_i$	Signal-to-interference-plus-noise ratio of link $i$
$\theta_{i,j}^t$	Angle between transmitter $i$ and receiver $j$ relative to transmitter boresight direction
$\theta_{i,j}^r$	Angle between receiver $j$ and transmitter $i$ relative to receiver boresight direction
$\varphi_i^t$	Beam-level transmitter beamwidth of link $i$
$\varphi_i^r$	Beam-level receiver beamwidth of link $i$
$\psi_i^t$	Sector-level transmitter beamwidth of link $i$
$\psi_i^r$	Sector-level receiver beamwidth of link $i$
$p_i$	Transmission power of transmitter $i$
$\tau_i$	Alignment delay
$g_i^t$	Antenna gain at transmitter $i$
$g_j^r$	Antenna gain at receiver $j$
$g_{i,j}^c$	Channel gain between transmitter $i$ and receiver $j$

which depends on  $p_i$ ,  $\varphi_i^t$ , and  $\varphi_j^r$ . SINR at receiver of link  $i$  is

$$\text{SINR}_i = \frac{p_i g_{i,i}^t g_{i,i}^c g_{i,i}^r}{\sum_{\substack{k=1 \\ k \neq i}}^N p_k g_{k,i}^t g_{k,i}^c g_{k,i}^r + n}. \quad (\text{C.5})$$

We assume that interference can be treated as noise at each receiver  $i$ , implying that, according to Shannon formula, link  $i$  can achieve a rate of  $\log_2(1 + \text{SINR}_i)$  for the remaining  $T - \tau_i$  seconds, which can be normalized by time slot duration  $T$  to derive the normalized throughput within a time slot.

Equation (C.5) indicates that narrower transmission and reception beamwidths lead to higher directivity gains and hence a higher data rate. As dictated by (C.1), this gain is obtained at the cost of higher alignment time  $\tau_i$  that leaves less time for data transmission. This reveals a tradeoff between the time devoted to alignment phase and the effective data rate. Notice also that decisions of different links are coupled through SINR, and hence scheduling multiple parallel transmissions within

a time slot is non-trivial.

### C.2.3 Maximizing Network Throughput

In this paper, we consider the problem of joint beamwidth selection and transmission scheduling that has to be solved by the coordinator in every time slot. In particular, we consider a generalized version of the latter where the optimal transmission power of each transmitter has to be selected such that the effective network throughput (or equivalently spectral efficiency) is maximized. If we collect all control variables  $\varphi_i^t$ ,  $\varphi_i^r$ , and  $p_i$  in vectors  $\boldsymbol{\varphi}^t$ ,  $\boldsymbol{\varphi}^r$ , and  $\mathbf{p}$ , respectively, the problem under consideration can be formally stated as:

$$\underset{\boldsymbol{\varphi}^t, \boldsymbol{\varphi}^r, \mathbf{p}}{\text{maximize}} \quad R = \sum_{i=1}^N \left(1 - \frac{\tau_i}{T}\right) \log_2 (1 + \text{SINR}_i), \quad (\text{C.6a})$$

$$\text{s.t.} \quad \varphi_i^t \leq \psi_i^t, \quad 1 \leq i \leq N, \quad (\text{C.6b})$$

$$\varphi_i^r \leq \psi_i^r, \quad 1 \leq i \leq N, \quad (\text{C.6c})$$

$$\psi_i^t \psi_j^r T_P / T \leq \varphi_i^t \varphi_j^r, \quad 1 \leq i, j \leq N, \quad (\text{C.6d})$$

$$0 \leq p_i \leq p^{\max}, \quad 1 \leq i \leq N. \quad (\text{C.6e})$$

Notice that for notational simplicity, function arguments have been discarded. Antenna beamwidths affect both  $\tau_i$  and  $\text{SINR}_i$ , whereas transmission powers only affect the latter. Optimization problem (C.6) is generally non-convex. In addition,  $\text{SINR}_i$  and consequently the objective function depend on the physical network topology, as dictated by  $\theta_{i,j}^t$  and  $\theta_{i,j}^r$  in (C.3) and (C.4). Such information cannot be available at the coordinator in most of WPAN and WLAN systems. In the next section, we investigate structural properties of problem (C.6), which enable us to propose two standard-compliant and easy to implement algorithms.

## C.3 Joint Beamwidth Selection and Transmission Scheduling

The optimization problem formulated in (C.6) is generally non-convex and difficult to solve. To derive some insight on the arising tradeoffs, we first focus on the single link case ( $N = 1$ ), which is also the case of existing mmWave standards [13]. Next, we consider the general problem of concurrent transmissions and demonstrate how it can be reduced to multiple parallel single link instances.

### C.3.1 Single Link Scenario

Consider a network consisting of a single link  $i$ , where no interference is experienced by the receiver. Once alignment procedure has been completed, both transmitter and receiver operate in their main lobes, hence  $\theta_{i,i}^t = \theta_{i,i}^r = 0$ . This implies that

SINR expression, formulated in (C.5), reduces to

$$\text{SNR}_i = \frac{g_{i,i}^c}{n} p_i \left( \frac{2\pi - (2\pi - \varphi_i^t)z}{\varphi_i^t} \right) \left( \frac{2\pi - (2\pi - \varphi_i^r)z}{\varphi_i^r} \right). \quad (\text{C.7})$$

Then, it is obvious that  $p^{\max}$  is the optimal transmission power, as increasing transmission power does not affect the alignment overhead, yet monotonically enhances  $\text{SNR}_i$ .

*Remark C.3.1.* Consider optimization problem (C.6) for a single link scenario. For parameters in the region of interest, the optimal antenna beamwidths  $(\varphi_i^t)^*$  and  $(\varphi_i^r)^*$  can be accurately approximated by a hyperbola  $(\varphi_i^t)^* (\varphi_i^r)^* = \varphi_i^*$ , where  $\varphi_i^*$  is determined by system parameters  $\psi_i^t, \psi_i^r, T_p, T, p^{\max}, z, g_{i,i}^c$  and  $n$ .

*Proof.* A proof is provided in [125].  $\square$

The above results imply that the dimension of the optimization problem in the single link scenario can be reduced from 3 variables, namely  $p_i, \varphi_i^t$  and  $\varphi_i^r$ , into a single one, namely  $\varphi_i \triangleq \varphi_i^t \varphi_i^r$ . Next, we derive an additional property of the objective function, which validates the existence of a tradeoff between alignment overhead and achievable throughput.

**Proposition C.3.** *Consider optimization problem (C.6) for a single link scenario. For system parameters in the region of interest, the optimal antenna beamwidth  $\varphi_i^*$  is the unique solution of  $\partial R / \partial \varphi_i = 0$ .*

*Proof.* A proof is provided in [125].  $\square$

Proposition C.3 implies that generally adopting extremely narrow beams (or equivalently excessively increasing the beamforming codebook size) is not optimal in terms of throughput due to the huge alignment overhead. Also, wide beams devastate the directivity gains, and hence they do not provide the maximum throughput. Given channel gain  $g_{i,i}^c$ , the network coordinator can find the optimal beamwidths  $\varphi_i^*$  through a simple gradient descent algorithm [126]. Next, we consider the multiple links case and we demonstrate how the coordinator can obtain an estimation of the channel gain between transmitter and receiver  $i$ .

### C.3.2 Multiple Links Scenario

Although current standards schedule a single link within each time slot, narrow beams promise significant throughput gain by exploiting concurrent transmissions. Optimization problem (C.6) provides the maximum network throughput, under the assumption that the coordinator knows the exact network topology. Here, we propose two topology-agnostic approaches. The first one is a conservative approach that generally overestimates the interference experienced by each link. In the second approach, we schedule transmissions under the assumption that resulting interference will be negligible, which is supported by the pseudo-wired abstraction of mmWave

communications [43]. In both cases, we show how a multiple links scenario can be decomposed into multiple single link scenarios.

### Overestimation of interference

The main idea behind this approach is to estimate interference at the sector level, which is generally higher than interference experienced at the beam-level. An IEEE 802.15.3c or 802.11ad compliant device has to be equipped with an orthogonal frequency division multiplexing (OFDM) transceiver, which enables different links to operate in different frequency channels at the same time. Inspired by FlashLinQ protocol proposed in [124], we can derive the following low-overhead protocol to estimate interference. First, the coordinator assigns orthogonal channels to different links, one to each link. Each transmitter  $i$  transmits with power  $p^{\max}$  inside its sector and on its dedicated channel, without introducing any interference to other links. Here, we assume that the sector of the intended receiver/transmitter can be derived from a local table [88]. Each receiver  $i$  measures SNR in link  $i$ , denoted by  $\text{SNR}_i$ , and also overhears the received power from every transmitter  $j$  with sector-level beam. The latter serves as an estimate of the interference-to-noise-ratio from transmitter  $j$ , denoted by  $\text{INR}_{ji}$ . Then, we need to check if a link can be activated concurrently with other links without receiving/causing harmful interference. From the analysis provided in [127], the sufficient condition for link  $i$  to be independent of link  $j$  (treating interference as noise) is

$$\sqrt{\text{SNR}_i} \geq \text{INR}_{ji} \quad \text{and} \quad \sqrt{\text{SNR}_i} \geq \text{INR}_{ij}. \quad (\text{C.8})$$

Each receiver  $i$  evaluates the interference level from transmitter  $j$  and according to sufficient conditions (C.8) creates the set of interferers, i.e., the set of links with which link  $i$  should not be activated simultaneously. Notice that interference has been estimated at sector level, whereas actual transmissions take place over fine-grained beams. Thus, this is an overestimation of the actual interference during communications with pencil beams, providing a conservative approach to ensure that no collisions occur. The receivers feedback their interferer sets to the coordinator. The coordinator then derives a conflict graph that shows the links that cannot be activated concurrently. Next, we provide a detailed description of the proposed scheme.

A conflict graph  $\mathcal{G} = (\mathcal{V}, \mathcal{E})$  is defined by a set of vertices  $\mathcal{V}$  and edges  $\mathcal{E}$ . A vertex  $i \in \mathcal{V}$  represents communication link  $i$  and an edge  $(i, j) \in \mathcal{E}$  indicates that links  $i$  and  $j$  cannot be activated simultaneously due to high mutual interference. In fact, the interferer set of link  $i$ , which is reported to the coordinator by receiver  $i$ , represents the set of neighbors of vertex  $i$  in the conflict graph. Finally, an independent set of graph  $\mathcal{G}$  is a subset of  $\mathcal{V}$  that contains no adjacent vertices, indicating that those vertices (links) can be concurrently activated without any harmful interference. This enables transformation of power allocation subproblem of (C.6) to a transmission scheduling instance. Thus, the coordinator, out of all independent sets, should activate at maximum power the links of the independent set that

---

**Protocol I** Interference-aware scheduling in mmWave communications

---

- 1: Initially, the coordinator assigns orthogonal channels to different links. A single channel is assigned to each.
  - 2: Each transmitter  $i$  transmits with power  $p^{\max}$  with sector-level beam on its dedicated channel.
  - 3: Each receiver  $i$  measures received power from transmitter  $i$  with sector-level beam and computes  $\text{SNR}_i$ .
  - 4: Each receiver  $i$  overhears the received power from each transmitter  $j$  with sector-level beam and computes  $\text{INR}_{j,i}$ .
  - 5: Each receiver  $i$  evaluates sufficient conditions (C.8) and creates the set of interferers.
  - 6: All receivers feedback their interferer sets to the coordinator.
  - 7: The coordinator creates a conservative conflict graph, and schedules links based on (C.9).
- 

achieves maximum throughput. For a given independent set and due to mutual independency of its links, the coordinator can optimize each link individually using a simple gradient descent, as already discussed in the single link scenario.

Let  $\mathcal{I}_k$  be independent set  $k$ , and  $\mathcal{I}$  be the set of all independent sets. Then, problem (C.6) can be cast as the following scheduling problem that activates the links of the independent set that maximizes the network throughput,

$$\begin{aligned} & \underset{\mathcal{I}_k \subseteq \mathcal{I}, \varphi^{\text{t}}, \varphi^{\text{r}}}{\text{maximize}} && \sum_{i \in \mathcal{I}_k} \left(1 - \frac{\tau_i}{T}\right) \log_2 (1 + \text{SNR}_i), \\ & \text{subject to} && \text{(C.6b)–(C.6d)}, \end{aligned} \tag{C.9}$$

where  $\text{SNR}_i$  is given by (C.7) with  $p_i = p^{\max}$ , since there is no interference inside an independent set of links operating with full power.

Given the independent sets, problem (C.9) can be solved efficiently by using gradient descent algorithms. However, finding all independent sets is an NP-hard problem in general [128]. For sparse conflict graphs, which is the case in mmWave networks with pencil beams, efficient solutions exist [129]. Protocol I describes the required steps to convert the joint beamwidth selection and power allocation problem (C.6) to a joint beamwidth selection and transmission scheduling problem (C.9).

**Underestimation of interference**

Alternatively, according to the pseudo-wired abstraction of mmWave communications [43], that is, a relatively small number of active links operating with narrow beams do not cause interference to each other, we may neglect interference. Thus, we may optimize each link independently, as if it was operating on its own. Then, the problem of joint optimization of antenna beamwidth and transmission power for  $N$  links can be decomposed into  $N$  parallel single link problems, and each can be solved in polynomial time as described in Section C.3.1. Protocol II describes the steps of the proposed underestimation approach. Its computational complexity



---

**Protocol II** Interference-agnostic scheduling in mmWave communications

---

- 1: Initially, the coordinator assigns orthogonal channels to different links. A single channel is assigned to each.
  - 2: Each transmitter  $i$  transmits with power  $p^{\max}$  with sector-level beam on its dedicated channel.
  - 3: Each receiver  $i$  estimates channel gain of link  $i$ , that is,  $g_{i,i}^c$ .
  - 4: All receivers feedback their channel gains.
  - 5: The coordinator optimizes beamwidth of every link individually, and each transceiver adjusts its beamwidth accordingly. All transmissions take place at maximum power  $p^{\max}$ .
- 

is significantly lower than the overestimation approach, since step 7 of Protocol I is not applied. Both approaches have almost the same signaling overhead, except that the underestimation one alleviates overhearing requirement.

## C.4 Numerical Results

We consider a WPAN scenario with several mmWave devices, randomly located in an area of  $10 \times 10 \text{ m}^2$ , operating in 60 GHz with maximum power of 2.5 mW, which are typical values in bluetooth-based WPAN. According to IEEE 802.15.3c, a single pilot transmission time  $T_p$  is  $20 \mu\text{s}$  [130], and the time slot duration  $T$  can be as high as  $65,535 \mu\text{s}$  [13]. We will mention the exact pilot transmission overhead  $T_p/T$  in every figure. We assume  $90^\circ$  sector-level beams both at transmitter and receiver side and  $z = 0.05$  directivity gain on the side lobe. Using Monte Carlo simulations, we evaluate the network throughput, in bits per time slot per hertz, over 100 random topologies.

Figure C.3 illustrates Remark C.3.1 by depicting contours of the throughput of a single link against transmission and reception beamwidths. The bold black curve shows the optimal beamwidth region for which throughput is maximized. This corresponds to  $\varphi_i^t \varphi_i^r = 240$ , for the example considered. Based on this result, for the rest of simulations, we assume that  $\varphi_i^t = \varphi_i^r$  for all  $i$ .

Figure C.4 demonstrates the alignment-throughput tradeoff for a single link mmWave network. For narrow beamwidths, beam-searching overhead is dominating, whereas as operating beamwidths increase, directivity gain becomes more important. Generally, the optimal point is a balance between directivity gain over the benefit of additional transmission time. Moreover, reduced overhead for single pilot transmission  $T_p/T$  allows executing more beam-searching iterations with the same time budget. As a result, performance is improved, and narrower beams are more beneficial.

Figure C.5 compares the performance of the proposed schemes in multiple links scenarios for  $T_p/T = 0.002$ . For benchmarking purposes, we depict also the performance of *Oracle*, which is the solution of optimization problem (C.6), as well as *Single Link Activation*, which is the network throughput achieved if only the

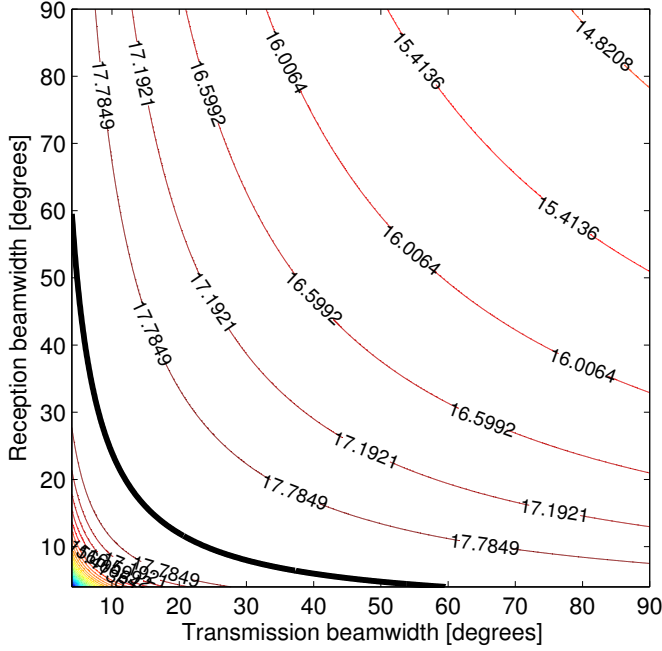


Figure C.3: Optimal region of transmission and reception beamwidths.

link of the highest SNR is activated. The following points can be made from this figure. First, allocating only one channel per time slot, which is the case in the existing standards, does not fully exploit the time slots of mmWave networks. This inefficiency increases with the number of links. In particular, with 10 links, 525%, 401%, and 177% performance enhancement can be achieved by the Oracle, interference under-estimator, and over-estimator, respectively. Given that the number of links in local networks is limited, typically less than 20, the underestimation approach can provide low complexity solutions that are close to the optimal. Good performance is expected for small scale networks, where users operate with narrow beams. For ultra dense networks, however, high levels of interference invalidate the basic pseudo-wired assumption, based on which the proposed underestimation approach has been developed. Instead, the conservative approach guarantees that no harmful interference arises at the cost of a significant throughput reduction; yet it outperforms the current single link activation scheme. This gain increases also with the number of links, since a higher number of links increases the probability of having more independent links. In general, deciding which is the most appropriate scheme depends heavily on the computation complexity that can be tolerated, the number of links, and quality of service requirements of individual links.

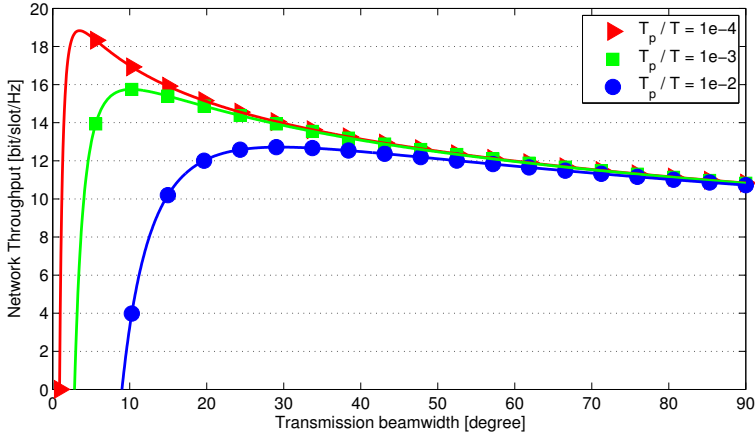


Figure C.4: Alignment-throughput tradeoff in mmWave networks.

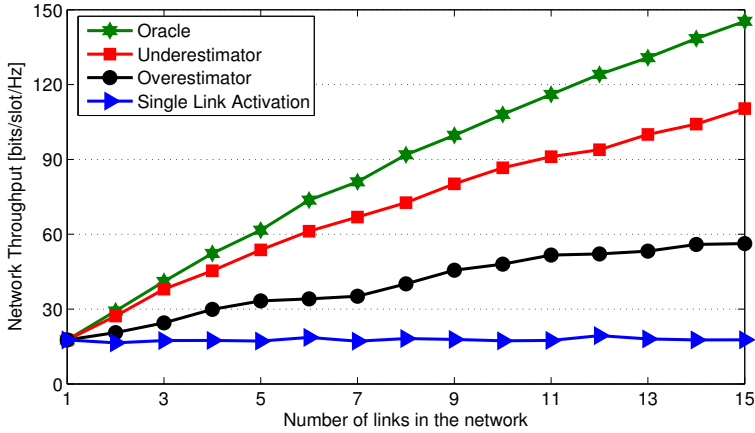


Figure C.5: Comparison of different concurrent transmission schemes in multiple links scenarios.

## C.5 Conclusion

Millimeter wave (mmWave) communications promise a significant improvement in spectral efficiency of next generation wireless networks. This paper demonstrated that existing standards do not leverage its full potential. This would require to optimize the alignment-throughput tradeoff and to devise novel transmission scheduling schemes. To this end, the problem of joint beamwidth selection and power control is formulated. This problem cannot be solved optimally, since the network topology needs to be known a priori. Thus, two low-complexity schemes are proposed that

rely on an overestimation and underestimation of interference and substantially improve the performance of existing standards.

In this work we focused on short range mmWave scenarios. Most of the identified tradeoffs arise also in cellular mmWave networks, where a hybrid digital-analog beamforming has to be conducted due to formidable complexity of pure digital beamforming design for large numbers of antennas [22]. Extending the proposed schemes and addressing the additional challenges that arise in the context of cellular networks is an interesting topic for future study.

---

# The Transitional Behavior of Interference in Millimeter Wave Networks

---

Hossein Shokri-Ghadikolaei and Carlo Fischione

Submitted to  
*IEEE Transactions on Communications*

©2015 IEEE

The layout has been revised.

# The Transitional Behavior of Interference in Millimeter Wave Networks

Hossein Shokri-Ghadikolaei and Carlo Fischione

## Abstract

Millimeter wave (mmWave) communication systems use large number of antenna elements that can potentially overcome severe channel attenuations by narrow beamforming. Pencil-beam operations in mmWave networks also reduce multiuser interference, introducing the concept of noise-limited wireless networks as opposed to interference-limited ones. The noise-limited or interference-limited regime heavily reflects on the medium access control (MAC) layer throughput and on proper resource allocation and interference management strategies. Yet, these regimes are ignored in current approaches to mmWave MAC layer design, with the potential disastrous consequences on the communication performance. In this paper, these regimes are investigated in terms of collision probability and throughput. Tractable closed-form expressions for collision probability and MAC layer throughput of mmWave ad hoc networks, operating under slotted ALOHA, are derived. The new analysis reveals that mmWave networks may exhibit a non-negligible transitional behavior from a noise-limited to an interference-limited behavior, depending on the density of transmitters, density and size of obstacles, transmission probability, operating beamwidth, and transmission power. Such a transitional behavior necessitates a new framework of adaptive hybrid resource allocation procedure, containing both contention-based and contention-free phases with on-demand realization of the contention-free phase. The contention-based phase may significantly improve network throughput performance with light signaling overhead, whereas a contention-free phase may deliver collided packets, so to guarantee a reliable physical layer. Moreover, conventional collision avoidance procedure in the contention-based phase should be revisited, due to the transitional behavior of interference, to maximize throughput/delay performance of a mmWave network. It is concluded that, unless proper hybrid schemes are investigated, the severity of the transitional behavior may significantly reduce or hinder throughput/delay performance of mmWave networks.

## D.1 Introduction

Increased demands for extremely high data rates and limited available spectrum for wireless systems in microwave bands motivate the use of millimeter wave (mmWave) communications to support multi-gigabit data rates. MmWave communication can support many diverse applications including Gbps short range wireless kiosks, augmented reality, massive wireless access in crowd public places, intra- and inter-vehicles connections, wireless connections in data centers, and mobile fronthaul-

ing and backhauling. The vast range of applications make mmWave communication a major technology for future short range and cellular wireless networks [1, 3–6, 22], and leads to several standardization activities such as ECMA 387 [52], IEEE 802.15.3c [13], IEEE 802.11ad [14], WirelessHD consortium, and wireless gigabit alliance (WiGig), and very recently IEEE 802.11ay study group on next generation 60 GHz, established in May 2015 and will support use cases with up to 1000 m range and with 40 Gbps data rate.<sup>1</sup> The Federal Communications Commission in the USA and the Ofcom in UK also published individual notice of inquiries in early 2015 to investigate if the mmWave bands should be re-purposed for mobile radio services [10, 11].

MmWave communications use the part of the electromagnetic spectrum between 30 and 300 GHz, which corresponds to wavelengths from 10 mm to 1 mm. The main characteristics of mmWave communications are short wavelength, large bandwidth, and high attenuation through most obstacles, called blockage [19]. Very small wavelengths allow the implementation of many antenna elements in the current size of radio chips, which promises a substantial increment in the link budget using beam-forming. Such a gain can largely or even completely compensate the high path-loss (that is, the distance-dependent component of the channel attenuation) without additional transmission power. Achieving this gain requires having very narrow beams both at the transmitter and at the receiver. These pencil-beams, besides boosting the link budget, reduce the interference from other transmitters [22]. In the extreme case, once such multiuser interference is no longer the main limiting factor of the throughput performance, we may face a noise-limited network where the achievable throughput is limited by the noise power.<sup>2</sup> The fundamental question is whether a mmWave network with pencil-beam operation is noise-limited as opposed to conventional interference-limited networks. This is a very important question at medium access control (MAC) layer; the answer will reveal the required complexity (and intelligence) for different MAC layer functions.

The network operating regime may determine which MAC protocol is better suited. For example, spatial time division multiple access (STDMA) protocol activates a set of transmitter-receiver pairs (links) with negligible mutual interference at a time slot, offering the maximum throughput for every link and for the network [55–58]. However, it requires knowledge of precise network topology a priori [57], which is not available in most of indoor WPAN scenarios, especially those with mobile devices. Scheduling based on partial knowledge of the network topology leads to a significant network throughput drop, e.g., 33% loss is reported

<sup>1</sup>Detailed information about these projects can be found at the following addresses: <http://www.wirelesshd.org> (WirelessHD), <http://wirelessgigabitalliance.org> (WiGig), and [http://www.ieee802.org/11/Reports/ng60\\_update.htm](http://www.ieee802.org/11/Reports/ng60_update.htm) (802.11ay), respectively. The study group of IEEE 802.11ay has not released any stable document so far, and the number are derived from the available proposals of the study group.

<sup>2</sup>Rigorously speaking, not being in an interference-limited regime does not necessarily imply that the noise power is the main bottleneck of the network throughput performance. Other sources such as beamforming (beam training) overhead may impact the achievable performance of a mmWave network [83]. In this paper, however, we focus on the interference behavior and neglect those overheads, and therefore the system will be either interference-limited or noise-limited.



in [59]. Discovering the topology (even partial knowledge) requires exchanging several control messages. Sending these control messages may be overwhelming in mmWave networks due to the characteristics of the physical control channel.<sup>3</sup> The optimal STDMA needs to solve an NP-hard problem for a given network topology [58–60], which may lead to largely suboptimal solutions in a network with very fast rescheduling requirements such as in mmWave networks [22]. To mitigate unaffordable signaling and computational overhead of STDMA, current mmWave standards adopt a very conservative approach of activating only one link at a time through a time division multiple access (TDMA)-based resource allocation [13, 14]. This conservative resource allocation, once again, is substantially suboptimal in mmWave networks [57, 62, 131], though achieves the performance of STDMA if there is mutual interference between any pair of links. The latter is very unlikely in mmWave networks with pencil-beam operation. Slotted ALOHA, as an alternative contention-based resource allocation solution, imposes no signaling and computational overhead and achieves the performance of STDMA provided that there is no mutual interference between any pair of links (a noise-limited regime). However, it cannot guarantee communications without collisions, which is important in many applications. Hybrid MAC approaches, mainly developed for interference-limited networks, can combine the strengths and offset the weaknesses of contention-based and contention-free resource allocation strategies [62, 63, 132–135].

To design a proper hybrid MAC for mmWave networks with pencil-beam operation, the first step is analyzing the collision, evaluating performance gain (in terms of throughput/delay) due to various resource allocation protocols, and investigating the signaling and computational complexities of those protocols. Roughly speaking, as the system goes to the noise-limited regime, the required complexity for proper resource allocation and interference avoidance functions at the MAC layer substantially reduces [43, 57, 70, 136–138]. For instance, in a noise-limited regime, a very simple resource allocation such as activating all links at the same time without any coordination among different links may outperform a complicated independent-set based resource allocation [57]. Instead, pencil-beam operation complicates negotiation among different devices in a network, as control message exchange may require time consuming antenna alignment procedure to avoid *deafness* [57]. Deafness refers to the situation in which the main beams of the transmitter and the receiver do not point to each other, preventing establishment of a communication link. Therefore, determining the network operating regime is essential to determine the best MAC layer protocol. How to make such a determination is largely an open problem for mmWave networks.

The seminal work in [43] shows the existence of *pseudowired* abstraction (noise-

---

<sup>3</sup>Due to high reliability and robustness requirements, the physical control channel has a significantly lower transmission rate compared to the data channel. IEEE 802.11ad, for instance, supports up to 27.7 Mbps for control packets (a “packet” is a message frame at the MAC layer) while 6.7 Gbps is supported for data packets [118]. Moreover, sending control packets in the mmWave bands may impose additional beam training overhead compared to sensing those in the microwave bands [22]. This alignment is necessary to avoid *deafness*, formally defined later in this section.

limited network) in outdoor mmWave mesh networks. However, as shown in [57, 123, 138, 139], indoor mmWave WPANs are not necessarily noise-limited. In particular, activating all links causes a significant performance drop compared to the optimal resource allocation [57], indicating that there may be situations in which a non-negligible multiuser interference is present; the noise power is not always the limiting factor. Such a performance degradation increases with the number of devices in the network [57]. This indeed means that the accuracy of the noise-limited assumption to model the actual network behavior reduces with the number of links. Similar conclusions are also made in mmWave cellular networks [67]. The increased directionality level in a mmWave network reduces multiuser interference; however, this reduction may not be enough to take an action (e.g., resource allocation) based on the assumption of being in a noise-limited regime. It follows that a pseudowired assumption may be detrimental for proper MAC layer design. However, the interference footprint may not be so large that we need to adopt very conservative resource allocation protocols such as TDMA, which activates only one link at a time.

In this paper, we investigate the fundamental performance indicators that will help in deciding which MAC is the best for which situation. To this end, we first introduce a novel blockage model that, unlike the existing models [48, 67, 140–142], captures the angular correlation of the blockage events as a function of size and density of the obstacles. We derive tractable closed-form expressions for collision probability, per-link throughput, and area spectral efficiency. We analytically evaluate the impact of the transmission/reception beamwidth, transmission power, and the densities of the transmitters and obstacles on the performance metrics. The new analysis shows that the pseudowired abstraction may not be accurate even for a modest-sized ad hoc network, and mmWave networks exhibit a transitional behavior from a noise-limited regime to an interference-limited regime. Using the established collision analysis, we investigate if either a contention-based or contention-free resource allocation protocol is a good option for a mmWave ad hoc network. To this end, we derive the exact expressions and tight bounds on the MAC layer throughput of a link, area spectral efficiency, and delay performance of STDMA, TDMA, and slotted ALOHA protocols. Comprehensive analysis reveals that STDMA is impractical due to massive signaling and computational overheads. A simple slotted ALOHA may achieve the performance of STDMA and significantly outperform TDMA in terms of network throughput/delay performance, while TDMA is still necessary to guarantee communication without any collision. We conclude that the transitional behavior of mmWave networks necessitates a collision-aware hybrid resource allocation procedure, containing both contention-based and contention-free phases with flexible phase duration. In particular, the contention-based phase with on-demand execution of the collision avoidance substantially improves throughput/delay performance of the network. Moreover, on-demand use of the contention-free phase to deliver only the collided packets guarantees a reliable physical layer with minimal drop in network throughput/delay performance. Detailed analysis of this paper clarifies the collision level and throughput performance of mmWave networks, and thereby provide required guidelines for designing proper resource allocation and interference management protocols for future mmWave networks.

The rest of this paper is organized as follows. In Section D.2, we describe the system model. The collision probability in mmWave ad hoc networks is derived in Section D.3, followed by evaluation of the MAC throughput and characterization of the network operating regime in Section D.4. Concluding remarks, along with possible future directions, are provided in Section D.5.

## D.2 System Model

We consider a mmWave wireless network, and a homogenous Poisson network of transmitters on the plane with density  $\lambda_t$  per unit area, each associated to a receiver. To evaluate the collision performance of the network, we consider a reference link (called typical link) between a reference receiver and its intended transmitter having geometrical/spatial length  $\ell$ , see Table D.6 for a list of the main symbols used in the paper. We call the receiver and the transmitter of the typical link as the typical receiver and the tagged transmitter. From Slivnyak's Theorem [89, Theorem 8.1] applied to homogenous Poisson point processes, the conditional distribution of potential interferers, excluding the tagged transmitter, given the typical receiver at the origin is another homogenous Poisson point process with the same density. We assume that if multiple neighbors are transmitting to the same receiver, at most one of them can be successfully decoded by that receiver. This natural assumption is due to lack of multiuser detection in many devices and thus existing mmWave standards [13, 14] adopts it. The assumption is also common in performance evaluation procedure [43, 48, 91, 92, 143]. Therefore, all transmitters in the network act as potential interferers for the typical receiver (the receiver of the typical link). The amount of interference depends on the density and location of the interferers relative to the typical receiver, transmission powers, channel model, the antenna radiation pattern, blockage model, and transmission and reception beamwidths.

We consider a slotted ALOHA protocol without power control to derive a lower bound on the performance.<sup>4</sup> That is, the transmission power of all links is  $p$ . We let every transmitter (interferer) be active with probability  $\rho_a$ , so the probability of transmitting in a slot is  $\rho_a$ . In the slotted ALOHA, the transmissions are regulated to start at the beginning of a time slot. The slotted ALOHA is a good model for the worst case analysis of a device-to-device (D2D) network underlying a cellular network, as devices are synchronous by using base station synchronization signals. Also, slotted ALOHA provides an upper bound on the throughput performance of pure ALOHA, where the transmission is started immediately upon a new packet arrival [144]. Although for mathematical tractability we choose slotted ALOHA, the analysis of this paper can be readily extended to the pure ALOHA case. Further, similar to [91, 92], we assume that transmitter of every link is spatially aligned with its intended receiver, so there is no beam training overhead. The

<sup>4</sup>Kleinrock's seminal work shows that simple CSMA protocols easily outperform both pure and slotted ALOHA protocols [144]. As will be shown in this paper, there is a non-negligible contention on the channel access, making it imperative to add a simple carrier sense functionality to the slotted ALOHA. However, as the system goes to the noise-limited regime, the performance gain due to this additional functionality vanishes.

Table D.6: Summary of main notations

Symbol	Definition
$A_d$	Area of circle sector with radius $d$ and angle $\theta_c$
$\text{ASE}_{\text{S-ALOHA}}$	Area spectral efficiency of slotted ALOHA
$\text{ASE}_{\text{TDMA}}$	Area spectral efficiency of TDMA
$d_{\max}$	Interference range
$\ell$	Geographical/spatial length of the typical link
$n_I$	The number of interferers
$n_o$	The number of obstacles
$r_{\text{S-ALOHA}}$	Average throughput of a link in slotted ALOHA
$r_{\text{TDMA}}$	Average throughput of a link in TDMA
$\theta$	Transmission/reception beamwidth
$\theta_c$	Coherence angle
$\lambda_I$	Density of potential interferers per unit area
$\lambda_t$	Density of transmitters (links) per unit area
$\lambda_o$	Density of obstacles per unit area
$\rho_a$	Transmission probability of slotted ALOHA
$\rho_{c \ell}$	Conditional collision probability given $\ell$
$\rho_{s \ell}$	Conditional probability of successful transmission given $\ell$

adverse impacts of the beam training overhead on per-link and network throughput performance is investigated in [57]. In this paper, instead, we have assumed pre-aligned transmitter-receiver pairs to analyze the impact of other parameters (such as density of the transmitters, operating beamwidth, density and size of the obstacles, and the blockage model) on the performance of mmWave networks. Moreover, the beam training procedure imposes same overhead on all resource allocation protocols we are considering in this paper, so it can be neglected from the comparative analysis and conclusions. If there is no obstacle on the link between transmitter  $i$  and the origin, we say that transmitter  $i$  has LoS condition respect to the typical receiver, otherwise it is in non-LoS (NLoS) condition. Moreover, similar to [43, 48, 67, 91, 92, 140–143], we consider only LoS links and neglect reflections.

We consider a distance-dependent path-loss with exponent  $\alpha$ , as commonly assumed for MAC layer performance evaluations [43, 88]. This simple model allows deriving tractable closed-form expressions for the collision probability and for the throughput, and, at the same time, enables us to draw general conclusions about the network operating regime. Note that the sparse scattering feature of mmWave frequencies along with a pencil beam operation makes the mmWave channel more deterministic compared to that of microwave systems that normally operate in rich

scattering environments and omnidirectional transmission [7]. Moreover, we use the *protocol model* of interference [39], which is common in the MAC layer analysis [43, 145–147]. In this model, for a given distance between a reference receiver and its intended transmitter, a *collision*<sup>5</sup> occurs if there is at least another interfering transmitter no farther than a certain distance from the reference receiver, hereafter called *interference range*. Besides its simplicity, the recent investigation in [50] reveals that the special characteristics of mmWave networks makes such a protocol model quite accurate for mmWave networks. Essentially, as the probability of having LoS condition on a link decreases exponentially with the distance [51], far away transmitters will be most probably blocked (in NLoS condition) and therefore cannot contribute in the interference a receiver experiences. Therefore, we may consider only the impact of spatially close interferers, and yet having negligible loss in the accuracy of the interference model.

At the MAC layer, the beamforming is represented by using an ideal sector antenna pattern [48, 91, 92], where the directivity gain is a constant for all angles in the main lobe and equal to a smaller constant in the side lobe. This model allows capturing the interplay between antenna gain, which ultimately affects transmission range, and half power beamwidth. We assume all devices in both transmission and reception modes operate with the same beamwidth  $\theta$ . Considering 2D beamforming, the directivity gain for each transmitter/receiver is

$$\begin{cases} \frac{2\pi - (2\pi - \theta)\epsilon}{\theta}, & \text{in the main lobe} \\ \epsilon, & \text{in the side lobe} \end{cases}, \quad (\text{D.1})$$

where typically  $0 \leq \epsilon \ll 1$ . The gain in the main lobe can be derived by fixing the total radiated power of the antennas over parameter space of  $\epsilon$  and  $\theta$ . Due to small value of  $\epsilon$  compared to the directivity gain in the main lobe, only the interferers that are aligned with the typical receiver can cause collision. In other words, there is no strong interference, so no collision, in the deafness condition.

Further, the extremely high penetration loss in mmWave networks almost vanishes the impact of any transmitter with non-LoS condition with respect to a receiver. To have quantitative insights, mmWave signals will be attenuated by 35 dB due to the human body and by up to 80 dB due to brick [19]. The extreme penetration loss not only blocks a link between a receiver and its intended transmitter, as argued in [88], it also vanishes the impact of unintended transmitters with non-LoS conditions (non-LoS interferers) on the aggregated interference level the receiver experiences. The negligible impact of the non-LoS interferers is also confirmed in [148].

**Blockage model:** As the operating beamwidth becomes narrower, the events of observing obstacles on the link between the typical receiver and individual interferers become more and more correlated, so the LoS condition for different interferers becomes correlated. Many interferers that are closely located in the angular

---

<sup>5</sup>Note that “collision” is defined as the outage event due to strong interference from other transmitters. Note that an outage can also occur due to low signal-to-noise ratio (SNR) even without any interference.

domain from the point of view of the receiver can be blocked by an obstacle between them and the receiver. Therefore, the assumption of independent LoS conditions on the links among the typical receiver and different interferers, as considered in [48, 67, 140–142], is not adequate for mmWave systems. The accuracy of this independent blockage model decreases if we increase the density of the transmitters or if the transmitters appear in spatial clusters. The consequence is that those blockage models may sometimes prevent to derive correct conclusions, especially for dense mmWave networks.

In this paper, assuming that the center of obstacles<sup>6</sup> follow a homogenous Poisson point process with density  $\lambda_o$  independent of the communication network, we use the following model to capture the aforementioned correlation among LoS conditions: we define a *coherence angle*  $\theta_c$  over which the LoS conditions are statistically correlated. That is, inside a coherence angle, an obstacle blocks all the interferers behind itself, so there is no LoS conditions in distances  $d \geq l$  with respect to the receiver of the typical link and consequently no LoS interferers, if there is an obstacle at distance  $l$ . However, there is no correlation between LoS condition events in different coherence angle intervals, i.e., in different circle sectors with angle  $\theta_c$ . The coherence angle depends on the size and density of obstacles in the environment. Note that different obstacles with different sizes and locations can cause different intervals  $\theta_c$  of the angular correlation of blockage events. However, we suggest using the average value of  $\theta_c$  to simplify the analysis, which otherwise would be intractable. We made this proposal inspired by the classic concept of coherence time and the coherence bandwidth for the wireless channel. The coherence time and coherence bandwidth are different for different users with different speeds and different surrounding environments; still, the common approach is assuming the same values for all users to simplify the analysis (see [149] and references therein). We validate the proposed blockage model in Section D.4 using extensive set of emulations.

### D.3 Collision Analysis

In this section, we investigate the collision probability in a mmWave network working with slotted ALOHA protocol. The derivation of such a result will play a major role in performance analysis of mmWave networks, presented in Section D.4.

We consider a typical receiver at the origin of the Polar coordinates and its intended transmitter at distance  $\ell$  and evaluate the collision probability due to other transmitters' operation located inside the circle sector with angle  $\theta$  and radius of the interference range. Let  $p$ ,  $\nu$ , and  $f_c$  be the signal transmission power, phase speed, and carrier frequency, respectively. In free space, the phase speed of electromagnetic signals is almost the speed of light. The channel gain between the typical receiver and an aligned non-blocked transmitter at distance  $d$  is  $(\nu/4\pi df_c)^\alpha$ .

---

<sup>6</sup>For sake of simplicity, we may use obstacle to refer the center of that obstacle throughout the paper.

We denote by  $d_{\max}$  the interference range, by  $\beta$  the minimum SINR threshold at the typical receiver, and by  $\sigma$  the noise power. The interference range  $d_{\max}$  is defined as the maximum distance an interferer can be from the receiver and still cause collision/outage. At the typical receiver, the SINR due to transmission of the intended transmitter and an aligned LoS interferer located at distance  $d$  is

$$\frac{p \left( \frac{2\pi - (2\pi - \theta)\epsilon}{\theta} \right)^2 \left( \frac{\nu}{4\pi\ell f_c} \right)^\alpha}{p \left( \frac{2\pi - (2\pi - \theta)\epsilon}{\theta} \right)^2 \left( \frac{\nu}{4\pi d f_c} \right)^\alpha + \sigma}.$$

Comparing the SINR expression to  $\beta$ , we get the interference range

$$d_{\max} = \left( \frac{\ell^{-\alpha}}{\beta} - \frac{\sigma}{p} \left( \frac{2\pi - (2\pi - \theta)\epsilon}{\theta} \right)^{-2} \left( \frac{\nu}{4\pi f_c} \right)^{-\alpha} \right)^{-1/\alpha}.$$

A transmitter at distance  $d$  from the typical receiver can cause collision provided that the following conditions hold: (a) it is active, (b) the typical receiver is inside its main lobe, (c) it is inside the main lobe of the typical receiver, (d) it is located inside the interference range  $d \leq d_{\max}$ , and (e) it is in LoS condition with respect to the typical receiver. These conditions are illustrated in Fig. D.1, where the tagged transmitter, interferers, and obstacles are represented by a green circle, red triangles, and blue rectangles, respectively. Also, the highlighted part is the sector from which the typical receiver is receiving signal. Interferers 1, 2, and 3 cannot cause collision at the typical receiver due to condition (c), (d), and (e), respectively. Due to random deployment of the devices, the probability that the typical receiver locates inside the main lobe of an active transmitter is  $\theta/2\pi$ . Therefore, if the density of transmitters per unit area is  $\lambda_t$  and if the average probability of being active for every transmitter is  $\rho_a$ , the interferers for which conditions (a) and (b) hold follow a homogenous Poisson point process with density  $\lambda_I = \rho_a \lambda_t \theta/2\pi$  per unit area. Conditions (c) and (d) reduces the area over which a potential interferer can make collision. For condition (e), we need to elaborate the blockage model. The typical receiver observes  $k = \lceil \theta/\theta_c \rceil$  sectors, each with angle  $\theta_c$ , where  $\lceil \cdot \rceil$  is the ceiling function. For the sake of simplicity, we assume that  $\theta/\theta_c$  is an integer; however the analysis can be extended, with more involved calculations, to the general case. We take the general assumption that the tagged transmitter is uniformly distributed in the circle sector with angle  $\theta$  that the typical receiver is pointing to, as shown by hashed lines in Fig. D.1. Having a fix coordinate for the tagged transmitter is a special case of our analysis. It is straightforward to see that the tagged transmitter is located in one of these  $k$  sectors with uniform distribution and its radial distance to the typical receiver  $L$  is a continuous random variable with density function  $f_L(\ell) = 2\ell/d_{\max}^2$ . Without loss of generality, we assume that the tagged transmitter is in sector  $k$ . It means that we have a combination of interferers and obstacles in the first  $k - 1$  sectors. In the last sector, we cannot have any obstacle in the circle sector with angle  $\theta_c$  and radius  $\ell$ , as the tagged transmitter in  $\ell$  should be in the LoS condition, otherwise the typical link will not be established and collision

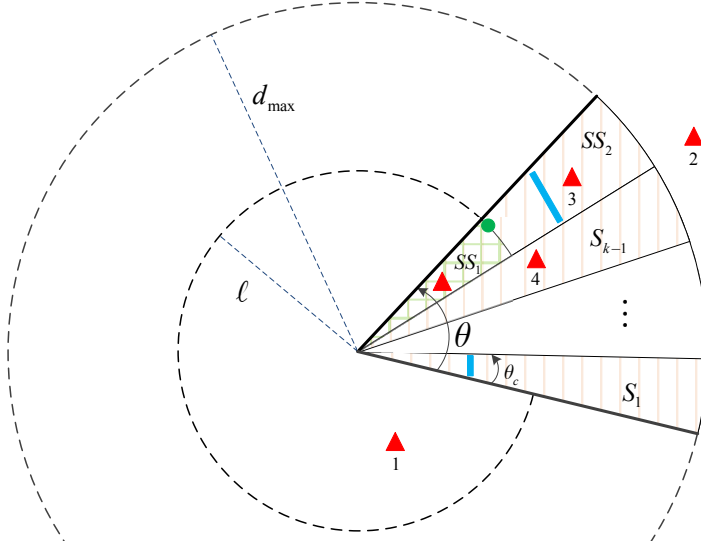


Figure D.1: Hatched lines show potential interference zone. Operating beamwidth  $\theta$  is divided into  $k$  sectors of angle  $\theta_c$ . The typical receiver is on the origin. The tagged transmitter, shown by a green circle, is on sector  $k$  at distance  $\ell$  of the typical receiver.  $S_i$  shows sector  $1 \leq i \leq k-1$ .  $SS_1$  and  $SS_2$  are two sub-sectors of sector  $k$ . Zones with orange hatched lines have both random interferers and obstacles, represented by a red triangle and a blue rectangle. Zones with green hatched lines have only random interferers.  $d_{\max}$  is the interference range.

cannot happen. Dividing the last sector into two sub-sectors, corresponding to the distances  $(0, \ell]$  and  $(\ell, d_{\max}]$ , the first sub-sector contains only interferers, whereas the second one has both interferers and obstacles. In the following, we first derive the probability of receiving collision from individual sectors and then compute the collision probability in general.

Let  $A_d$  be the area of a circle sector with radius  $d$  and angle  $\theta_c$ . The number of interferers and obstacles in every sector  $s$ ,  $1 \leq s \leq k-1$ , are Poisson random variables with average  $\lambda_I A_d$  and  $\lambda_o A_d$ , where  $\lambda_I$  and  $\lambda_o$  are the density of potential interferers and obstacles per unit area. Let  $n_I$  and  $n_o$  be the number of interferers and obstacles, which are independent Poisson random variables with densities  $\lambda_I$  and  $\lambda_o$ . Given sector  $s$ ,  $1 \leq s \leq k-1$ , we have three possible cases:

1.  $n_I = 0, n_o \geq 0$ : There is no interferer, and consequently the probability of LoS interference is 0.
2.  $n_I \geq 1, n_o = 0$ : In this case, every interferer in the sector is a LoS interferer that causes collisions. The probability of LoS interference in this case is 1.



3.  $n_I \geq 1, n_o \geq 1$ : In this case, we have a combination of interferers and obstacles located randomly inside the sector. Let  $\{x_1, x_2, \dots, x_{n_I}\}$  and  $\{y_1, y_2, \dots, y_{n_o}\}$  be the set of distances of  $n_I$  interferers and  $n_o$  obstacles from the origin, where  $n_I$  and  $n_o$  are Poisson random variables. We define random variables  $X_{(1)} = \min\{x_1, x_2, \dots, x_{n_I}\}$  and  $Y_{(1)} = \min\{y_1, y_2, \dots, y_{n_o}\}$ . Given  $n_I \geq 1$  and  $n_o \geq 1$ , the typical receiver observes at least one LoS interferer provided that  $X_{(1)} < Y_{(1)}$ . We characterize the probability of having at least one LoS interferer in the following propositions.

**Lemma D.1.** *Consider the blockage model, described in Section C.2 and Fig. D.1. Given sector  $s$ , the number of interferers  $n_I \geq 1$ , and the number of obstacles  $n_o \geq 1$ , joint probability density function  $X_{(1)}$ ,  $Y_{(1)}$ ,  $n_I$ , and  $n_o$  is*

$$f_{X_{(1)}, Y_{(1)}, n_I, n_o}(x, y, n, m | n \geq 1, m \geq 1) = \frac{2nx}{d_{\max}^2} \left(1 - \frac{x^2}{d_{\max}^2}\right)^{n-1} \frac{2my}{d_{\max}^2} \left(1 - \frac{y^2}{d_{\max}^2}\right)^{m-1} \\ \times \frac{e^{-\lambda_I A_{d_{\max}}}}{1 - e^{-\lambda_I A_{d_{\max}}}} \frac{(\lambda_I A_{d_{\max}})^n}{n!} \frac{e^{-\lambda_o A_{d_{\max}}}}{1 - e^{-\lambda_o A_{d_{\max}}}} \frac{(\lambda_o A_{d_{\max}})^m}{m!}. \quad (\text{D.2})$$

Also, the probability of having at least one LoS interferer is

$$\frac{\lambda_o}{(1 - e^{-\lambda_I A_{d_{\max}}})(1 - e^{-\lambda_o A_{d_{\max}}})} \left( \frac{1 - e^{-\lambda_o A_{d_{\max}}}}{\lambda_o} - \frac{1 - e^{-(\lambda_o + \lambda_I) A_{d_{\max}}}}{\lambda_o + \lambda_I} \right). \quad (\text{D.3})$$

*Proof.* A proof is given in Appendix A.  $\square$

Using Lemma D.1, we can find the probability of having LoS interference in sector  $s$ ,  $1 \leq s \leq k-1$ .

**Proposition D.4.** *Consider the blockage model, described in Section C.2 and in Fig. D.1. Given sector  $s$ ,  $1 \leq s \leq k-1$ , the probability of having at least one LoS interferer is*

$$\frac{\lambda_I}{\lambda_o + \lambda_I} \left( 1 - e^{-(\lambda_o + \lambda_I) A_{d_{\max}}} \right), \quad (\text{D.4})$$

where  $\lambda_I = \rho_a \lambda_t \theta / 2\pi$  and  $A_{d_{\max}} = \theta_c d_{\max}^2 / 2$ .

*Proof.* For sake of notation simplicity, we denote by  $\Pr[\text{LI}]$  the probability of having at least one LoS interferer in a given sector  $s$ ,  $1 \leq s \leq k-1$ . Let  $n_I = n$  and  $n_o = m$ . Considering the discussions at the beginning of this subsection and mutual independence of the number of interferers and obstacles, we have

$$\begin{aligned} \Pr[\text{LI}] &= \Pr[\text{LI} | n = 0] \Pr[n = 0] + \Pr[\text{LI} | n \geq 1, m = 0] \Pr[n \geq 1, m = 0] \\ &\quad + \Pr[\text{LI} | n \geq 1, m \geq 1] \Pr[n \geq 1, m \geq 1] \\ &= \Pr[\text{LI} | n \geq 1, m = 0] \Pr[n \geq 1] \Pr[m = 0] \\ &\quad + \Pr[\text{LI} | n \geq 1, m \geq 1] \Pr[n \geq 1] \Pr[m \geq 1], \end{aligned} \quad (\text{D.5})$$

where  $\Pr[\text{LI} | n \geq 1, m = 0] = 1$ ,  $\Pr[n \geq 1] = 1 - e^{-\lambda_I A_{d_{\max}}}$ ,  $\Pr[m = 0] = e^{-\lambda_o A_{d_{\max}}}$ ,  $\Pr[\text{LI} | n \geq 1, m \geq 1]$  is given in (D.3), and  $\Pr[m \geq 1] = 1 - e^{-\lambda_o A_{d_{\max}}}$ . After some algebraic manipulations, we have

$$\begin{aligned} \Pr[\text{LI}] &= (1 - e^{-\lambda_I A_{d_{\max}}}) e^{-\lambda_o A_{d_{\max}}} + \lambda_o \left( \frac{1 - e^{-\lambda_o A_{d_{\max}}}}{\lambda_o} - \frac{1 - e^{-(\lambda_o + \lambda_I) A_{d_{\max}}}}{\lambda_o + \lambda_I} \right) \\ &= \frac{\lambda_I}{\lambda_o + \lambda_I} \left( 1 - e^{-(\lambda_o + \lambda_I) A_{d_{\max}}} \right), \end{aligned} \quad (\text{D.6})$$

which concludes the proof.  $\square$

In order to numerically illustrate Proposition D.4 and derive some insights on the behavior of LoS interference probability formulated in (D.4), we simulate an ad hoc network with random number of mmWave links, operating with beamwidth  $\theta = 20^\circ$  at 60 GHz. The transmission probability of every link is 1, so all links are always active. We assume a 2.5 mW transmission power, a coherence angle  $\theta_c = 5^\circ$ , and an interference range  $d_{\max} = 15$  m. Using Monte Carlo simulations, we evaluate the average probability of having a LoS interference over  $10^6$  random topologies. Changing  $\lambda_t$ ,  $\lambda_o$ ,  $\theta$ , and  $d_{\max}$  we can cover a wide variety of future mmWave applications. These spans the following cases: long range, low mobility, low density usage applications such as mobile fronthauling/backhauling use case (corresponds to high  $d_{\max}$  and small  $\theta$ ,  $\lambda_o$ , and  $\lambda_t$ ); short range, high mobility, massive wireless access usage applications such as crowded public place use case (corresponds to small  $d_{\max}$ , wider  $\theta$ , and higher  $\lambda_o$  and  $\lambda_t$ ).

Fig. D.2a shows the probability of having LoS interference from a given sector  $s$ ,  $1 \leq s \leq k - 1$ , as a function of link density  $\lambda_t$ . First of all, Proposition D.4 holds for all curves. Not surprisingly, increasing the link density increases LoS interference probability, but in a saturating manner. Also, higher obstacle density increases blockage probability, so reduces LoS interference probability. As can be observed in the figure, for the density of 1 transmitter (interferer) in a  $3 \times 3$  m<sup>2</sup> area, increasing the density obstacles by a factor of 100, from 0.0025 to 0.25, leads to only 62% reduction on the probability of observing an LoS interferer. To better understand the impact of obstacle density  $\lambda_o$ , we report the probability of having LoS interference from a given sector  $s$ ,  $1 \leq s \leq k - 1$ , as a function of  $\lambda_o$ . LoS interference probability is not too sensitive to the changes of  $\lambda_o$  for small obstacle densities. However, the sensitivity increases by  $\lambda_o$ , leading to a very fast reduction in LoS interference probability by a small increment of  $\lambda_o$ , for instance, for  $\lambda_o > 1$ .

Although (D.4) describes LoS interference probability from every sector 1 to  $k - 1$ , for sector  $k$  we need to extend (D.4) according to the corresponding blockage and interference models. As shown in Fig. D.1, sector  $k$  consists of two sub-sectors, corresponding to the distances  $(0, \ell]$  and  $(\ell, d_{\max}]$ . In the first sub-sector, there is no obstacle, whereas we have regular appearance of the obstacles in the second sub-sector, see Fig. D.1. Following the same steps taken in Appendix A and in Proposition D.4, and after some algebraic manipulations, we can derive the proba-

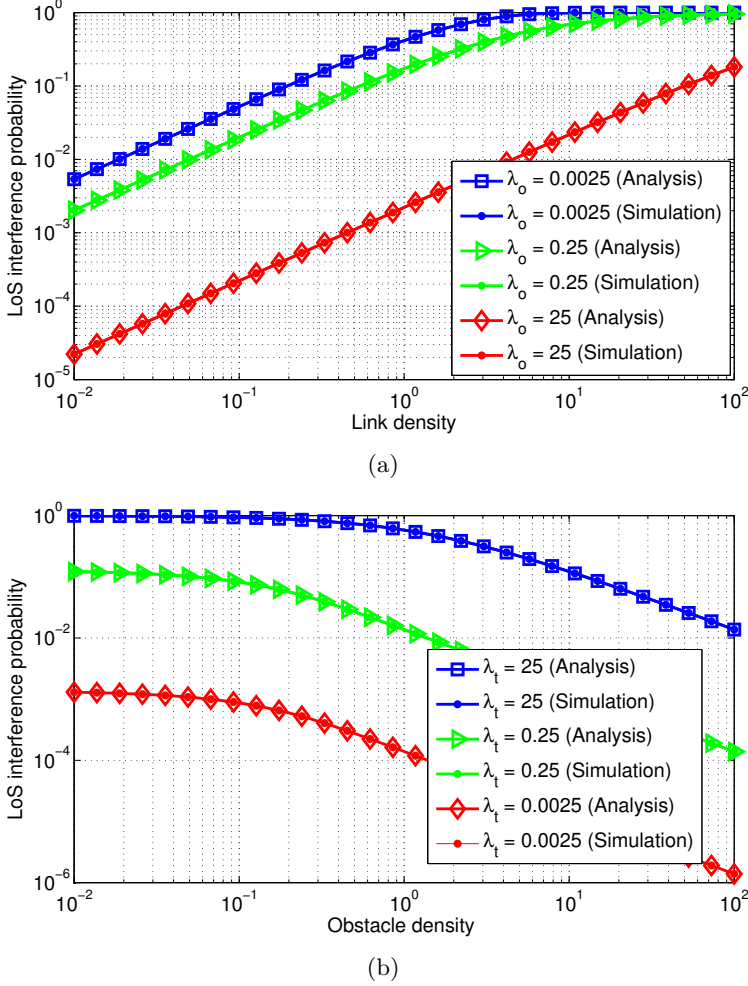


Figure D.2: The probability of having LoS interference from sector  $s$ ,  $1 \leq s \leq k-1$ , as a function of (a) link density and (b) obstacle density, as computed by Equation (D.3) and Monte Carlo simulations.

bility of receiving LoS interference from sector  $k$ :

$$1 - e^{-\lambda_I A_\ell} + \frac{\lambda_I}{\lambda_o + \lambda_I} \left( e^{-(\lambda_o + \lambda_I) A_\ell} - e^{-(\lambda_o + \lambda_I) A_{d_{\max}}} \right). \quad (\text{D.7})$$

**Proposition D.5.** Let  $\lambda_t$  and  $\lambda_o$  denote the density of the interferers and obstacles per unit area. Let  $\rho_a$  be the probability that an interferer is active. Consider blockage and interference models, described in Fig. D.1. Let  $d_{\max}$ ,  $\theta$ , and  $\theta_c$  be the

interference range, operating beamwidth, and coherence angle, respectively. Given that the typical link at length  $\ell$  can be established, the conditional collision probability, denoted by  $\rho_{c|\ell}$ , is

$$\rho_{c|\ell} = 1 - \left( \frac{\lambda_o + \lambda_I e^{-(\lambda_o + \lambda_I) A_{d_{\max}}}}{\lambda_o + \lambda_I} \right)^{\lceil \theta / \theta_c \rceil - 1} \times \left( e^{-\lambda_I A_\ell} - \frac{\lambda_I}{\lambda_o + \lambda_I} \left( e^{-(\lambda_o + \lambda_I) A_\ell} - e^{-(\lambda_o + \lambda_I) A_{d_{\max}}} \right) \right), \quad (\text{D.8})$$

where  $\lambda_I = \rho_a \lambda_t \theta / 2\pi$ ,  $A_{d_{\max}} = \theta_c d_{\max}^2 / 2$  and  $A_\ell = \theta_c \ell^2 / 2$ .

*Proof.* Given that the typical link is established, the collision probability is equal to the probability of having at least one LoS interferer, irrespective of the sectors in which the LoS interferer(s) are. To derive the collision probability, we first find its complementary, that is, the probability of having no LoS interferer in any sector. The latter is equal to complementary of the event of having collision in any sector, given by (D.4) and (D.7). Considering mutual independence of different sectors, the proof is straightforward.  $\square$

We can draw several fundamental remarks from the closed-form expression of the collision probability of Equation (D.8).

*Remark D.3.1.* The collision probability, formulated in (D.8), implies the following asymptotic results:

$$\begin{aligned} \lambda_I \rightarrow 0 &\Rightarrow \rho_{c|\ell} \rightarrow 0, \\ \lambda_o \rightarrow 0 &\Rightarrow \rho_{c|\ell} \rightarrow 1 - \left( e^{-\lambda_I A_{d_{\max}}} \right)^{\lceil \theta / \theta_c \rceil}, \\ \lambda_I \rightarrow \infty, \lambda_o < \infty &\Rightarrow \rho_{c|\ell} \rightarrow 1, \\ \lambda_o \rightarrow \infty, \lambda_I < \infty &\Rightarrow \rho_{c|\ell} \rightarrow 1 - e^{-\lambda_I A_\ell}, \\ \theta \rightarrow 0, \theta = \theta_c &\Rightarrow \rho_{c|\ell} \rightarrow 0, \\ \theta_c \rightarrow 0, \theta \gg \theta_c &\Rightarrow \rho_{c|\ell} \rightarrow 1 - e^{-\lambda_I d_{\max}^2 \theta / 2}. \end{aligned}$$

Note that the last remark, which can be simply proved by relaxing ceiling function in (D.8) and using a Taylor expansion, is basically equivalent to assume that different interferers experience independent LoS events, as considered in [48]. Remark D.3.1 shows asymptotic performance bounds on the conditional collision probability and provides benchmarks for the analysis.

The last step of characterizing the collision probability is taking an average of (D.8) over distribution of the length of the typical link, which is  $2\ell/d_{\max}^2$ . The

resulting collision probability is

$$\rho_c = 1 - \int_{\ell=0}^{d_{\max}} \frac{2\ell}{d_{\max}^2} \left( \frac{\lambda_o + \lambda_I e^{-(\lambda_o + \lambda_I)\theta_c d_{\max}^2/2}}{\lambda_o + \lambda_I} \right)^{\lceil \theta/\theta_c \rceil - 1} \times \left( e^{-\lambda_I \theta_c \ell^2/2} + \frac{\lambda_I}{\lambda_o + \lambda_I} \left( e^{-(\lambda_o + \lambda_I)\theta_c \ell^2/2} - e^{-(\lambda_o + \lambda_I)\theta_c d_{\max}^2/2} \right) \right) d\ell. \quad (\text{D.9})$$

**Proposition D.6.** *Let  $\lambda_t$  and  $\lambda_o$  denote the density of the interferers and obstacles per unit area. Let  $\rho_a$  be the probability that an interferer is active. Consider blockage and interference models, described in Fig. D.1. Let  $d_{\max}$ ,  $\theta$ , and  $\theta_c$  be the interference range, operating beamwidth, and coherence angle, respectively. The collision probability is bounded as*

$$1 - \left( \frac{\lambda_o + \lambda_I e^{-(\lambda_o + \lambda_I)\theta_c d_{\max}^2/2}}{\lambda_o + \lambda_I} \right)^{\lceil \theta/\theta_c \rceil} \leq \rho_c$$

$$\rho_c \leq 1 - e^{-\lambda_I \theta_c d_{\max}^2/2} \left( \frac{\lambda_o + \lambda_I e^{-(\lambda_o + \lambda_I)\theta_c d_{\max}^2/2}}{\lambda_o + \lambda_I} \right)^{\lceil \theta/\theta_c \rceil - 1}, \quad (\text{D.10})$$

where  $\lambda_I = \rho_a \lambda_t \theta / 2\pi$ .

*Proof.* We first observe that the collision probability given by (D.9) is strictly increasing with  $\ell$ . Therefore, its lower and upper bounds are achieved by substituting  $\ell = 0$  and  $\ell = d_{\max}$  into (D.9), respectively. This completes the proof.  $\square$

Using simulation parameters similar to those used in Fig. D.2, we depict the collision probability against the length of the typical link  $\ell$  in Fig. D.3. As stated in Proposition D.6, the collision probability is an increasing function of  $\ell$  with lower and upper bounds, formulated in (D.10). First, Proposition D.5 holds for all curves, and there is a perfect coincidence between numerical and analytical results. Moreover, both upper and lower bounds are tight for all examples considered in the figure, implying that the approximated closed-form expressions (D.10) can be effectively used for pessimistic/optimistic MAC layer designs, instead of the exact but less tractable expression. For the example of 1 transmitter in a  $3 \times 3 \text{ m}^2$  area and operating beamwidth  $\theta = 20^\circ$ , the maximum error due to those approximations, that is, the difference between upper and lower bounds is only 0.005. This error reduces as the operating beamwidth or link densities reduces, see Fig. D.3.

In the next section, we will use the collision probability to derive several performance metrics of a mmWave ad hoc network.

## D.4 Throughput and Delay Analysis

The closed-form expression of collision probability and its bounds, formulated in (D.8)–(D.10), allow deriving the effective MAC layer throughput, analyzing the

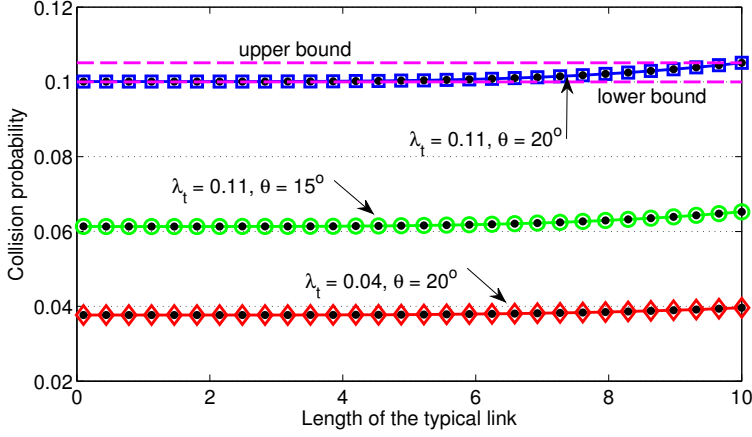


Figure D.3: The probability of collision as a function of the length of the typical link  $\ell$ , as computed by Equations (D.8) and Monte Carlo simulations, marked by filled circles. Upper and lower bounds are computed by Equation (D.10).

regime at which the network operates, highlighting inefficiency of hybrid MAC protocols of existing standards, and providing insightful discussions on the proper resource allocation and interference management protocols for future mmWave networks.

#### D.4.1 Noise-limited or Interference-limited

To compute per-link throughput, we note that the tagged transmitter is active with probability  $\rho_a$ . Its transmission to the receiver at distance  $\ell$  is successful if there is no blockage, which occurs with probability  $e^{-\lambda_o A_\ell}$ , and no collision, which occurs with probability  $(1 - \rho_{c|\ell})$ . Therefore, the conditional probability of successful transmission in a slot given  $\ell$ , denoted by  $\rho_{s|\ell}$ , is

$$\rho_{s|\ell} = \rho_a e^{-\lambda_o A_\ell} (1 - \rho_{c|\ell}) . \quad (\text{D.11})$$

Let  $r_{\text{S-ALOHA}}$  be the average MAC throughput of slotted ALOHA. Assuming transmission of one packet per slot, the average per-link throughput is equal to the average successful transmission probability, hence

$$r_{\text{S-ALOHA}} = \int_{\ell=0}^{d_{\max}} \rho_{s|\ell} f_L(\ell) d\ell = \int_{\ell=0}^{d_{\max}} \rho_a e^{-\lambda_o A_\ell} (1 - \rho_{c|\ell}) \frac{2\ell}{d_{\max}^2} d\ell , \quad (\text{D.12})$$

where  $f_L(\ell)$  is the distribution function of the link length. Since  $\rho_{s|\ell}$  is strictly decreasing with  $\ell$ , we can find upper and lower bounds of  $r_{\text{S-ALOHA}}$  by substituting

$\ell = 0$  and  $\ell = d_{\max}$  into  $\rho_s|_{\ell}$ . We have

$$\begin{aligned} \rho_a e^{-(\lambda_o + \lambda_I)\theta_c d_{\max}^2/2} \left( \frac{\lambda_o + \lambda_I e^{-(\lambda_o + \lambda_I)\theta_c d_{\max}^2/2}}{\lambda_o + \lambda_I} \right)^{\lceil \theta/\theta_c \rceil - 1} &\leq r_{\text{S-ALOHA}} \\ r_{\text{S-ALOHA}} &\leq \rho_a \left( \frac{\lambda_o + \lambda_I e^{-(\lambda_o + \lambda_I)\theta_c d_{\max}^2/2}}{\lambda_o + \lambda_I} \right)^{\lceil \theta/\theta_c \rceil}. \end{aligned} \quad (\text{D.13})$$

For a given  $\rho_a$ , the throughput is uniquely determined by the collision probability. It follows that we can study the collision probability, instead of the throughput, to identify the operating regime. By definition, we are in the *noise-limited* regime if the collision probability is too small for given density of the obstacles, density of the transmitters, and operating beamwidth, among the main parameters. On the other hand, if there is at least one LoS interferer, which limits the throughput performance of the link, the link is in *LoS interference-limited* regime. This suggests the following conclusion. A mmWave network with directional communication exhibits a *transitional behavior*, that is, a transition from a noise-limited regime to an LoS interference-limited regime. This transition depends on the density of interferers and obstacles, transmission probability, operating beamwidth, transmission powers, and coherence angle.

We use the same simulation parameters as of Fig. D.2 to investigate the collision probability as a function of  $\lambda_t$  and  $\lambda_o$ , depicted in Fig. D.4. From Fig. D.4a, collision probability is not negligible even for a modest-size network. For instance, for 1 transmitter in a 3x3 m<sup>2</sup> area and 1 obstacle in a 20x20 m<sup>2</sup> area, the collision probability is as much as 0.26. Increasing the density of obstacles to 1 obstacle in a 3x3 m<sup>2</sup> area, which is not shown in Fig. D.4a for the sake of clarity, the collision probability reduces to 0.17, which is still high enough to invalidate the assumption of being in a noise-limited regime. This conclusion becomes even more clear in Fig. D.4b, where the green curve represent a collision probability as high as 0.48 for not so dense WPANs (1 transmitter in a 2x2 m<sup>2</sup>). Moreover, as can be observed in all curves of Fig. D.4a, there is a transition from the noise-limited regime to the LoS interference-limited one. For benchmarking purposes, we also simulate a network with omnidirectional communications. Fixing all other parameters, we only increase the transmission power to achieve the same interference range as the corresponding directional communications and investigate the collision probability. As shown in Fig. D.4, traditional networks with omnidirectional communications always experience an interference-limited regime without any transitional behavior.

### D.4.2 Proper Resource Allocation Protocol

In this subsection, we compare the MAC layer throughput of a single link, area spectral efficiency (network throughput normalized to the network size), and delay performance of slotted ALOHA to those of TDMA in a mmWave network. We define delay as the difference between the time a new packet is inserted to the

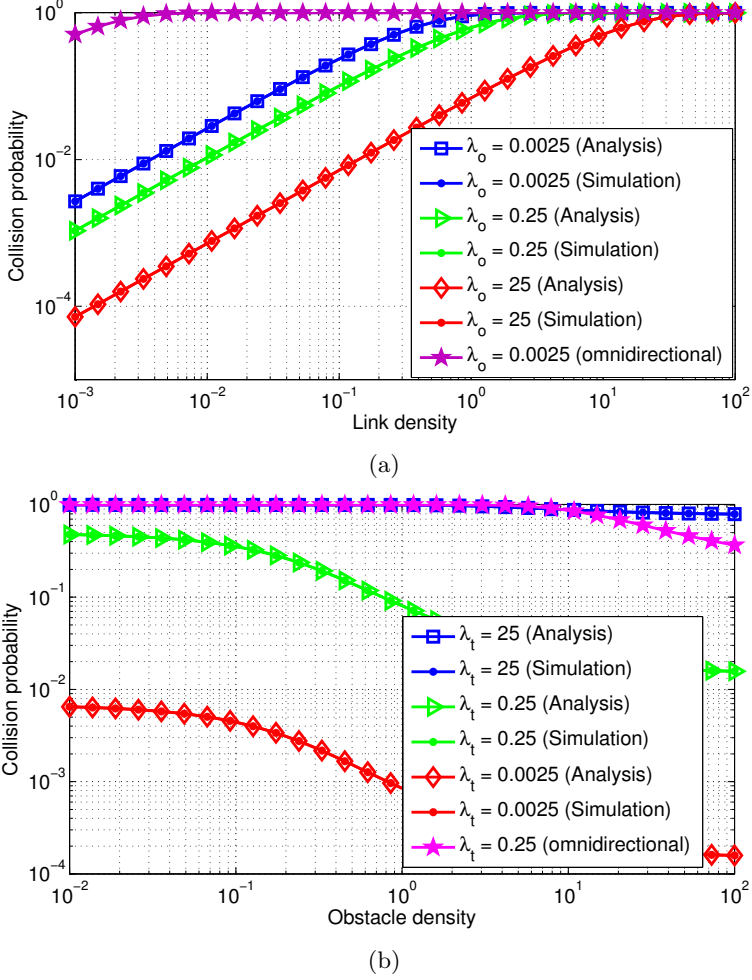


Figure D.4: The probability of collision as a function of (a) link density and (b) obstacle density. The length of the typical link is  $\ell = 5$  m.

transmission queue of the transmitter and the time it is correctly received at the receiver.

The throughput of an individual link is derived in (D.12). To evaluate the area spectral efficiency (ASE) of slotted ALOHA, we consider a large region with area  $A$ . The number of transmitters (links) inside this region is  $1 + n_t$ , where  $n_t$  follows a Poisson distribution with mean  $A\lambda_t$ . We assume that, at each transmission attempt, and regardless of the number of retransmissions suffered, each packet collides with constant and independent probability  $\rho_c$  (given by Equation (D.9)), which is



also independent of the number of transmitters. This is a common assumption in throughput analysis of IEEE 802.15.4 [150, 151] and IEEE 802.11 [152–155], which can be extended to the general case using similar approach taken in [156]. Also, we show the validity of this assumption in Figs. D.5 and D.8a. With this independence assumption, the network throughput is  $(1 + n_t) r_{\text{S-ALOHA}}$ , leading to an average network throughput of  $(1 + A\lambda_t) r_{\text{S-ALOHA}}$ . Thus, the ASE of slotted ALOHA, denoted by  $\text{ASE}_{\text{S-ALOHA}}$ , is

$$\text{ASE}_{\text{S-ALOHA}} = \frac{1 + A\lambda_t}{A} r_{\text{S-ALOHA}} = \frac{1 + A\lambda_t}{A} \int_{\ell=0}^{d_{\max}} \frac{2\rho_a}{d_{\max}^2} e^{-\lambda_o A \ell} (1 - \rho_{c|\ell}) \ell d\ell, \quad (\text{D.14})$$

which can be tightly approximated by  $\lambda_t r_{\text{S-ALOHA}}$  if  $A\lambda_t \gg 1$ . This condition holds for networks with high density of transmitters (high  $\lambda_t$ ) or for those with large size (high  $A$ ).

We can also use the derived collision probability to analyze the delay performance of slotted ALOHA. In the following, we only show the main steps and leave the exact calculations for future studies. Let  $\rho_s$  denote the probability of successful transmission, derived in (D.11) and (D.12). Let  $n_r$  be the number of retransmissions in the typical link until successful reception.  $n_r$  can be accurately approximated by a geometric distribution [157], that is,

$$\Pr[n_r = n_{r_0}] = \rho_s (1 - \rho_s)^{n_{r_0}}.$$

Let  $w_i$  be the contribution of  $i$ -the transmission/retransmission on the total delay, where  $w_0$  is the delay due to initial transmission. Each  $w_i$  contains round-trip propagation, packet transmission, and backoff delays [157]. Then, the delay is  $\sum_{i=0}^{n_r} w_i$ . Detailed analysis of the delay is out of the scope of this work, and we use Monte Carlo simulations to find the delay performance.

Unlike slotted ALOHA, TDMA protocol activates only one link at a time, regardless of the number of links. This guarantees a collision-free communication. We derive the throughput of a link and ASE of TDMA in the following proposition:

**Proposition D.7.** *Consider the blockage model, described in Fig. D.1. Let  $\lambda_o$  be the density of the obstacles,  $\theta_c$  be the coherence angle, and  $d_{\max}$  be the interference range. Consider a typical link. Let  $A$  denote the area over which TDMA regulates the transmissions of  $1 + n_t$  links, including the typical link, where  $n_t$  is Poisson random variable with density  $\lambda_t$  per unit area. Average per-link throughput under TDMA scheduler is*

$$r_{\text{TDMA}} = \left( \frac{1 - e^{-\lambda_t A}}{\lambda_t A} \right) \left( \frac{1 - e^{-\lambda_o A d_{\max}}}{\lambda_o A d_{\max}} \right). \quad (\text{D.15})$$

where  $A d_{\max} = \theta_c d_{\max}^2 / 2$ . Moreover, ASE under TDMA scheduler is

$$\text{ASE}_{\text{TDMA}} = \frac{1 - e^{-\lambda_o A d_{\max}}}{A \lambda_o A d_{\max}}. \quad (\text{D.16})$$

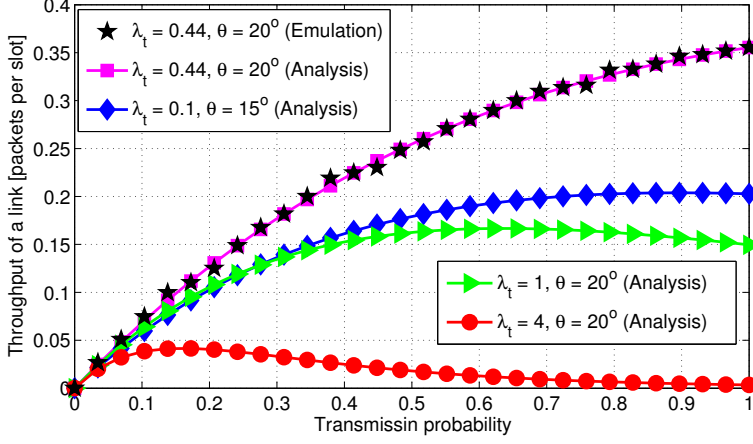


Figure D.5: The effective MAC throughput against transmission probability  $\rho_a$ , as computed by the emulator and by Equation (D.12). The obstacle density is  $\lambda_o = 0.11$  per unit area.

*Proof.* A proof is given in Appendix B. □

**Corollary 1.** *Throughput under TDMA scheduler are upper bounded by*

$$r_{TDMA} \leq \frac{1 - e^{-A\lambda_t}}{A\lambda_t}, \quad ASE_{TDMA} \leq \frac{1}{A}.$$

*Proof.* We first note that  $(1 - e^{-x})/x$  is strictly decreasing for any  $x > 0$ , and that  $x = \lambda_o A d_{\max} > 0$ . Therefore, (D.15) and (D.16) can be upper bounded by letting  $x \rightarrow 0^+$ . Using  $\lim_{x \rightarrow 0^+} (1 - e^{-x})/x \rightarrow 1$ , we conclude the proof. □

**Corollary 2.** *Consider Corollary 1. Per-link throughput under TDMA scheduler goes to zero as the average number of links in the network  $A\lambda_t$  grows large. Moreover, ASE of TDMA protocol goes to zero as the network size  $A$  grows large.*

Corollaries 1 and 2 explicitly show the inefficiency of TDMA protocol to share resources among massive number of devices in a mmWave network. Besides poor throughput performance, the delay of TDMA increases with the number of activate transmitters, as a transmitter should wait more to access the channel [158]. In the following, we numerically compare the throughput and delay performance of slotted ALOHA to TDMA.

To validate the blockage model as well as the assumption of independency of  $\rho_c$  and the number of transmitters, introduced in the throughput analysis, we build an NS3-based mmWave emulator. We consider a random number of aligned mmWave links (aligned transmitter-receiver pairs) on 2D space, all operating with the same beamwidth at 60 GHz. Transmitters and receivers are uniformly distributed in a

10x10 m<sup>2</sup> area. We also uniformly distribute a random number of obstacles with density  $\lambda_o$  in the environment. The obstacles are in the shape of lines with random orientation and their length is uniformly distributed between 0 and 1 m. Every transmitter generates traffic with constant bit rate (CBR) 384 Mbps, the size of all packets is 5 kB, time slot duration is 100  $\mu$ s, transmission rate is 1 packet per slot (link capacity around 1.5 Gbps), the transmitters have infinite buffer to save and transmit the packets, and the emulation time is 1 s.

We first start with a mmWave network operating with slotted ALOHA protocol. Fig. D.5 shows per-link throughput as a function of transmission probability. First of all, there is an excellent match between the results obtained from the emulator and those from Equation (D.12), which confirms the validity of both blockage model and the independence assumption. Moreover, for relatively not dense networks, for instance, 1 transmitter in a 1.5x1.5 m<sup>2</sup> area ( $\lambda_t = 0.44$ ), increasing the transmission probability is always beneficial, as the multiuser interference level is small enough that activating more links will not substantially reduce the average throughput of a link but increases the number of time slots over which the link is active. As the link density increases, higher collision probability introduces a tradeoff on increasing the transmission probability and reducing the interference. In a very dense network, for instance, with  $\lambda_t = 4$ , we should adopt a very small transmission probability to maximize MAC throughput.

Fig. D.6 illustrates the achievable regions of per-link throughput and ASE of slotted ALOHA with  $\rho_a = 1$  and  $\lambda_o = 0.11$ . Hotter colors correspond to higher values. For instance, with operating beamwidth  $\theta = 50^\circ$  and on average 2 transmitters in a square meter, a per-link throughput of 0.5 packets per slot is not achievable, and to achieve that, we should reduce either the operating beamwidth or the link density (or equivalently the transmission probability). It is worth noting that blockage due to obstacles may destroy the typical link, and therefore it avoids per-link throughput of 1 packet per slot even without any collision in the network. From Fig. D.6, there is a tradeoff between operating beamwidth and link density. To maintain a certain level of per-link throughput or ASE, we can either increase the operating beamwidth or link density. Furthermore, these figures confirm that without alignment overhead, mmWave networks benefit from narrower operating beamwidth and denser deployment. However, as mentioned in [57], the adoption of extremely narrow beams is not throughput optimal in general due to the alignment overhead.

Fig. D.7 shows the behavior of the optimal transmission probability of slotted ALOHA (that maximizes per-link throughput) as a function of link density  $\lambda_t$  and operating beamwidth  $\theta$ . Thanks to this figure, we can explicitly answer why there is a throughput degradation, as observed in [57], if we activate all links at the same time and under which conditions such a degradation will disappear. From Fig. D.7a, in many cases, the optimal transmission probability is 1, implying that we can simply activate all links and still achieve the maximum MAC throughput. In fact, there is negligible multiuser interference in those cases, so the performance of one of the simplest collision-based resource allocation (slotted ALOHA) is almost equivalent to the optimal collision-free resource allocation (STDMA) with much

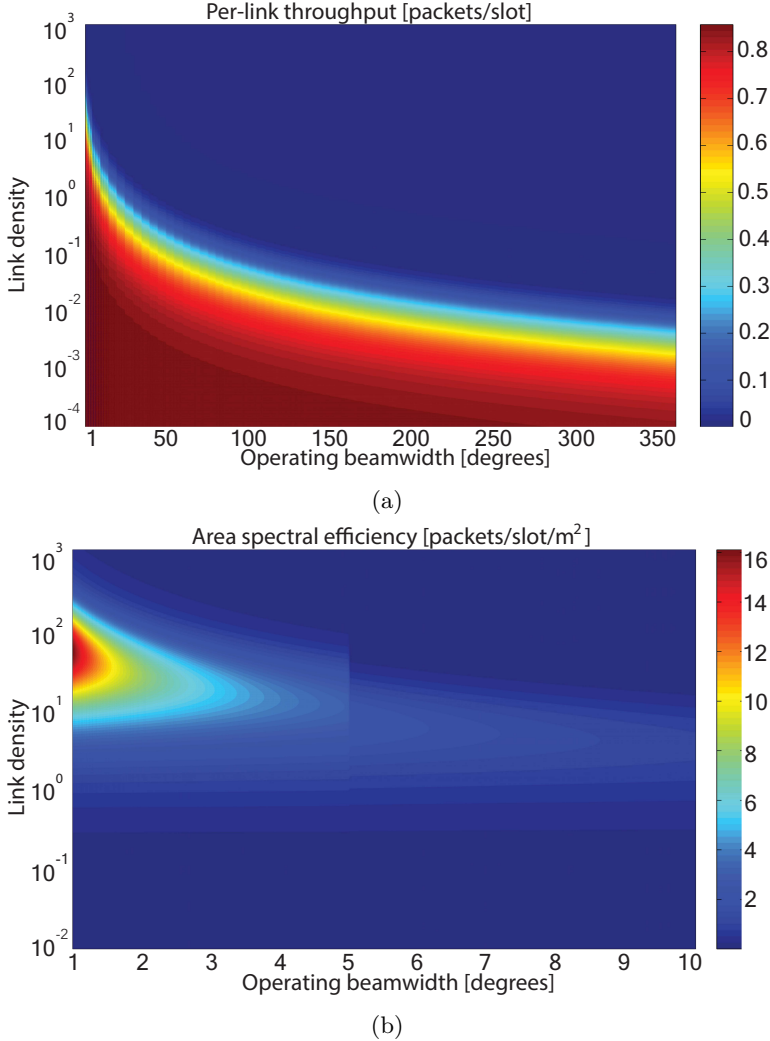
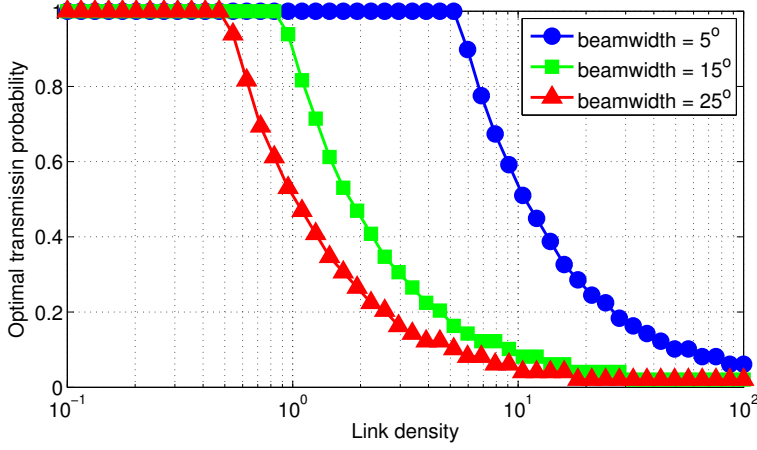


Figure D.6: Achievable regions of (a) per-link throughput and (b) area spectral efficiency of slotted ALOHA with  $\rho_a = 1$ .

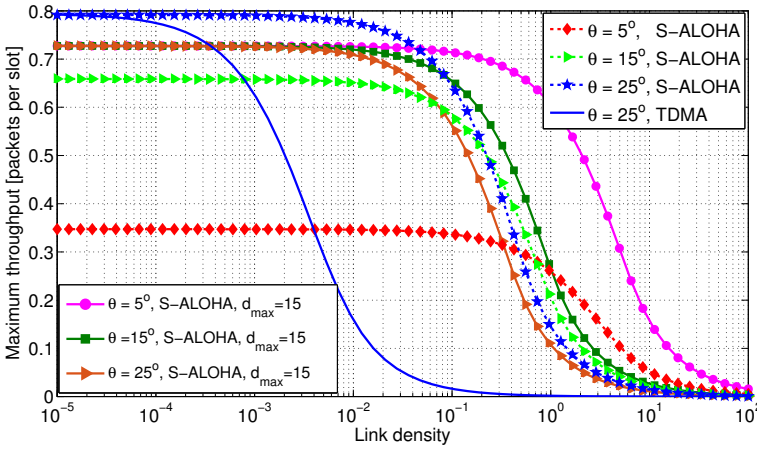
lower signaling and computational overhead. However, as the operating beamwidth or the link density increases, we should think of more intelligent resource allocation strategies as the mmWave network may transit to the interference-limited regime. This further invalidates the generality of noise-limited mmWave networks and indicates that we may adopt a very small transmission probability to decrease the contention level in an ultra dense mmWave network. Fig. D.7b demonstrates the

maximum throughput of a link in slotted ALOHA, associated with the optimal transmission probability. In the first set of curves of this figure, we fixed the interference range  $d_{\max}$  to 15, while in the second set we let  $d_{\max}$  change according to  $\theta$ , see Appendix A. Fixing either link length or  $d_{\max}$  (only the latter is depicted for the sake of clarity in the figure), the throughput of a link in slotted ALOHA will be decreased with  $\theta$ . That is because, according to (D.8) and (D.11), narrower beams reduce the collision probability, so increase  $\rho_{s|\ell}$  for any given  $\ell$ , leading to a higher average  $r_{\text{S-ALOHA}}$ . Therefore, with fixed  $d_{\max}$ , we always have *lower beamwidth higher throughput* rule. However, if we do not manually fix  $d_{\max}$  (e.g., by changing the transmission power), lower  $\theta$  causes another effect, namely extended length at which a link can be established. This extended link length, in turn, increases the blockage probability and may consequently reduce the achievable throughput. In other words, two parameters with a non-trivial interplay affect the average throughput: blockage and collision. For sparse networks, the reduced blockage probability due to a higher  $\theta$  dominates the increased collision probability, and we can observe *higher beamwidth higher throughput* rule. However, higher link density introduces more collisions to the network and highlights the impact of the collision term on the average throughput. After a critical link density, the reduced blockage probability due to a higher  $\theta$  cannot compensate for the increased collision probability, so we can observe *lower beamwidth higher throughput* rule. Furthermore, slotted ALOHA significantly outperforms TDMA as illustrated in Fig. D.7a. The main reason is that TDMA realizes an orthogonal use of time resources, irrespective of the collision level, whereas slotted ALOHA re-uses all the time resources and benefits from spatial gain. This gain leads to 390% and 4270% throughput enhancements over TDMA for the cases of 1 transmitter in a 10x10 m<sup>2</sup> and in a 3x3 m<sup>2</sup> area with  $\theta = 25^\circ$ , respectively. Note that, from Fig. D.7a, the optimal transmission probability is 1 in both cases, further highlighting simplicity of the corresponding slotted ALOHA. Furthermore, per-link throughput in TDMA is strictly decreasing with density of the transmitters, whereas that of slotted ALOHA remains almost unchanged as long as the collision term, shown in (D.11) and (D.12), is almost negligible. As stated in Corollary 2, the throughput of TDMA goes to zero very fast. Although slotted ALOHA shows the same asymptotic zero throughput behavior, it has much slower rates of convergence to this asymptotic point. Considering any arbitrary small  $\zeta$  for the per-link throughput, from Fig. D.7b, the per-link throughput of both TDMA and slotted ALOHA become lower than  $\zeta$  for sufficiently large  $\lambda_t$ ; however, slotted ALOHA reaches that point with almost two orders of magnitude more links in the network (e.g., see  $\zeta = 0.1$ ), indicating its efficiency on handling massive wireless access in mmWave networks.

We use the developed mmWave emulator to find ASE and the average delay performance. Fig. D.8a illustrates ASE of slotted ALOHA and TDMA as a function of link density. Again, there is a perfect coincidence the analytical results obtained from Equations (D.14) and (D.16) and those of the emulator. Increasing the number of links of the network does not affect ASE of TDMA. The average network



(a)

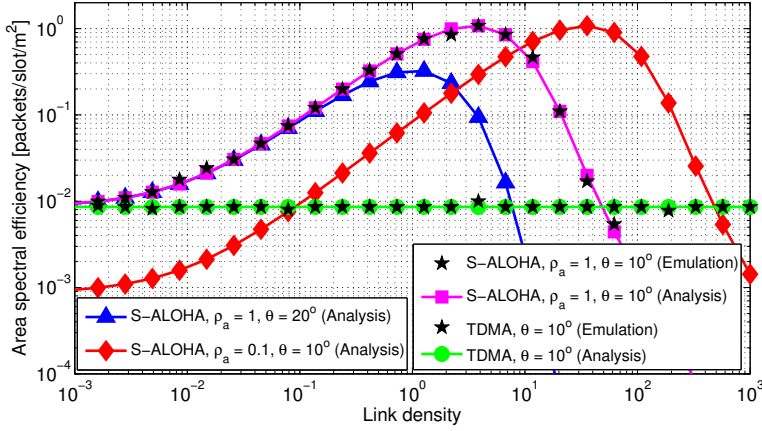


(b)

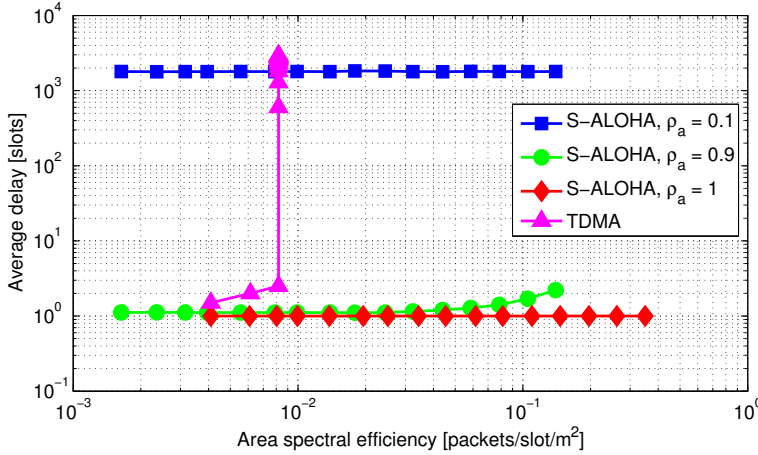
Figure D.7: (a) the optimal transmission probability and (b) the maximum per-link throughput against link density. “S-ALOHA” stands for slotted ALOHA.

throughput of TDMA is slightly lower than one packet per slot,<sup>7</sup> and it achieves the upper bound if the obstacle density goes to zero, see Corollary 2. Slotted ALOHA with transmission probability  $\rho_a = 1$  provides the highest ASE, which is firstly

<sup>7</sup>Note that TDMA can increase the network throughput if individual transmitters do not have enough payload to occupy the whole time slot. In this case, TDMA divides one long time slot to smaller pieces, each for one transmitter, leading to a more utilized time slot. However, in this paper, we have assumed that every packet of a transmitter requires one time slot, so the TDMA channel is already saturated if the transmitters have always packets to transmit.



(a)



(b)

Figure D.8: Area spectral efficiency and delay performance of slotted ALOHA and TDMA. Area size is  $10 \times 10 \text{ m}^2$ . Different points of (b) represent different link densities from 0.02 to 2 links per unit area. The obstacle density is  $\lambda_o = 0.25$  per unit area. Operating beamwidth in (b) is  $10^\circ$ . Slotted ALOHA provides higher ASE with lower delay significantly. These performance gains may improve with the number of links.

increasing with the link density and then shows a strictly decreasing behavior once the throughput loss, due to the collision term, overweighs the throughput enhancement due to the first term of (D.14). For the example of  $\rho_a = 1$  and  $\theta = 10^\circ$ , the optimal density of transmitters that maximizes the ASE is, on average, 3.5 transmit-

ters per square meter. This example number indeed means that mmWave networks benefits from dense deployment. Slotted ALOHA with  $\rho_a = 0.1$  outperforms that with  $\rho_a = 1$  in ultra dense WPANs ( $\lambda_t > 9$  in Fig. D.8a), as lower transmission probability leads to fewer active links. Moreover, narrower beams provide higher ASE.

Fig. D.8b reports ASE and the corresponding delay of TDMA and those of slotted ALOHA. Slotted ALOHA with transmission probability 1 is the best strategy from both ASE and delay perspectives. It introduces only one slot delay, that is, a packet transmission time. However, if a link observes a collision at its first transmission attempt, it cannot successfully transmit anymore, as we do not have any randomization in the transmission time (e.g., with random backoff techniques). Using slotted ALOHA with transmission probability 0.9, the aforementioned issue can be solved at the expense of extra delay with exponential growth at very high network throughput (equivalently ASE). Note that this delay is still around 2 slots for a very dense WPAN with 2 transmitters in a unit area, in the example considered. Moreover, while slotted ALOHA with transmission probability 0.1 may provide higher ASE than that with 1 in ultra dense WPANs (see Fig. D.8a), the corresponding delay becomes very large. Expectedly, the delay in TDMA increases with the link density without any significant network throughput gain, as shown in Fig. D.8b. Considering traffic generation rate of this example, which is 0.25 of the link capacity, the network will be saturated roughly with 4 links in the environment, and further increasing the number of links will not improve the network throughput, but reduces the time share of every link and consequently reduces the average throughput of a link. Note that with a fixed packet generation rate, *effective link capacity* (links capacity multiplied by its time share) in TDMA reduces with the number of links in the network, so the queues of the transmitter may become unstable. The delay in slotted ALOHA is not significantly affected by total the number of transmitters; rather it depends on the number of transmitters in the collision domain of the typical receiver –those that can cause collision to the typical receiver. This may be much smaller than the total number of transmitters in mmWave networks, thanks to the pencil-beam operation and also blockage. Furthermore, due to time-reuse, the effective link capacity of slotted ALOHA is significantly higher than that of TDMA. Superior throughput and delay performances of slotted ALOHA is due to spatial gain. As the network goes to the noise-limited regime, spatial gain and consequently throughput/delay gains improve.

### D.4.3 Collision-aware Hybrid MAC

Although slotted ALOHA may outperform TDMA in terms of throughput/delay, the latter guarantees communication with no collisions, which is necessary for specific applications. The transitional behavior of interference in mmWave networks indicates inefficacy of existing standards and suggests a dynamic incorporation of both contention-based and contention-free phases in the resource allocation. The current mmWave standards such as IEEE 802.15.3c and IEEE 802.11ad adopt similar resource allocation approaches as those developed for interference-limited mi-



crowwave networks, e.g., by IEEE 802.15.4 [150]. In particular, they introduce a contention-based phase mainly to register channel access requests of the devices inside the mmWave network. These requests are served on the following contention-free phase, called service period in IEEE 802.11ad [14]. In fact, though some data packets with low QoS requirements may be transmitted in the contention-based phase, the network traffic is mostly served in the contention-free phase irrespective of the network operating regime. Instead, we can (and should) leverage the transitional behavior of mmWave networks to dynamically serve the network traffic partially on the contention-based and partially on the contention-free phase, according to the actual network operating regime. More specifically, a data transfer interval<sup>8</sup> that is, a set of consecutive time slot over which devices will be scheduled for data transmission, can consist of a two phases:

- *phase 1*: a distributed contention-based resource allocation, which is more suitable for the noise-limited regime.
- *phase 2*: a centralized contention-free resource allocation, which is more suitable for the interference-limited regime.

While all devices can contend to access the channel in the first phase, only devices with collided packets will be scheduled on the second phase. Therefore, the proposed resource allocation framework reduces the duration of the contention-free phase to cover only the links with strong mutual interference. For a noise-limited regime, automatically, most of the traffics will be served on the first phase due to negligible multiuser interference. In an interference-limited regime, however, many links may register their collisions –so channel access requests– to be scheduled on the following contention-free phase. Using flexible phase duration, adjusted according to the collision level of the networks, we can realize an on-demand use of the inefficient contention-free phase, improve the network throughput (especially as the network goes to the noise-limited regime), and also guarantee a communication without collision. Developing a proper adaptive hybrid resource allocation framework for mmWave networks will be undertaken in future studies.

## D.5 Concluding Remarks

Millimeter wave (mmWave) communication systems use highly directional transmission/reception to compensate severe channel attenuation. This pencil-beam operation significantly reduces interference footprint, promising a significant spatial gain that is largely ignored in resource allocation of current mmWave standards. In this paper, a tractable closed-form expression for collision probability in a mmWave ad hoc network operating under slotted ALOHA was derived. This derivation allowed investigation of MAC layer throughput of a mmWave network, as a function of the density of transmitters, density of obstacles, transmission probability, operating

---

<sup>8</sup>Data transfer interval is introduced in IEEE 802.11ad [14]. Similar interval in the superframe of IEEE 802.15.3c consists of contention access period and channel time allocation period [13].

beamwidth, and transmission power, among the main parameters. Comprehensive analysis revealed that mmWave networks exhibit a transitional behavior from a noise-limited network to an interference-limited network. This transitional behavior necessitates novel frameworks of collision-aware hybrid MAC, containing both contention-based and contention-free phases with adaptive phase duration. Mathematical and numerical analysis of the per-link throughput, area spectral efficiency (network sum throughput divided by the network size), and the delay performance, indicated inefficacy of TDMA in mmWave network with small multiuser interference. Instead, slotted ALOHA efficiently leverages spatial gain and provides substantially higher throughput with lower average delay. These gains increase with the number of links in the network, making contention-based strategies more justifiable in massive mmWave access scenarios. Inspired by these results, on-demand use of inefficient contention-free strategies to only guarantee a reliable physical layer was proposed.

This paper provided a novel blockage model for mmWave networks, a new framework for analyzing the performance of mmWave networks with blockage and deafness, derived closed-form expressions for collision probability in mmWave networks along with link throughput and area spectral efficiency of slotted ALOHA as well as those of TDMA, clarified the collision level in a mmWave network with uncoordinated transmitters, discovered the transitional behavior of mmWave networks, identified the inefficiency of resource allocation of existing mmWave standards, and raised the necessity of on-demand contention-free resource allocation.

Moreover, in this paper, we evaluated the performance of slotted ALOHA for the contention-based phase. While being adopted by current mmWave standards for the contention-based phase, CSMA/CA is substantially throughput-suboptimal due to the overhead of channel reservation control messages [66]. Motivated by collision analysis of this paper and transitional behavior of mmWave networks, a fundamental question is if a mmWave transmitter still needs to reserve a channel and avoid potential collisions with expensive and inefficient control messages, irrespective of the actual network operating regime. This suggests investigation of new contention-based protocols with on-demand collision avoidance capability.

In this study, we did not consider the alignment (beam-searching) overhead [57]. That is, the time required for finding the best set of beams at the transmitter and at the receiver to establish a proper link. Boosting link budget and suppressing interference in mmWave systems with pencil-beam operation come at the expense of more complicated connection management (establishment, maintenance, and recovery) strategies. Upon missing the established channel, either due to appearance of a random obstacle or loss of precise beamforming information (e.g., due to mobility/channel change), the transmitter and receiver should trigger a time consuming alignment procedure to find another channel. Using narrower beams increases the frequency of alignment executions. Therefore, the alignment overhead may be overwhelming and dictates the overall performance of the network, especially for massive uncoordinated access and highly mobile networks [22]. Introducing the alignment overhead in the performance evaluation is an interesting future direction.

## Appendix A: Proof of Lemma D.1

In this appendix, we find probability of having at least one LoS interferer given the number of interferers  $n_I \geq 1$  and the number of obstacles  $n_o \geq 1$ . We have the following lemma:

**Lemma D.2.** *Let  $\{x_1, x_2, \dots, x_{n_I}\}$  be a set of  $n_I$  i.i.d. continuous random variables with CDF  $F_x(x) = x^2/d_{\max}^2$  and PDF  $f_x(x) = 2x/d_{\max}^2$ , where  $n_I$  is a zero-truncated Poisson random variable with density  $\lambda_I$ . Define  $X_{(1)} = \min\{x_1, \dots, x_{n_I}\}$ . Given  $n_I = n \geq 1$ , the joint PDF of  $X_{(1)}$  and  $n_I$  is given by*

$$f_{X_{(1)}, n_I}(X_{(1)} = x, n_I = n | n \geq 1) = \frac{2nx}{d_{\max}^2} \left(1 - \frac{x^2}{d_{\max}^2}\right)^{n-1} \frac{e^{-\lambda_I}}{1 - e^{-\lambda_I}} \frac{\lambda_I^n}{n!}. \quad (\text{D.17})$$

*Proof.* We define  $k$ -order statistic of  $\{x_i\}_1^{n_I}$ , denoted by  $X_{(k)}$ , as  $k$ -th smallest value of  $\{x_i\}_1^{n_I}$  [159]. Therefore,  $X_{(1)} = \min\{x_1, x_2, \dots, x_{n_I}\}$  is the first order statistic whose PDF is [159]

$$f_{X_{(1)}}(x) = n f_X(x) \left(1 - F_X(x)\right)^{n-1}. \quad (\text{D.18})$$

Noting that  $n_I = n \geq 1$  is a random variable with zero-truncated Poisson distribution, thus [116]

$$\Pr[n_I = n | n \geq 1] = \frac{e^{-\lambda_I}}{1 - e^{-\lambda_I}} \frac{\lambda_I^n}{n!}. \quad (\text{D.19})$$

Now, replacing replacing PDF and CDF of random variables  $\{x_i\}_1^{n_I}$  in (D.18) and multiplying the result by (D.19), we have

$$\begin{aligned} f_{X_{(1)}, n_I}(X_{(1)} = x, n_I = n | n \geq 1) &= f_{X_{(1)} | n_I}(x | n_I = n, n \geq 1) \Pr[n_I = n | n \geq 1] \\ &= \frac{2nx}{d_{\max}^2} \left(1 - \frac{x^2}{d_{\max}^2}\right)^{n-1} \frac{e^{-\lambda_I}}{1 - e^{-\lambda_I}} \frac{\lambda_I^n}{n!}. \end{aligned} \quad (\text{D.20})$$

This concludes the proof.  $\square$

Due to mutual independence of blockage and interferer processes, and using Lemma D.2, we obtain

$$f_{X_{(1)}, Y_{(1)}, n_I, n_o}(x, y, n, m | n, m \geq 1) = f_{X_{(1)}, n_I}(x, n | n \geq 1) f_{Y_{(1)}, n_o}(y, m | m \geq 1). \quad (\text{D.21})$$

Applying Lemma D.2 to  $f_{X_{(1)}, n_I}(x, n | n \geq 1)$  and  $f_{Y_{(1)}, n_o}(y, m | m \geq 1)$ , the first part of Lemma D.1 is straightforward. All we need to do is substituting the average number of interferers and obstacles in a sector  $\lambda_I A_{d_{\max}}$  and  $\lambda_o A_{d_{\max}}$  into (D.17).

The next step is finding the probability of having at least one LoS interferer given  $n_I \geq 1, n_o \geq 1$ , which we denote by  $I_{\text{LoS}}$ . We have

$$\begin{aligned}
I_{\text{LoS}} &= \Pr[x < y | n \geq 1, m \geq 1] \\
&= \int_{y=0}^{d_{\max}} \int_{x=0}^y \sum_{n=1}^{\infty} \sum_{m=1}^{\infty} f_{X_{(1)}, n_I}(x, n | n \geq 1) f_{Y_{(1)}, n_o}(y, m | m \geq 1) dx dy \\
&\stackrel{(D.17)}{=} \frac{4\lambda_I \lambda_o A_{d_{\max}}^2}{d_{\max}^4} \int_{y=0}^{d_{\max}} \int_{x=0}^y \left\{ \frac{xy e^{-(\lambda_I + \lambda_o) A_{d_{\max}}}}{(1 - e^{-\lambda_I A_{d_{\max}}})(1 - e^{-\lambda_o A_{d_{\max}}})} \right. \\
&\quad \times \sum_{n=1}^{\infty} \frac{\left( \left(1 - \frac{x^2}{d_{\max}^2}\right) \lambda_I A_{d_{\max}} \right)^{n-1}}{(n-1)!} \sum_{m=1}^{\infty} \frac{\left( \left(1 - \frac{y^2}{d_{\max}^2}\right) \lambda_o A_{d_{\max}} \right)^{m-1}}{(m-1)!} dx dy \left. \right\} \\
&\stackrel{(\star)}{=} \frac{4\lambda_I \lambda_o A_{d_{\max}}^2}{d_{\max}^4 (1 - e^{-\lambda_I A_{d_{\max}}})(1 - e^{-\lambda_o A_{d_{\max}}})} \\
&\quad \times \int_{y=0}^{d_{\max}} \int_{x=0}^y e^{-(\lambda_I + \lambda_o) A_{d_{\max}}} e^{(1-x^2/d_{\max}^2) \lambda_I A_{d_{\max}}} e^{(1-y^2/d_{\max}^2) \lambda_o A_{d_{\max}}} xy dx dy \\
&= \frac{4\lambda_I \lambda_o A_{d_{\max}}^2}{d_{\max}^4 (1 - e^{-\lambda_I A_{d_{\max}}})(1 - e^{-\lambda_o A_{d_{\max}}})} \\
&\quad \times \int_{y=0}^{d_{\max}} y e^{-\lambda_o A_{d_{\max}} y^2 / d_{\max}^2} \int_{x=0}^y x e^{-\lambda_I A_{d_{\max}} x^2 / d_{\max}^2} dx dy \\
&= \frac{\lambda_o}{(1 - e^{-\lambda_I A_{d_{\max}}})(1 - e^{-\lambda_o A_{d_{\max}}})} \left( \frac{1 - e^{-\lambda_o A_{d_{\max}}}}{\lambda_o} - \frac{1 - e^{-(\lambda_o + \lambda_I) A_{d_{\max}}}}{\lambda_o + \lambda_I} \right), \tag{D.22}
\end{aligned}$$

where  $(\star)$  follows from the Taylor series of the exponential function. This completes the proof of Lemma D.1.  $\square$

## Appendix B: Throughput Analysis of TDMA

Consider a network of area  $A$ , TDMA-based channel access, and  $1 + n_t$  links including the typical link, where  $n_t$  is a Poisson random variable with mean  $A\lambda_t$ . Also, assume that the intended receiver of each transmitter  $i$  is located at distance  $0 < \ell_i \leq d_{\max}$  at the cone where the transmitter's signal is pointed. Having a natural assumption of independency of the lengths of different links,  $\{\ell_i\}_{i=1}^{1+n_t}$  become i.i.d random variables with density function  $f_L(\ell) = 2\ell/d_{\max}^2$ . Let  $z_{\ell_i}$  be a binary random variable taking 1 if and only if link  $i$  has the LoS condition (no blockage). As there is no simultaneous transmissions in TDMA, the success probability for TDMA given  $\ell_i$  and  $n_t$  is equal to having no obstacle on link  $i$  that occurs with

probability  $\Pr[z_{\ell_i} = 1 | \ell_i, n_t] = e^{-\lambda_o A_{\ell_i}}$ , see Fig. D.1. In long term, TDMA scheduler allocates only  $1/(1 + n_t)$  shares of the total resources to every link. Assuming transmission of one packet per slot, the MAC throughput of each link  $i$  in TDMA is

$$\begin{aligned} r_{\text{TDMA}} &= \sum_{n_t=0}^{\infty} \frac{e^{-A\lambda_t}}{(1+n_t)} \frac{(A\lambda_t)^{n_t}}{n_t!} \int_{\ell_i=0}^{d_{\max}} e^{-\lambda_o \theta_c \ell_i^2/2} \frac{2\ell_i}{d_{\max}^2} d\ell_i \\ &= \left( \frac{1 - e^{-A\lambda_t}}{A\lambda_t} \right) \frac{2}{d_{\max}^2} \left( \frac{1 - e^{-\lambda_o A d_{\max}}}{\lambda_o \theta_c} \right). \end{aligned} \quad (\text{D.23})$$

Recalling  $A_{d_{\max}} = \theta_c d_{\max}^2/2$ , (D.23) simplifies to (D.15). To find the area spectral efficiency of TDMA scheduler, we assume that  $z_{\ell_i}$  and  $z_{\ell_j}$  are independent for all  $\ell_i, \ell_j, i$ , and  $j$ , where  $j \neq i$ .<sup>9</sup> The area spectral efficiency of TDMA is

$$\begin{aligned} \text{ASE}_{\text{TDMA}} &= \frac{1}{A} \sum_{n_t=0}^{\infty} e^{-A\lambda_t} \frac{(A\lambda_t)^{n_t}}{n_t!} \text{ASE}_{\text{TDMA}|n_t} \\ &= \frac{1}{A} \sum_{n_t=0}^{\infty} \frac{e^{-A\lambda_t}}{1+n_t} \frac{(A\lambda_t)^{n_t}}{n_t!} \int_{\ell_1=0}^{d_{\max}} \cdots \int_{\ell_{1+n_t}=0}^{d_{\max}} \left\{ \sum_{i=1}^{1+n_t} \Pr[z_{\ell_i} = 1 | \ell_1, \dots, \ell_{1+n_t}, n_t] f(\ell_1, \dots, \ell_{1+n_t}) d\ell_1 \dots d\ell_{1+n_t} \right\} \\ &= \frac{1}{A} \sum_{n_t=0}^{\infty} \frac{e^{-A\lambda_t}}{1+n_t} \frac{(A\lambda_t)^{n_t}}{n_t!} \sum_{i=1}^{1+n_t} \left\{ \left( \int_{\ell_i=0}^{d_{\max}} \Pr[z_{\ell_i} = 1 | \ell_i, n_t] f(\ell_i) d\ell_i \right) \right. \\ &\quad \left. \times \prod_{\substack{j=1 \\ j \neq i}}^{1+n_t} \int_{\ell_j=0}^{d_{\max}} f(\ell_j) d\ell_j \right\} \\ &= \frac{1}{A} \sum_{n_t=0}^{\infty} \frac{e^{-A\lambda_t}}{1+n_t} \frac{(A\lambda_t)^{n_t}}{n_t!} \sum_{i=1}^{1+n_t} \int_{\ell_i=0}^{d_{\max}} e^{-\lambda_o \theta_c \ell_i^2/2} \frac{2\ell_i}{d_{\max}^2} d\ell_i \\ &= \frac{1}{A} \sum_{n_t=0}^{\infty} \frac{e^{-A\lambda_t}}{1+n_t} \frac{(A\lambda_t)^{n_t}}{n_t!} (1+n_t) \left( \frac{1 - e^{-\lambda_o A d_{\max}}}{\lambda_o A d_{\max}} \right) = \frac{1 - e^{-\lambda_o A d_{\max}}}{A \lambda_o A d_{\max}}, \end{aligned} \quad (\text{D.24})$$

<sup>9</sup>This independency means that the event of having obstacle on the path between different transmitter-receiver pairs are independent. Still, we have correlated LoS conditions on the channels between a reference receiver and different transmitters.

where  $f_{L_1, \dots, L_{1+n_t}}(\ell_1, \dots, \ell_{1+n_t})$  is joint distribution of links lengths and  $\text{ASE}_{\text{TDMA}|n_t}$  is the area spectral efficiency of TDMA given  $n_t$ . This concludes the proof.  $\square$

---

## Bibliography

---

- [1] Y. Niu, Y. Li, D. Jin, L. Su, and A. Vasilakos, “Survey of millimeter wave communications (mmWave) for 5G: Opportunities and challenges,” *Wireless Networks*, pp. 1–20, Apr. 2015.
- [2] T. S. Rappaport, R. Heath, R. C. Daniels, and J. N. Murdock, *Millimeter Wave Wireless Communications*. Pearson Education, 2014.
- [3] T. Rappaport, S. Sun, R. Mayzus, H. Zhao, Y. Azar, K. Wang, G. Wong, J. Schulz, M. Samimi, and F. Gutierrez, “Millimeter wave mobile communications for 5G cellular: It will work!” *IEEE Access*, vol. 1, pp. 335–349, May 2013.
- [4] F. Boccardi, R. Heath, A. Lozano, T. L. Marzetta, and P. Popovski, “Five disruptive technology directions for 5G,” *IEEE Commun. Mag.*, vol. 52, no. 2, pp. 74–80, Feb. 2014.
- [5] J. G. Andrews, S. Buzzi, W. Choi, S. Hanly, A. Lozano, A. C. Soong, and J. C. Zhang, “What will 5G be?” *IEEE J. Sel. Areas Commun.*, vol. 32, no. 6, pp. 1065–1082, Jun. 2014.
- [6] A. Osseiran, F. Boccardi, V. Braun, K. Kusume, P. Marsch, M. Maternia, O. Queseth, M. Schellmann, H. Schotten, H. Taoka *et al.*, “Scenarios for 5G mobile and wireless communications: the vision of the METIS project,” *IEEE Commun. Mag.*, vol. 52, no. 5, pp. 26–35, May 2014.
- [7] T. S. Rappaport, G. R. MacCartney, M. K. Samimi, and S. Sun, “Wideband millimeter-wave propagation measurements and channel models for future wireless communication system design,” *IEEE Trans. Commun.*, 2015, to be published.
- [8] Z. Pi and F. Khan, “An introduction to millimeter-wave mobile broadband systems,” *IEEE Commun. Mag.*, vol. 49, no. 6, pp. 101–107, Jun. 2011.
- [9] Federal Communications Commission, “Fcc-154,” Oct. 2014. [Online]. Available: <http://apps.fcc.gov/edocspublic/attachmatch/FCC-14-154A1.pdf>
- [10] —, “Fcc-177,” Jan. 2015. [Online]. Available: <http://apps.fcc.gov/ecfs/proceeding/view?name=14-177>

- [11] Ofcom, "Spectrum above 6 ghz for future mobile communications," Feb. 2015. [Online]. Available: [http://stakeholders.ofcom.org.uk/binaries/consultations/above-6ghz/summary/spectrum\\_above\\_6\\_GHz\\_CFI.pdf](http://stakeholders.ofcom.org.uk/binaries/consultations/above-6ghz/summary/spectrum_above_6_GHz_CFI.pdf)
- [12] T. S. Rappaport, J. N. Murdock, and F. Gutierrez, "State of the art in 60-GHz integrated circuits and systems for wireless communications," *Proc. IEEE*, vol. 99, no. 8, pp. 1390–1436, Aug. 2011.
- [13] "IEEE 802.15.3c Part 15.3: Wireless medium access control (MAC) and physical layer (PHY) specifications for high rate wireless personal area networks (WPANs) amendment 2: Millimeter-wave-based alternative physical layer extension," Oct. 2009.
- [14] "IEEE 802.11ad. Part 11: Wireless LAN medium access control (MAC) and physical layer (PHY) specifications - amendment 3: Enhancements for very high throughput in the 60 GHz band," Dec. 2012.
- [15] W. Hong, K.-H. Baek, Y. Lee, Y. Kim, and S.-T. Ko, "Study and prototyping of practically large-scale mmWave antenna systems for 5G cellular devices," *IEEE Commun. Mag.*, vol. 52, no. 9, pp. 63–69, Sept. 2014.
- [16] *IEEE Commun. Mag.*, special issue on, "Millimeter-wave communications for 5G: Fundamental: Part I," vol. 52, no. 9, Sept. 2014.
- [17] —, "Millimeter-wave communications for 5G: Application: Part II," vol. 53, no. 1, Jan. 2015.
- [18] C. Dehos, J. Gonzalez, A. Domenico, D. Ktenas, and L. Dussopt, "Millimeter-wave access and backhauling: The solution to the exponential data traffic increase in 5G mobile communications systems?" *IEEE Commun. Mag.*, vol. 52, no. 9, pp. 88–95, Sept. 2014.
- [19] S. Rangan, T. Rappaport, and E. Erkip, "Millimeter wave cellular wireless networks: Potentials and challenges," *Proc. IEEE*, vol. 102, no. 3, pp. 366–385, Mar. 2014.
- [20] E. Torkildson, U. Madhow, and M. Rodwell, "Indoor millimeter wave MIMO: Feasibility and performance," *IEEE Trans. Wireless Commun.*, vol. 10, no. 12, pp. 4150–4160, Dec. 2011.
- [21] Y. Zhang, P. Wang, and A. Goldsmith, "Rainfall effect on the performance of millimeter-wave MIMO systems," *IEEE Trans. Wireless Commun.*, 2015, to be published.
- [22] H. Shokri-Ghadikolaei, C. Fischione, G. Fodor, P. Popovski, and M. Zorzi, "Millimeter wave cellular networks: A MAC layer perspective," *IEEE Trans. Commun.*, 2015, to be published.



- [23] P. Demestichas, A. Georgakopoulos, D. Karvounas, K. Tsagkaris, V. Stavroulaki, J. Lu, C. Xiong, and J. Yao, "5G on the horizon: Key challenges for the radio-access network," *IEEE Veh. Technol. Mag.*, vol. 8, no. 3, pp. 47–53, Sept. 2013.
- [24] F. Haider, X. Gao, X.-H. You, Y. Yang, D. Yuan, H. M. Aggoune, and H. Haas, "Cellular architecture and key technologies for 5G wireless communication networks," *IEEE Commun. Mag.*, pp. 123–130, Feb. 2014.
- [25] S. Sun, T. Rappapport, R. Heath, A. Nix, and S. Rangan, "MIMO for millimeter wave wireless communications: Beamforming, spatial multiplexing, or both?" *IEEE Commun. Mag.*, vol. 52, no. 12, pp. 110–121, Dec. 2014.
- [26] J. Mo and R. Heath, "High SNR capacity of millimeter wave MIMO systems with one-bit quantization," in *Proc. IEEE Information Theory and Applications Workshop (ITA)*, 2014, pp. 1–5.
- [27] A. Alkhateeb, J. Mo, N. González-Prelcic, and R. Heath, "MIMO precoding and combining solutions for millimeter-wave systems," *IEEE Commun. Mag.*, vol. 52, no. 12, pp. 122–130, Dec. 2014.
- [28] V. Venkateswaran and A. J. Veen, "Analog beamforming in MIMO communications with phase shift networks and online channel estimation," *IEEE Trans. Sign. Proces.*, vol. 58, no. 8, pp. 4131–4143, Aug. 2010.
- [29] S. Han, I. Chih-Lin, Z. Xu, and C. Rowell, "Large-scale antenna systems with hybrid analog and digital beamforming for millimeter wave 5G," *IEEE Commun. Mag.*, vol. 53, no. 1, pp. 186–194, Jan. 2015.
- [30] T. Kim, J. Park, J.-Y. Seol, S. Jeong, J. Cho, and W. Roh, "Tens of Gbps support with mmWave beamforming systems for next generation communications," in *Proc. IEEE Global Communications Conference (GLOBECOM)*, Dec. 2013, pp. 3685–3690.
- [31] T. Obara, S. Suyama, J. Shen, and Y. Okumura, "Joint fixed beamforming and eigenmode precoding for super high bit rate massive mimo systems using higher frequency bands," in *Proc. IEEE Personal, Indoor and Mobile Radio Communications (PIMRC)*, Sept. 2014, pp. 1–5.
- [32] H. Ghauch, M. Bengtsson, T. Kim, and M. Skoglund, "Subspace estimation and decomposition for hybrid analog-digital millimetre-wave mimo systems," in *Proc. IEEE International Workshop on Signal Processing Advances in Wireless Communications (SPAWC)*, 2015.
- [33] A. Alkhateeb, O. El Ayach, G. Leus, and R. Heath, "Channel estimation and hybrid precoding for millimeter wave cellular systems," *IEEE J. Sel. Top. Sign. Proces.*, vol. 8, no. 5, pp. 831–846, Oct. 2014.

- [34] S. Rajagopal, S. Abu-Surra, and M. Malmirchegini, "Channel feasibility for outdoor non-line-of-sight mmwave mobile communication," in *Proc. IEEE Vehicular Technology Conference (VTC Fall)*, 2012, pp. 1–6.
- [35] J. Lu, D. Steinbach, P. Cabrol, and P. Pietraski, "Modeling the impact of human blockers in millimeter wave radio links," *ZTE Commun. Mag.*, vol. 10, no. 4, pp. 23–28, Jan. 2012.
- [36] K. C. Allen, N. DeMinco, J. Hoffman, Y. Lo, and P. Papazian, *Building Penetration Loss Measurements at 900 MHz, 11.4 GHz, and 28.8 MHz*. US Department of Commerce, National Telecommunications and Information Administration Rep. 94-306, 1994.
- [37] A. V. Alejos, M. G. Sánchez, and I. Cuiñas, "Measurement and analysis of propagation mechanisms at 40 GHz: Viability of site shielding forced by obstacles," *IEEE Trans. Veh. Technol.*, vol. 57, no. 6, pp. 3369–3380, Nov. 2008.
- [38] H. Zhao, R. Mayzus, S. Sun, M. Samimi, J. K. Schulz, Y. Azar, K. Wang, G. N. Wong, F. Gutierrez, and T. S. Rappaport, "28 GHz millimeter wave cellular communication measurements for reflection and penetration loss in and around buildings in New York City," in *Proc. IEEE International Conference on Communications (ICC)*, 2013, pp. 5163–5167.
- [39] P. Gupta and P. R. Kumar, "The capacity of wireless networks," *IEEE Trans. Inform. Theory*, vol. 46, no. 2, pp. 388–404, Mar. 2000.
- [40] P. Kyasanur and N. H. Vaidya, "Capacity of multichannel wireless networks under the protocol model," *IEEE/ACM Trans. Netw.*, vol. 17, no. 2, pp. 515–527, Apr. 2009.
- [41] A. El Gamal, J. Mammen, B. Prabhakar, and D. Shah, "Optimal throughput-delay scaling in wireless networks-part I: The fluid model," *IEEE Trans. Inform. Theory*, vol. 52, no. 6, pp. 2568–2592, Jun. 2006.
- [42] T. Nandagopal, T.-E. Kim, X. Gao, and V. Bharghavan, "Achieving MAC layer fairness in wireless packet networks," in *Proc. ACM International Conference on Mobile Computing and Networking (MobiCom)*, 2000, pp. 87–98.
- [43] S. Singh, R. Mudumbai, and U. Madhow, "Interference analysis for highly directional 60-GHz mesh networks: The case for rethinking medium access control," *IEEE/ACM Trans. Netw.*, vol. 19, no. 5, pp. 1513–1527, Oct. 2011.
- [44] G. D. Celik, G. Zussman, W. F. Khan, and E. Modiano, "MAC for networks with multipacket reception capability and spatially distributed nodes," *IEEE Trans. Mobile Comput.*, vol. 9, no. 2, pp. 226–240, Aug. 2010.
- [45] H. Dahrouj and W. Yu, "Coordinated beamforming for the multicell multi-antenna wireless system," *IEEE Trans. Wireless Commun.*, vol. 9, no. 5, pp. 1748–1759, May 2010.

- [46] M. Sharif and B. Hassibi, "On the capacity of MIMO broadcast channels with partial side information," *IEEE Trans. Inform. Theory*, vol. 51, no. 2, pp. 506–522, Feb. 2005.
- [47] F. Rashid-Farrokhi, L. Tassiulas, and K. Liu, "Joint optimal power control and beamforming in wireless networks using antenna arrays," *IEEE Trans. Commun.*, vol. 46, no. 10, pp. 1313–1324, Oct. 1998.
- [48] T. Bai and R. Heath, "Coverage and rate analysis for millimeter wave cellular networks," *IEEE Trans. Wireless Commun.*, vol. 14, no. 2, pp. 1100–1114, Feb. 2015.
- [49] H. Q. Ngo, E. G. Larsson, and T. L. Marzetta, "Energy and spectral efficiency of very large multiuser MIMO systems," *IEEE Trans. Commun.*, vol. 61, no. 4, pp. 1436–1449, Feb. 2013.
- [50] H. Shokri-Ghadikolaei, C. Fischione, and E. Modiano, "The right interference model for millimeter wave networks," *KTH Royal Institute of Technology, Tech. Rep.*, July 2015, available upon request.
- [51] T. Bai, R. Vaze, and R. Heath, "Analysis of blockage effects on urban cellular networks," *IEEE Trans. Wireless Commun.*, vol. 13, no. 9, pp. 5070–5083, Sept. 2014.
- [52] ECMA-TC48, ECMA standard 387, "High rate 60 GHz PHY, MAC and HDMI PAL," Dec. 2008.
- [53] F. Rossetto and M. Zorzi, "A low-delay MAC solution for MIMO ad hoc networks," *IEEE Trans. Wireless Commun.*, vol. 8, no. 1, pp. 130–135, Jan. 2009.
- [54] J. Polastre, J. Hill, and D. Culler, "Versatile low power media access for wireless sensor networks," in *Proc. ACM international conference on embedded networked sensor systems (SenSys)*, 2004, pp. 95–107.
- [55] R. Nelson and L. Kleinrock, "Spatial TDMA: A collision-free multihop channel access protocol," *IEEE Trans. Commun.*, vol. 33, no. 9, pp. 934–944, Sept. 1985.
- [56] X. An and R. Hekmat, "Directional MAC protocol for millimeter wave based wireless personal area networks," in *Proc. IEEE Vehicular Technology Conference (VTC Spring)*, 2008, pp. 1636–1640.
- [57] H. Shokri-Ghadikolaei, L. Gkatzikis, and C. Fischione, "Beam-searching and transmission scheduling in millimeter wave communications," in *Proc. IEEE International Conference on Communications (ICC)*, 2015.

- [58] P. Bjorklund, P. Varbrand, and D. Yuan, "Resource optimization of spatial tdma in ad hoc radio networks: A column generation approach," in *Proc. IEEE International Conference on Computer Communications (INFOCOM)*, 2003, pp. 818–824.
- [59] J. Grönkvist and A. Hansson, "Comparison between graph-based and interference-based stdma scheduling," in *Proc. ACM international symposium on Mobile ad hoc networking & computing (MobiHoc)*, 2001, pp. 255–258.
- [60] S. Ramanathan, "A unified framework and algorithm for (T/F/C) DMA channel assignment in wireless networks," in *Proc. IEEE International Conference on Computer Communications (INFOCOM)*, 1997, pp. 900–907.
- [61] G.-Z. Yang and M. Yacoub, "Body sensor networks," 2006.
- [62] I. Rhee, A. Warriar, M. Aia, J. Min, and M. L. Sichitiu, "Z-MAC: A hybrid MAC for wireless sensor networks," *IEEE/ACM Trans. Netw.*, vol. 16, no. 3, pp. 511–524, 2008.
- [63] T. Van Dam and K. Langendoen, "An adaptive energy-efficient MAC protocol for wireless sensor networks," in *Proc. PACM*.
- [64] B. Krishnamachari, *Networking wireless sensors*. Cambridge University Press, 2005.
- [65] P. Karn, "Maca-a new channel access method for packet radio," in *ARRL/CRRL Amateur radio 9th computer networking conference*, vol. 140, 1990, pp. 134–140.
- [66] E. Magistretti, O. Gurewitz, and E. W. Knightly, "802.11ec: Collision avoidance without control messages," *IEEE/ACM Trans. Netw.*, vol. 22, no. 6, pp. 1845–1858, Dec. 2014.
- [67] M. Di Renzo, "Stochastic geometry modeling and analysis of multi-tier millimeter wave cellular networks," *IEEE Trans. Wireless Commun.*, 2015, to be published.
- [68] M. Kim, S.-E. Hong, and J. Kim, "Analysis of directional communication via relaying devices in mmWave WPANs," *Communications Letters, IEEE*, vol. 16, no. 3, pp. 342–345, Mar. 2012.
- [69] H. Shokri-Ghadikolaei and C. Fischione, "The transitional behavior of interference in millimeter wave networks," *submitted to IEEE Trans. Commun.*, May 2015.
- [70] J. Qiao, X. Shen, J. Mark, Q. Shen, Y. He, and L. Lei, "Enabling device-to-device communications in millimeter-wave (5G) cellular networks," *IEEE Commun. Mag.*, vol. 53, no. 1, pp. 209–215, Jan. 2015.

- [71] R. Baldemair, T. Irnich, K. Balachandran, E. Dahlman, G. Mildh, Y. Selen, S. Parkvall, M. Meyer, and A. Osseiran, "Ultra-dense networks in millimeter-wave frequencies," *IEEE Commun. Mag.*, vol. 53, no. 1, pp. 202–208, Jan. 2015.
- [72] N. Bhushan, J. Li, D. Malladi, R. Gilmore, D. Brenner, A. Damnjanovic, R. Sukhavasi, C. Patel, and S. Geirhofer, "Network densification: The dominant theme for wireless evolution into 5G," *IEEE Commun. Mag.*, vol. 52, no. 2, pp. 82–89, Feb. 2014.
- [73] B. Bangerter, S. Talwar, R. Arefi, and K. Stewart, "Networks and devices for the 5G era," *IEEE Commun. Mag.*, vol. 52, no. 2, pp. 90–96, Feb. 2014.
- [74] J. Mitola, J. Guerri, J. Reed, Y.-D. Yao, Y. Chen, T. Clancy, J. Dwyer, H. Li, H. Man, R. McGwier *et al.*, "Accelerating 5G QoE via public-private spectrum sharing," *IEEE Commun. Mag.*, vol. 52, no. 5, pp. 77–85, May 2014.
- [75] S. Shalmashi, E. Bjornson, M. Kountouris, K. W. Sung, and M. Debbah, "Energy efficiency and sum rate when massive MIMO meets device-to-device communication," in *Proc. IEEE International Conference on Communications (ICC)*, 2015.
- [76] A. Asadi, Q. Wang, and V. Mancuso, "A survey on device-to-device communication in cellular networks," *IEEE Commun. Surveys Tuts.*, vol. 16, no. 4, pp. 1801–1819, Fourth Quarter 2014.
- [77] S. Hur, T. Kim, D. J. Love, J. V. Krogmeier, T. A. Thomas, and A. Ghosh, "Millimeter wave beamforming for wireless backhaul and access in small cell networks," *IEEE Trans. Commun.*, vol. 61, no. 10, pp. 4391–4403, Oct. 2013.
- [78] O. El Ayach, S. Rajagopal, S. Abu-Surra, Z. Pi, and R. Heath, "Spatially sparse precoding in millimeter wave MIMO systems," *IEEE Trans. Wireless Commun.*, vol. 13, no. 3, pp. 1499–1513, Mar. 2014.
- [79] P. Schniter and A. Sayeed, "Channel estimation and precoder design for millimeter-wave communications: The sparse way," in *Proc. IEEE Asilomar Conference on Signals, Systems and Computers*, 2014, pp. 273–277.
- [80] D. Astely, E. Dahlman, G. Fodor, S. Parkvall, and J. Sachs, "LTE release 12 and beyond," *IEEE Commun. Mag.*, vol. 51, no. 7, pp. 154–160, Jul. 2013.
- [81] K. Zheng, L. Zhao, J. Mei, M. Dohler, W. Xiang, and Y. Peng, "10 Gb/s HetSNetS with millimeter-wave communications: Access and networking – challenges and protocols," *IEEE Commun. Mag.*, vol. 53, no. 1, pp. 222–231, Jan. 2015.
- [82] H. Ishii, Y. Kishiyama, and H. Takahashi, "A novel architecture for LTE-B: C-plane/U-plane split and Phantom Cell concept," in *Proc. IEEE Global Communications Conference (GLOBECOM) Workshops*, 2012, pp. 624–630.

- [83] H. Shokri-Ghadikolaei, C. Fischione, P. Popovski, and M. Zorzi, "Design aspects of short range millimeter wave wireless networks: A MAC layer perspective," *submitted to IEEE Network*, May 2015.
- [84] L. Lu, G. Y. Li, A. L. Swindlehurst, A. Ashikhmin, and R. Zhang, "An overview of massive MIMO: Benefits and challenges," *IEEE J. Sel. Areas Commun.*, vol. 8, no. 5, pp. 742–758, Oct. 2014.
- [85] K. Guo, Y. Guo, G. Fodor, and G. Ascheid, "Uplink power control with MMSE receiver in multi-cell MU-massive-MIMO systems," in *Proc. IEEE International Conference on Communications (ICC)*, 2014, pp. 5184–5190.
- [86] G. Fodor, P. Di Marco, and M. Telek, "Performance analysis of block and comb type channel estimation for massive MIMO systems," in *Proc. IEEE International Conference on 5G for Ubiquitous Connectivity (5GU)*, 2014, pp. 62–69.
- [87] T. E. Bogale and L. B. Le, "Beamforming for multiuser massive MIMO systems: Digital versus hybrid analog-digital," in *Proc. IEEE Global Communications Conference (GLOBECOM)*, Dec. 2014, pp. 4066–4071.
- [88] S. Singh, F. Ziliotto, U. Madhow, E. Belding, and M. Rodwell, "Blockage and directivity in 60 GHz wireless personal area networks: From cross-layer model to multihop MAC design," *IEEE J. Sel. Areas Commun.*, vol. 27, no. 8, pp. 1400–1413, Oct. 2009.
- [89] M. Haenggi, *Stochastic Geometry for Wireless Networks*. Cambridge University Press, 2013.
- [90] J. Liu, R. Love, K. Stewart, and M. Buckley, "Design and analysis of LTE physical downlink control channel," in *Proc. IEEE Vehicular Technology Conference (VTC Spring)*, 2009, pp. 1–5.
- [91] A. M. Hunter, J. G. Andrews, and S. Weber, "Transmission capacity of ad hoc networks with spatial diversity," *IEEE Trans. Wireless Commun.*, vol. 7, no. 12, pp. 5058–5071, Dec. 2008.
- [92] J. Wildman, P. H. Nardelli, M. Latva-aho, and S. Weber, "On the joint impact of beamwidth and orientation error on throughput in wireless directional poisson networks," *IEEE Trans. Wireless Commun.*, vol. 13, no. 12, pp. 7072–7085, Dec. 2014.
- [93] B. Liu and D. Towsley, "A study of the coverage of large-scale sensor networks," in *Proc. IEEE International Conference on Mobile Ad hoc and Sensor Systems (MASS)*, 2004, pp. 475–483.
- [94] C.-F. Hsin and M. Liu, "Randomly duty-cycled wireless sensor networks: Dynamics of coverage," *IEEE Trans. Wireless Commun.*, vol. 5, no. 11, pp. 3182–3192, Nov. 2006.

- [95] S. Sesia, I. Toufik, and M. Baker, *LTE: The UMTS long term evolution*. Wiley Online Library, 2009.
- [96] Q. C. Li, H. Niu, G. Wu, and R. Q. Hu, “Anchor-booster based heterogeneous networks with mmwave capable booster cells,” in *Proc. IEEE Global Communications Conference (GLOBECOM) Workshops*, 2013, pp. 93–98.
- [97] G. Jakllari, J. Broustis, T. Korakis, S. V. Krishnamurthy, and L. Tassiulas, “Handling asymmetry in gain in directional antenna equipped ad hoc networks,” in *Proc. IEEE International Symposium on Personal, Indoor and Mobile Radio Communications (PIMRC)*, 2005, pp. 1284–1288.
- [98] C. Jeong, J. Park, and H. Yu, “Random access in millimeter-wave beamforming cellular networks: Issues and approaches,” *IEEE Commun. Mag.*, vol. 53, no. 1, pp. 180–185, Jan. 2015.
- [99] G. Athanasiou, C. Weeraddana, C. Fischione, and L. Tassiulas, “Optimizing client association in 60 GHz wireless access networks,” *IEEE/ACM Trans. Netw.*, vol. 23, no. 3, pp. 836–850, Jun. 2015.
- [100] J. He, T. Kim, H. Ghauch, K. Liu, and G. Wang, “Millimeter wave MIMO channel tracking systems,” in *Proc. IEEE Global Communications Conference (GLOBECOM) Workshops*, 2014, pp. 416–421.
- [101] A. Adhikary, J. Nam, J. Ahn, and G. Caire, “Joint spatial division and multiplexing—the large-scale array regime,” *IEEE Trans. Inform. Theory*, vol. 59, no. 10, pp. 6441–6463, Feb. 2013.
- [102] R. Taori and A. Sridharan, “Point-to-multipoint in-band mmwave backhaul for 5G networks,” *IEEE Commun. Mag.*, vol. 53, no. 1, pp. 195–201, Jan. 2015.
- [103] J. Nam, A. Adhikary, J. Ahn, and G. Caire, “Joint spatial division and multiplexing: Opportunistic beamforming, user grouping and simplified downlink scheduling,” *IEEE J. Sel. Areas Commun.*, vol. 8, no. 5, pp. 876–890, Oct. 2014.
- [104] A. Adhikary, E. Safadi, M. Samimi, R. Wang, G. Caire, T. Rappaport, and A. Molisch, “Joint spatial division and multiplexing for mm-Wave channels,” *IEEE J. Sel. Areas Commun.*, vol. 32, no. 6, pp. 1239–1255, Jun. 2014.
- [105] S. Sun, G. R. MacCartney, M. K. Samimi, S. Nie, and T. S. Rappaport, “Millimeter wave multi-beam antenna combining for 5G cellular link improvement in New York City,” in *Proc. IEEE International Conference on Communications (ICC)*, 2014, pp. 5468–5473.
- [106] E. G. Larsson, O. Edfors, F. Tufvesson, and T. L. Marzetta, “Massive MIMO for next generation wireless systems,” *IEEE Commun. Mag.*, vol. 52, no. 2, pp. 186–195, Feb. 2014.

- [107] A. L. Swindlehurst, E. Ayanoglu, P. Heydari, and F. Capolino, "Millimeter-wave massive MIMO: The next wireless revolution," *IEEE Commun. Mag.*, vol. 52, no. 9, pp. 56–62, Sept. 2014.
- [108] J. G. Andrews, S. Singh, Q. Ye, X. Lin, and H. S. Dhillon, "An overview of load balancing in HetNets: Old myths and open problems," *IEEE Wireless Commun.*, vol. 21, no. 2, pp. 18–25, Apr. 2014.
- [109] H.-S. Jo, Y. J. Sang, P. Xia, and J. G. Andrews, "Heterogeneous cellular networks with flexible cell association: A comprehensive downlink SINR analysis," *IEEE Trans. Wireless Commun.*, vol. 11, no. 10, pp. 3484–3495, Oct. 2012.
- [110] Q. Ye, B. Rong, Y. Chen, M. Al-Shalash, C. Caramanis, and J. G. Andrews, "User association for load balancing in heterogeneous cellular networks," *IEEE Trans. Wireless Commun.*, vol. 12, no. 6, pp. 2706–2716, Jun. 2013.
- [111] M. Haenggi, J. G. Andrews, F. Baccelli, O. Dousse, and M. Franceschetti, "Stochastic geometry and random graphs for the analysis and design of wireless networks," *IEEE J. Sel. Areas Commun.*, vol. 27, no. 7, pp. 1029–1046, Sept. 2009.
- [112] G. Andrews, F. Baccelli, and R. Ganti, "A tractable approach to coverage and rate in cellular networks," *IEEE Trans. Commun.*, vol. 59, no. 11, pp. 3122–3134, Nov. 2011.
- [113] H. S. Dhillon, R. K. Ganti, F. Baccelli, and J. G. Andrews, "Modeling and analysis of k-tier downlink heterogeneous cellular networks," *IEEE J. Sel. Areas Commun.*, vol. 30, no. 3, pp. 550–560, Apr. 2012.
- [114] W. Xia, Y. Wen, C. H. Foh, D. Niyato, and H. Xie, "A survey on software-defined networking," *IEEE Commun. Surveys Tuts.*, vol. 17, no. 1, pp. 27–51, First Quarter 2015.
- [115] R. Jain, D. Chiu, and W. Hawe, "A quantitative measure of fairness and discrimination for resource allocation in shared computer systems," *Digital Equipment Corp., Tech. Rep.*, 1998.
- [116] N. L. Johnson, A. W. Kemp, and S. Kotz, *Univariate discrete distributions*. John Wiley & Sons, 2005, vol. 444.
- [117] C. A. Balanis, *Antenna theory: analysis and design*. John Wiley & Sons, 2012.
- [118] T. Nitsche, C. Cordeiro, A. B. Flores, E. W. Knightly, E. Perahia, and J. C. Widmer, "IEEE 802.11ad: Directional 60 GHz communication for multi-Gigabit-per-second Wi-Fi," *IEEE Commun. Mag.*, vol. 52, no. 12, pp. 132–141, Dec. 2014.



- [119] B. Li, Z. Zhou, W. Zou, X. Sun, and G. Du, "On the efficient beam-forming training for 60GHz wireless personal area networks," *IEEE Trans. Wireless Commun.*, vol. 12, no. 2, pp. 504–515, Feb. 2013.
- [120] R. Ramanathan, J. Redi, C. Santivanez, D. Wiggins, and S. Polit, "Ad hoc networking with directional antennas: A complete system solution," *IEEE J. Sel. Areas Commun.*, vol. 23, no. 3, pp. 496–506, Mar. 2005.
- [121] J. Qiao, L. Cai, X. Shen, and J. Mark, "Enabling multi-hop concurrent transmissions in 60 GHz wireless personal area networks," *IEEE Trans. Wireless Commun.*, vol. 10, no. 11, pp. 3824–3833, Nov. 2011.
- [122] J. Kim, Y. Tian, S. Mangold, and A. F. Molisch, "Joint scalable coding and routing for 60 ghz real-time live HD video streaming applications," *IEEE Trans. Broadcast.*, vol. 59, no. 3, pp. 500–512, Sept. 2013.
- [123] J. Qiao, L. X. Cai, X. Shen, and J. Mark, "STDMA-based scheduling algorithm for concurrent transmissions in directional millimeter wave networks," in *Proc. IEEE International Conference on Communications (ICC)*, 2012, pp. 5221–5225.
- [124] X. Wu, S. Tavildar, S. Shakkottai, T. Richardson, J. Li, R. Laroia, and A. Jovicic, "FlashLinQ: A synchronous distributed scheduler for peer-to-peer ad hoc networks," *IEEE/ACM Trans. on Netw.*, vol. 21, no. 4, pp. 1215–1228, 2013.
- [125] H. Shokri-Ghadikolaei, L. Gkatzikis, and C. Fischione, "Beam-searching and transmission scheduling in millimeter wave communications," *arXiv <http://arxiv.org/abs/1501.02516>*, 2015.
- [126] S. Boyd and L. Vandenberghe, *Convex Optimization*. New York, NY, USA: Cambridge University Press, 2004.
- [127] R. H. Etkin, D. N. Tse, and H. Wang, "Gaussian interference channel capacity to within one bit," *IEEE Trans. Inform. Theory*, vol. 54, no. 12, pp. 5534–5562, 2008.
- [128] G. Sharma, R. R. Mazumdar, and N. B. Shroff, "On the complexity of scheduling in wireless networks," in *Proc. of the 12th ACM annual international conference on Mobile computing and networking*, 2006, pp. 227–238.
- [129] V. V. Lozin and M. Milanić, "A polynomial algorithm to find an independent set of maximum weight in a fork-free graph," *Journal of Discrete Algorithms*, vol. 6, no. 4, pp. 595–604, 2008.
- [130] J. Kim and A. F. Molisch, "Fast millimeter-wave beam training with receive beamforming," *J. Commun. and Netw.*, vol. 16, no. 5, pp. 512–522, 2014.

- [131] I. K. Son, S. Mao, M. X. Gong, and Y. Li, "On frame-based scheduling for directional mmWave WPANs," in *Proc. IEEE International Conference on Computer Communications (INFOCOM)*, 2012, pp. 2149–2157.
- [132] A. Ephremides and O. A. Mowafi, "Analysis of a hybrid access scheme for buffered users-probabilistic time division," *IEEE Trans. Software Eng.*, no. 1, pp. 52–61, Jan. 1982.
- [133] M. Rios and N. D. Georganas, "A hybrid multiple-access protocol for data and voice-packet over local area networks," *IEEE Trans. Comput.*, vol. 100, no. 1, pp. 90–94, Jan. 1985.
- [134] W. Ye, J. Heidemann, and D. Estrin, "Medium access control with coordinated adaptive sleeping for wireless sensor networks," *IEEE/ACM Trans. Netw.*, vol. 12, no. 3, pp. 493–506, Jun. 2004.
- [135] M. C. Vuran and I. F. Akyildiz, "A-MAC: Adaptive medium access control for next generation wireless terminals," *IEEE/ACM Trans. Netw.*, vol. 15, no. 3, pp. 574–587, Jun. 2007.
- [136] Y. Niu, Y. Li, D. Jin, L. Su, and D. Wu, "Blockage robust and efficient scheduling for directional mmWave WPANs," *IEEE Trans. Veh. Technol.*, vol. 64, no. 2, pp. 728–742, Feb. 2015.
- [137] I. Son, S. Mao, M. Gong, and Y. Li, "On frame-based scheduling for directional mmWave WPANs," in *Proc. IEEE International Conference on Computer Communications (INFOCOM)*, 2012, pp. 2149–2157.
- [138] M. Park and P. Gopalakrishnan, "Analysis on spatial reuse and interference in 60-GHz wireless networks," *IEEE J. Sel. Areas Commun.*, vol. 27, no. 8, pp. 1443–1452, Oct. 2009.
- [139] C. Sum, Z. Lan, R. Funada, J. Wang, T. Baykas, M. A. Rahman, and H. Harada, "Virtual time-slot allocation scheme for throughput enhancement in a millimeter-wave multi-Gbps WPAN system," *IEEE J. Sel. Areas Commun.*, vol. 27, no. 8, pp. 1379–1389, Oct. 2009.
- [140] J. Park, S.-L. Kim, and J. Zander, "Tractable resource management in millimeter-wave overlaid ultra-dense cellular networks," *arXiv preprint arXiv:1507.04658*, 2015.
- [141] W. Lu and M. Di Renzo, "Stochastic geometry modeling of cellular networks: Analysis, simulation and experimental validation," *arXiv preprint arXiv:1506.03857*, 2015.
- [142] S. Singh, M. N. Kulkarni, A. Ghosh, and J. G. Andrews, "Tractable model for rate in self-backhauled millimeter wave cellular networks," *IEEE J. Sel. Areas Commun.*, 2015, to be published.

- [143] C. Pyo and H. Harada, "Throughput analysis and improvement of hybrid multiple access in IEEE 802.15.3c mm-wave WPAN," *IEEE J. Sel. Areas Commun.*, vol. 27, no. 8, pp. 1414–1424, Oct. 2009.
- [144] L. Kleinrock and F. A. Tobagi, "Packet switching in radio channels: Part I—carrier sense multiple-access modes and their throughput-delay characteristics," *IEEE Trans. Commun.*, vol. 23, no. 12, pp. 1400–1416, Dec. 1975.
- [145] K. Xu, M. Gerla, and S. Bae, "How effective is the IEEE 802.11 RTS/CTS handshake in ad hoc networks?" in *Proc. IEEE Global Telecommunications Conference (GLOBECOM)*, 2002, pp. 72–76.
- [146] A. Iyer, C. Rosenberg, and A. Karnik, "What is the right model for wireless channel interference?" *IEEE Trans. Wireless Commun.*, vol. 8, no. 5, pp. 2662–2671, May 2009.
- [147] P. Cardieri, "Modeling interference in wireless ad hoc networks," *IEEE Commun. Surveys Tuts.*, vol. 12, no. 4, pp. 551–572, Fourth Quarter 2010.
- [148] A. Thornburg, T. Bai, and R. Heath, "MmWave ad hoc network coverage and capacity," in *Proc. IEEE International Conference on Communications (ICC)*, 2015.
- [149] A. Goldsmith, S. A. Jafar, N. Jindal, and S. Vishwanath, "Capacity limits of MIMO channels," *IEEE J. Sel. Areas Commun.*, vol. 21, no. 5, pp. 684–702, Jun. 2003.
- [150] P. Park, P. Di Marco, P. Soldati, C. Fischione, and K. H. Johansson, "A generalized Markov chain model for effective analysis of slotted IEEE 802.15.4," in *Proc. IEEE Mobile Adhoc and Sensor Systems (MASS)*, 2009, pp. 130–139.
- [151] S. Pollin, M. Ergen, S. Ergen, B. Bougard, L. Der Perre, I. Moerman, A. Bahai, P. Varaiya, and F. Catthoor, "Performance analysis of slotted carrier sense IEEE 802.15.4 medium access layer," *IEEE Trans. Wireless Commun.*, vol. 7, no. 9, pp. 3359–3371, Sept. 2008.
- [152] G. Bianchi, "Performance analysis of the IEEE 802.11 distributed coordination function," *IEEE J. Sel. Areas Commun.*, vol. 18, no. 3, pp. 535–547, Mar. 2000.
- [153] J. Hui and M. Devetsikiotis, "A unified model for the performance analysis of IEEE 802.11e EDCA," *IEEE Trans. Commun.*, vol. 53, no. 9, pp. 1498–1510, Sept. 2005.
- [154] D. Malone, K. Duffy, and D. Leith, "Modeling the 802.11 distributed coordination function in nonsaturated heterogeneous conditions," *IEEE/ACM Trans. Netw.*, vol. 15, no. 1, pp. 159–172, Feb. 2007.

- [155] M. Garetto, T. Salonidis, and E. W. Knightly, "Modeling per-flow throughput and capturing starvation in CSMA multi-hop wireless networks," *IEEE/ACM Trans. Netw.*, vol. 16, no. 4, pp. 864–877, Aug. 2008.
- [156] B. Jang and M. L. Sichitiu, "IEEE 802.11 saturation throughput analysis in the presence of hidden terminals," *IEEE/ACM Trans. Netw.*, vol. 20, no. 2, pp. 557–570, Apr. 2012.
- [157] Y. Yang and T. Yum, "Delay distributions of slotted ALOHA and CSMA," *IEEE Trans. Commun.*, vol. 51, no. 11, pp. 1846–1857, Nov. 2003.
- [158] N. Benvenuto and M. Zorzi, *Principles of communications Networks and Systems*. Wiley Online Library, 2011.
- [159] H. A. David and H. N. Nagaraja, *Order statistics*. Wiley Online Library, 2003, third Edition.